The
PHILOSOPHICAL MAGAZINE

FIRST PUBLISHED IN 1798

L. 44 SEVENTH SERIES No. 350 March 1953

UNIVERSITY OF HAWAII
LIBRARY
APR 13 '53

A Journal of Theoretical Experimental and Applied Physics

EDITOR
PROFESSOR N. F. MOTT, M.A., D.Sc., F.R.S.

EDITORIAL BOARD
SIR LAWRENCE BRAGG, O.B.E., M.C., M.A., D.Sc., F.R.S.
SIR GEORGE THOMSON, M.A., D.Sc., F.R.S.
PROFESSOR A. M. TYNDALL, C.B.E., D.Sc., F.R.S.

PRICE 15s. 0d.
Annual Subscription £8 0s. 0d. payable in advance

D AND PUBLISHED BY TAYLOR & FRANCIS LTD., RED LION COURT, FLEET ST., LONDON, E.C.4.

Early Scientific Publications

ALERE FLAMMAM

DIARY OF ROBERT HOOKE, M.A., M.D., F.R.S.
1672-1680

Edited by **H. W. ROBINSON** and **W. ADAMS**
Recommended for publication by the Royal Society, London

25/-
net

"This vivid record of the scientific, artistic and social activities of a remarkable man during remarkable years has too long remained in obscurity."—Extract from foreword by Sir Frederick Gowland Hopkins, O.M., President of the Royal Society.

MATHEMATICAL WORK OF JOHN WALLIS, D.D., F.R.S.

By **J. F. SCOTT, Ph.D., B.A.**

12/6
net

"His work will be indispensable to those interested in the early history of The Royal Society. I commend to all students of the Seventeenth Century, whether scientific or humane, this learned and lucid book."—Extract from foreword by Prof. E. N. da C. Andrade, D.Sc., Ph.D., F.R.S.
Recommended for publication by University of London

CORRESPONDENCE AND PAPERS OF EDMOND HALLEY

21/-
net

Arranged and Edited by **EUGENE FAIRFIELD MACPIKE**

First published on behalf of The History of Science Society by Oxford University Press. Now re-issued by Taylor & Francis, Ltd.

MEMOIRS OF SIR ISAAC NEWTON'S LIFE

5/-
net

By **WILLIAM STUKELEY, M.D., F.R.S., 1752**
From an Original Manuscript
Now in the possession of the Royal Society, London

HEVELIUS, FLAMSTEED AND HALLEY

12/6
net

Three Contemporary Astronomers and their Mutual Relations
By **EUGENE FAIRFIELD MACPIKE**
Published by arrangement with The History of Science Society

Established over 150 years

TAYLOR & FRANCIS, LTD.
RED LION COURT, FLEET ST., LONDON E.C.
PRINTERS & PUBLISHERS OF SCIENTIFIC BOOKS

XXV. *The Onset of Convection by Thermal Instability in Spherical Shells*

By S. Chandrasekhar, F.R.S.
Yerkes Observatory, University of Chicago*

[Received November 1, 1952]

Summary

In this paper the problem of the thermal instability of an incompressible sphere consisting of an inviscid core and a viscous mantle is considered, and it is shown that the pattern of convection which sets in, at marginal stability, in the mantle shifts to harmonics of the higher orders as the thickness of the mantle decreases. Thus, when the mantle extends to a depth of half the radius of the sphere, the harmonics of orders three and four set in about simultaneously, while the harmonic of order five follows very soon afterwards. The bearing of this result on the problem of convection in the earth's mantle and of the interpretation of the earth's topographic features is indicated.

§1. Introduction

In a recent paper (Chandrasekhar 1952 : this paper will be referred to hereafter as I) the problem of the thermal instability of a fluid sphere heated within has been treated. In this paper the related problem of the onset of convection in spherical shells will be treated. The interest in this latter problem arises, in part, in connection with Vening Meinesz's (1951) interpretation of a feature of the earth's topography, to which he drew attention at the same time. The feature in question is this : Using Prey's (1922) development in spherical harmonics of the earth's topography, Vening Meinesz combined the coefficients of the $(2l+1)$ tesseral harmonics belonging to a given order l to obtain the root mean square amplitude with which a harmonic of order l is present in the development ; and he showed that, apart from the strong first-order term (corresponding to the near separation of the land and the sea hemispheres on the earth), the orders most predominantly present are three, four and five. From this predominance of the orders three, four and five Vening Meinesz concluded that phenomena in which these orders play an important part must have occurred at some time in the earth ; and he suggested that thermally induced convection might be the principal responsible phenomenon. On this suggestion the differentiation of the surface of the earth into a land and a sea hemisphere (i.e. into a hemisphere of high, respectively, low topographic elevation and corresponding differences in crustal composition) is assumed to have taken place at a time when the whole earth was a highly viscous fluid sphere of nearly uniform

---

* Communicated by the Author.

density, and the easiest pattern of convection to excite (and the last which might be expected to survive in a cooling earth) is a spherical harmonic of order one (cf. I). And the predominance of the orders three, four and five in the topography is traced to a subsequent stage in the development of the earth when it had reached a constitution not unlike the present with a core and a mantle of thickness of about 2900 km. The surmise here is that convection in the mantle at this later stage 'tore' the land hemisphere into something like its present topographic distribution (cf. also Jeffreys 1952 in this connection). The validity of this surmise requires that in a mantle extending to approximately half the radius of the sphere the modes of convections most easily excited are those of orders three, four and five; we shall see that this is confirmed by the detailed calculations presented in this paper.

§ 2. THE FORMULATION OF THE PROBLEM

Consider an incompressible sphere of radius R in which a stationary temperature distribution of the form (I, eqn. (2))

$$T=\beta(R^2-r^2) \quad . \quad . \quad . \quad . \quad . \quad . \quad . \quad . \quad . \quad (1)$$

can be maintained in virtue of a uniform distribution of heat sources imbedded in it. We shall suppose that though the sphere is of nearly uniform density it consists of an inviscid fluid core extending to a fraction η of the radius of the sphere and a viscous mantle overlying the core. We wish to determine, under these circumstances, the criterion for the onset of convection by thermal instability in the mantle.

For the application to the earth's mantle contemplated in § 1 the model we are adopting is admittedly a very idealized one: for, in the earth, what principally distinguishes the mantle from the core is the existence of a relatively sharp discontinuity of density between them. In the model we have described we are not allowing for any such discontinuity. On the other hand, by assuming that the core is inviscid and the mantle viscous, we are making the interface between them a *free surface* across which no tangential viscous stresses can act (cf. I, § 3); and we may expect that this latter condition, appropriate for a free surface, will be actually fulfilled in the earth at the interface between the core and the mantle. Consequently it would not appear unreasonable to hope that the consideration of the model we have described would disclose the essential features of the convection patterns which may predominate in the earth's mantle.

Under the conditions we have stated the equations governing the problem are the same as in I. In particular, the criterion for the onset of convection in the mantle as a disturbance in the form of a spherical harmonic of order l will be determined by the conditions that the equation (cf. I, eqns. (41) to (43))

$$\left[\frac{d^2}{dr^2}+\frac{2}{r}\frac{d}{dr}-\frac{l(l+1)}{r^2}\right]^3 W=-l(l+1)C_l W \quad . \quad . \quad . \quad (2)$$

admits a solution satisfying the boundary conditions

$$W=\frac{d^2W}{dr^2}=\left[\frac{d^2}{dr^2}+\frac{2}{r}\frac{d}{dr}-\frac{l(l+1)}{r^2}\right]^2 W=0 \text{ at } r=1 \text{ and } r=\eta, \quad . \quad (3)$$

where it may be recalled that r is now measured in units of R and (I, eqn. (42))

$$C_l=\frac{2\beta\gamma}{\kappa\nu}R^6. \quad . \quad . \quad . \quad . \quad . \quad . \quad . \quad . \quad (4)$$

(For the meanings of the other symbols see I.)

§ 3. THE VARIATIONAL SOLUTION OF THE PROBLEM

It can be readily verified that the variational principle established in I, § 5 is applicable, with suitable modifications, to the problem on hand, and that it can be used to solve the characteristic value problem formulated in § 2 in the following manner.

Letting

$$\left[\frac{d^2}{dr^2}+\frac{2}{r}\frac{d}{dr}-\frac{l(l+1)}{r^2}\right]^2 W=F, \quad . \quad . \quad . \quad . \quad . \quad . \quad (5)$$

assume a form for F (containing one or more parameters A_j) which vanishes at $r=1$ and $r=\eta$; then solve eqn. (5) for W and arrange that it satisfies the remaining boundary conditions

$$W=\frac{d^2W}{dr^2}=0 \quad \text{at } r=1 \text{ and } r=\eta; \quad . \quad . \quad . \quad . \quad . \quad (6)$$

and finally, evaluate C_l according to the formula (cf. I, eqn. (54))

$$C_l=\frac{1}{l(l+1)}\frac{\int_\eta^1 \{r^2(dF/dr)^2+l(l+1)F^2\}\,dr}{\int_\eta^1 r^2WF\,dr} \quad . \quad . \quad . \quad . \quad (7)$$

and minimize it with respect to the parameters A_j. In this way we shall obtain the best value of C_l for the chosen form of F.

The form of the equation to be solved for W suggests that we assume for F a solution of Bessel's equation of order $(l+\frac{1}{2})$ which vanishes at $r=1$ and $r=\eta$. Thus, writing

$$F=aJ_{l+1/2}(\alpha r)+bJ_{-(l+1/2)}(\alpha r), \quad . \quad . \quad . \quad . \quad . \quad . \quad (8)$$

where a, b and α are constants, we shall arrange that F vanishes at $r=1$ and $r=\eta$. For this purpose we proceed as follows: Let

$$\mathscr{C}_{l+1/2,\nu}(z)=J_{-(l+1/2)}(\alpha\eta)J_\nu(z)-J_{l+1/2}(\alpha\eta)J_{-\nu}(z), \quad . \quad . \quad . \quad (9)$$

where α is a constant unspecified for the present. Then,

$$\mathscr{C}_{l+1/2,\,l+1/2}(\alpha r)=J_{-(l+1/2)}(\alpha\eta)J_{l+1/2}(\alpha r)-J_{l+1/2}(\alpha\eta)J_{-(l+1/2)}(\alpha r) \quad . \quad . \quad . \quad (10)$$

clearly vanishes at $r=\eta$; it will also vanish at $r=1$ provided

$$J_{-(l+1/2)}(\alpha\eta)J_{l+1/2}(\alpha)-J_{l+1/2}(\alpha\eta)J_{-(l+1/2)}(\alpha)=0. \quad . \quad . \quad . \quad (11)$$

It is known (cf. Gray and Mathews 1922, p. 82, theorem X) that eqn. (11) admits an infinite number of roots all of which are real and simple; and that if α_j $(j=1, 2, \ldots)$ are the distinct roots of the equation, the functions $\mathscr{C}_{l+1/2,\, l+1/2}(\alpha_j r)$ $(j=1, 2, \ldots)$ form an orthogonal set with the integral property

$$\int_\eta^1 r\mathscr{C}_{l+1/2,\, l+1/2}(\alpha_j r)\mathscr{C}_{l+1/2,\, l+1/2}(\alpha_k r)\, dr=N_{j,\, l+1/2}\delta_{jk}, \quad . \quad . \quad (12)$$

where δ_{jk} denotes the usual Kronecker symbol and

$$N_{j,\, l+1/2}=\frac{2}{\alpha_j^2\pi^2}\left\{\frac{J^2{}_{l+1/2}(\alpha_j\eta)}{J^2{}_{l+1/2}(\alpha_j)}-1\right\}. \quad . \quad . \quad . \quad . \quad (13)$$

For later use we may note here that the derivatives of $\mathscr{C}_{l+1/2,\, l+1/2}(\alpha_j r)$ at $r=1$ and $r=\eta$ (which we shall denote by $\mathscr{C}'_{l+1/2}(\alpha_j)$ and $\mathscr{C}'_{l+1/2}(\alpha_j\eta)$ respectively) are given by

$$\mathscr{C}'_{l+1/2}(\alpha_j)=\left[\frac{d}{dr}\mathscr{C}_{l+1/2,\, l+1/2}(\alpha_j r)\right]_{r=1}=(-1)^l\frac{2}{\pi}\frac{J_{l+1/2}(\alpha_j\eta)}{J_{l+1/2}(\alpha_j)} \quad (14)$$

and

$$\mathscr{C}'_{l+1/2}(\alpha_j\eta)=\left[\frac{d}{dr}\mathscr{C}_{l+1/2,\, l+1/2}(\alpha_j r)\right]_{r=\eta}=(-1)^l\frac{2}{\pi\eta}. \quad . \quad . \quad (15)$$

(Equations (12) to (15) can be derived by following the procedure given by Carslaw and Jaeger 1947, § 79, in obtaining similar relations involving the Bessel functions of order zero.)

Also, since $\mathscr{C}_{l+1/2,\nu}(z)$ represents a solution of Bessel's equation of order ν it must clearly satisfy the relations implied by the equations

$$\left.\begin{aligned}&\frac{d}{dz}\{z^{\nu+1}\mathscr{C}_{l+1/2,\, \nu+1}(z)\}=+z^{\nu+1}\mathscr{C}_{l+1/2,\nu}(z)\\ &\text{and}\\ &\frac{d}{dz}\{z^{-\nu+1}\mathscr{C}_{l+1/2,\, \nu-1}(z)\}=-z^{-\nu+1}\mathscr{C}_{l+1/2,\nu}(z).\end{aligned}\right\} \quad . \quad . \quad (16)$$

Returning to the variational solution of the problem described in the beginning of this section, we shall assume for F the trial function

$$F(r)=\frac{1}{\sqrt{r}}\Sigma_j A_j\mathscr{C}_{l+1/2,\, l+1/2}(\alpha_j r), \quad . \quad . \quad . \quad . \quad (17)$$

where the A_j's are the variational parameters. With this choice, F vanishes at $r=1$ and $r=\eta$ as required. Moreover, with F given by eqn. (17), eqn. (5) governing W can be explicitly solved and we have (cf. I, eqns. (68) to (73))

$$W=\frac{1}{\sqrt{r}}\Sigma_j\frac{A_j}{\alpha_j^4}\mathscr{C}_{l+1/2,\, l+1/2}(\alpha_j r)+B_1r^l+B_2r^{l+2}+B_3r^{-(l+1)}+B_4r^{-(l-1)}, \quad . \quad (18)$$

where B_1, B_2, B_3 and B_4 are constants of integration to be determined by the boundary conditions (6). These boundary conditions lead to the equations

$$B_1+B_2+B_3+B_4=0, \qquad (19)$$

$$B_1\eta^l+B_2\eta^{l+2}+B_3\eta^{-(l+1)}+B_4\eta^{-(l-1)}=0, \qquad (20)$$

$$l(l-1)(B_1+B_4)+(l+1)(l+2)(B_2+B_3)=2\Sigma_j(A_j/\alpha_j^3)\mathscr{C}'_{l+1/2}(\alpha_j) \qquad (21)$$

and

$$\begin{aligned} l(l-1)(B_1\eta^{l-2}+B_4\eta^{-(l+1)})&+(l+1)(l+2)(B_2\eta^l+B_3\eta^{-(l+3)}) \\ &=2\eta^{-3/2}\Sigma_j(A_j/\alpha_j^3)\mathscr{C}'_{l+1/2}(\alpha_j\eta), \end{aligned} \qquad (22)$$

where $\mathscr{C}'_{l+1/2}(\alpha_j)$ and $\mathscr{C}'_{l+1/2}(\alpha_j\eta)$ are defined as in eqns. (14) and (15). Combining eqns. (19) and (21), and similarly (20) and (22), we obtain

$$B_1+B_4=-(B_2+B_3)=-\frac{1}{2l+1}\Sigma_j\frac{A_j}{\alpha_j^3}\mathscr{C}'_{l+1/2}(\alpha_j) \qquad (23)$$

and

$$\begin{aligned} B_1\eta^l+B_4\eta^{-(l-1)}&=-(B_2\eta^{l+2}+B_3\eta^{-(l+1)}) \\ &=-\frac{\sqrt{\eta}}{2l+1}\Sigma_j\frac{A_j}{\alpha_j^3}\mathscr{C}'_{l+1/2}(\alpha_j\eta)\,; \end{aligned} \qquad (24)$$

and solving these equations for B_2 and B_4 we have

$$B_2=\frac{1}{(2l+1)(1-\eta^{2l+3})}\Sigma_j\frac{A_j}{\alpha_j^3}\Big[\mathscr{C}'_{l+1/2}(\alpha_j)-\eta^{l+3/2}\mathscr{C}'_{l+1/2}(\alpha_j\eta)\Big] \qquad (25)$$

and

$$B_4=\frac{1}{(2l+1)(\eta^{-2l+1}-1)}\Sigma_j\frac{A_j}{\alpha_j^3}\Big[\mathscr{C}'_{l+1/2}(\alpha_j)-\eta^{-l+1/2}\mathscr{C}'_{l+1/2}(\alpha_j\eta)\Big]. \qquad (26)$$

Turning next to the evaluation of C_l, we find that for F and W given by eqns. (17) and (18) the integrals occurring in (7) can be reduced in a manner quite analogous to that followed in the reduction of the corresponding integrals in I (cf. I, eqns. (76) to (78)). Thus, on using the orthogonality relation (12), we now find that

$$\int_\eta^1\left\{r^2\left(\frac{dF}{dr}\right)^2+l(l+1)F^2\right\}dr=\Sigma_jA_j^2\alpha_j^2N_{j,\,l+1/2} \qquad (27)$$

and

$$\begin{aligned} \int_\eta^1 r^2WF\,dr&=\Sigma_j(A_j^2/\alpha_j^4)N_{j,\,l+1/2} \\ &+\Sigma_jA_j\int_\eta^1\mathscr{C}_{l+1/2,\,l+1/2}(\alpha_jr)[B_1r^{l+3/2}+B_2r^{l+7/2}+B_3r^{-l+1/2}+B_4r^{-l+5/2}]\,dr. \end{aligned} \qquad (28)$$

The remaining integrals on the right-hand side of (28) can be evaluated if proper use is made of eqns. (16), (23) and (24); and we find, after some lengthy reductions, that

$$\begin{aligned} \int_\eta^1 r^2WF\,dr=\Sigma_j(A_j^2/\alpha_j^4)N_{j,\,l+1/2} &-2B_2\Sigma_j(A_j/\alpha_j^2)[\mathscr{C}_{l+1/2,\,l+5/2}(\alpha_j)-\eta^{l+5/2}\mathscr{C}_{l+1/2,\,l+5/2}(\alpha_j\eta)] \\ &-2B_4\Sigma_j(A_j/\alpha_j^2)[\mathscr{C}_{l+1/2,\,l-3/2}(\alpha_j)-\eta^{-l+3/2}\mathscr{C}_{l+1/2,\,l-3/2}(\alpha_j\eta)]. \end{aligned} \qquad (29)$$

The resulting expression for C_l is, therefore,

$$\begin{aligned}C_l=\frac{2l+1}{l(l+1)}[\Sigma_j A_j^2\alpha_j^2 N_{j,\,l+1/2}]\Big\{&(2l+1)\Sigma_j(A_j^2/\alpha_j^4)N_{j,\,l+1/2}\\ &-\frac{2}{(1-\eta^{2l+3})}\Sigma_j\frac{A_j}{\alpha_j^3}[\mathscr{C}'_{l+1/2}(\alpha_j)\\ &-\eta^{l+3/2}\mathscr{C}'_{l+1/2}(\alpha_j\eta)]\Sigma_k\frac{A_k}{\alpha_k^2}[\mathscr{C}_{l+1/2,\,l+5/2}(\alpha_k)-\eta^{l+5/2}\mathscr{C}_{l+1/2,\,l+5/2}(\alpha_k\eta)]\\ &-\frac{2}{(\eta^{-2l+1}-1)}\Sigma_j\frac{A_j}{\alpha_j^3}[\mathscr{C}'_{l+1/2}(\alpha_j)\\ &-\eta^{-l+1/2}\mathscr{C}'_{l+1/2}(\alpha_j\eta)]\Sigma_k\frac{A_k}{\alpha_k^2}[\mathscr{C}_{l+1/2,\,l-3/2}(\alpha_k)\\ &-\eta^{-l+3/2}\mathscr{C}_{l+1/2,\,l-3/2}(\alpha_k\eta)]\Big\}^{-1},\qquad (30)\end{aligned}$$

where we have substituted for B_2 and B_4 according to eqns. (25) and (26). By minimizing this last expression with respect to the A_j's we shall obtain the 'best' value for C_l for the chosen form of F.

Table 1. The Characteristic Numbers C_l for Various Values of l and η

l	$\eta=0{\cdot}2$	$\eta=0{\cdot}4$	$\eta=0{\cdot}5$	$\eta=0{\cdot}6$	$\eta=0{\cdot}8$
1	$4{\cdot}141\times10^3$	$2{\cdot}140\times10^4$	$5{\cdot}373\times10^4$	$1{\cdot}734\times10^5$	$8{\cdot}604\times10^6$
2	$3{\cdot}826\times10^3$	$1{\cdot}041\times10^4$	$2{\cdot}347\times10^4$	$6{\cdot}962\times10^4$	$3{\cdot}017\times10^6$
3	$5{\cdot}790\times10^3$	$9{\cdot}730\times10^3$	$1{\cdot}803\times10^4$	$4{\cdot}602\times10^4$	$1{\cdot}626\times10^6$
4	$9{\cdot}441\times10^3$	$1{\cdot}200\times10^4$	$1{\cdot}839\times10^4$	$3{\cdot}938\times10^4$	$1{\cdot}075\times10^6$
5	$1{\cdot}486\times10^4$	$1{\cdot}649\times10^4$	$2{\cdot}175\times10^4$	$3{\cdot}939\times10^4$	$8{\cdot}070\times10^5$
6		$2{\cdot}331\times10^4$	$2{\cdot}767\times10^4$	$4{\cdot}340\times10^4$	$6{\cdot}610\times10^5$
7		$3{\cdot}281\times10^4$	$3{\cdot}633\times10^4$	$5{\cdot}072\times10^4$	$5{\cdot}779\times10^5$
8			$4{\cdot}808\times10^4$	$6{\cdot}130\times10^4$	$5{\cdot}312\times10^5$
9			$6{\cdot}340\times10^4$	$7{\cdot}545\times10^4$	$5{\cdot}079\times10^5$
10			$8{\cdot}276\times10^4$	$9{\cdot}358\times10^4$	$5{\cdot}012\times10^5$
11			$1{\cdot}067\times10^5$	$1{\cdot}162\times10^5$	$5{\cdot}073\times10^5$
12			$1{\cdot}357\times10^5$	$1{\cdot}439\times10^5$	$5{\cdot}239\times10^5$
13			$1{\cdot}705\times10^5$	$1{\cdot}774\times10^5$	$5{\cdot}499\times10^5$
14			$2{\cdot}115\times10^5$	$2{\cdot}172\times10^5$	$5{\cdot}848\times10^5$
15			$2{\cdot}594\times10^5$	$2{\cdot}640\times10^5$	$6{\cdot}282\times10^5$

The simplest trial function for F of the chosen form is

$$F=\frac{1}{\sqrt{r}}\mathscr{C}_{l+1/2,\,l+1/2}(\alpha_1 r),\qquad (31)$$

where α_1 is the first zero of the expression on the right-hand side of eqn. (11); $\mathscr{C}_{l+1/2,\,l+1/2}(\alpha_1 r)$ has then no node between $r=\eta$ and $r=1$.

For this choice of F there is no variational parameter with respect to which we have to minimize, and eqn. (30) directly gives

$$\begin{aligned} C_l = \frac{2l+1}{l(l+1)} \alpha_1{}^7 N_{1,\, l+1/2} \Big\{ & (2l+1)\alpha_1 N_{1,\, l+1/2} \\ & - \frac{2}{(1-\eta^{2l+3})} [\mathscr{C}'_{l+1/2}(\alpha_1) - \eta^{l+3/2} \mathscr{C}'_{l+1/2}(\alpha_1\eta)][\mathscr{C}_{l+1/2,\, l+5/2}(\alpha_1) \\ & - \eta^{l+5/2} \mathscr{C}_{l+1/2,\, l+5/2}(\alpha_1\eta)] - \frac{2}{(\eta^{-2l+1}-1)} [\mathscr{C}'_{l+1/2}(\alpha_1) \\ & - \eta^{-l+1/2} \mathscr{C}'_{l+1/2}(\alpha_1\eta)][\mathscr{C}_{l+1/2,\, l-3/2}(\alpha_1) - \eta^{-l+3/2} \mathscr{C}_{l+1/2,\, l-3/2}(\alpha_1\eta)] \Big\}^{-1} . \end{aligned} \qquad (32)$$

Fig. 1

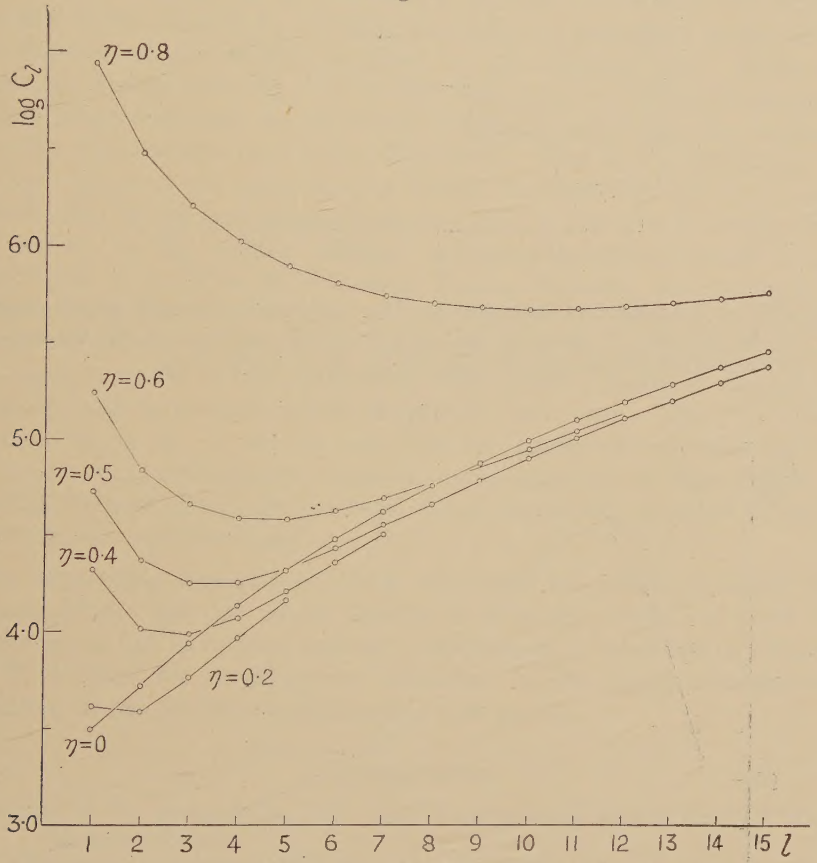

The criterion (C_l) for the onset of convection in the mantle as a spherical harmonic disturbance of order l for various thicknesses of the mantle. The different curves are distinguished by the values of the fraction (η) of the radius of the sphere occupied by the inviscid core.

In table 1 are listed the values of C_l obtained with the aid of formula (32) and the recent tabulation of Chandrasekhar and Donna Elbert (1953) of the roots of eqn. (11). The dependence of C_l on l and η is further illustrated in fig. 1.

Fig. 2

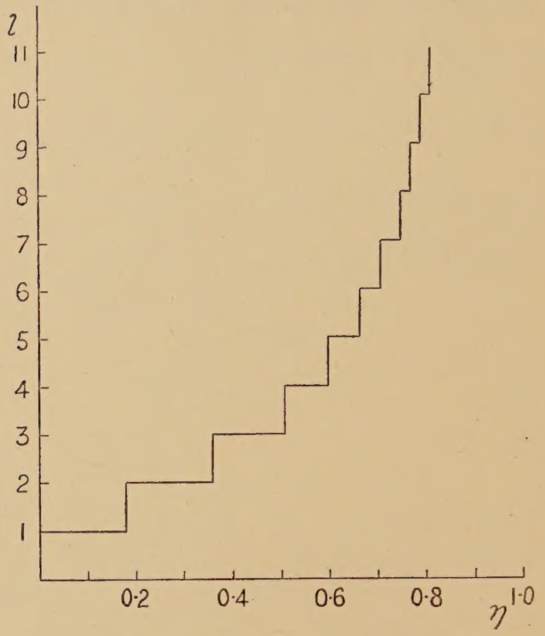

The order of the spherical harmonic l of the convection pattern which appears in the mantle, at marginal stability, in its dependence on the fraction (η) of the radius of the sphere occupied by the inviscid core.

Fig. 3

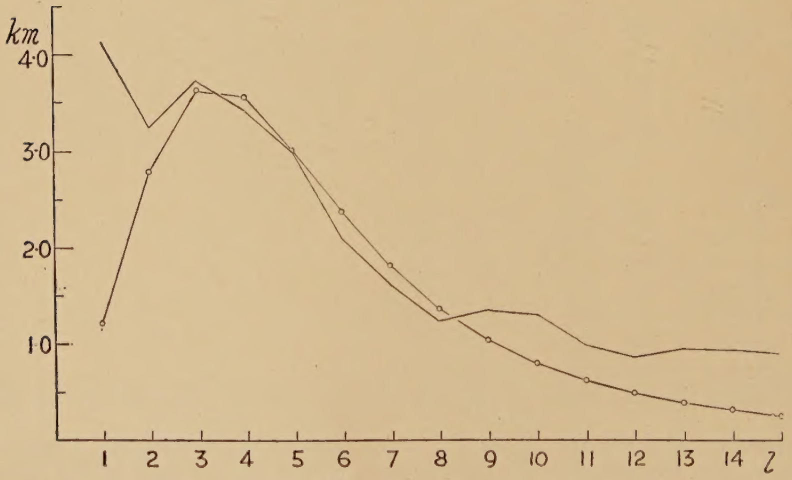

Comparison of the root mean square amplitude (in km) of a spherical harmonic of order l in the topographic analysis of the earth's surface (the full line discontinuous curve) after Vening Meinesz with $1/C_l$ (the discontinuous curve passing through the open circles) in the case when the mantle extends to a depth of one-half of the radius of the sphere. (The curves have been adjusted to agree at $l=5$.)

The values given by (32) could be improved by including a second term in F. However, in view of the fact that for the case $\eta=0$ the first approximation already gave values accurate to a fraction of a per cent (cf. I, table 1), it was not considered necessary to carry out this improvement.

§ 4. DISCUSSION OF THE RESULTS AND APPLICATION TO CONVECTION IN THE EARTH'S MANTLE

From fig. 1 it is at once apparent that, as the thickness of the mantle decreases, the pattern of convection which first appears at marginal stability shifts progressively to harmonics of the higher orders. This is shown more clearly in fig. 2, in which the order of the harmonic which is the first to be excited by thermal instability is plotted as a function of the fraction of the radius occupied by the inviscid core. From this figure, as well as from fig. 1, it is seen that for $\eta \sim 0{\cdot}5$ the harmonics of orders three and four set in about simultaneously, while the harmonic of order five follows very soon afterwards. This is a confirmation (so far as it goes) of the suggestion of Vening Meinesz that the topographic distribution in the land hemisphere may have arisen as a consequence of convection in the earth's mantle. A more quantitative test of this hypothesis is possible if, following Vening Meinesz, we compare the relative amplitudes with which the spherical harmonics of the various orders are present in the topographic analysis of the earth's surface, with $1/C_l$ as a measure of the probability with which a mode of disturbance of order l will be present in fully developed convection. This comparison is made in fig. 3. It will be seen that the agreement between the two curves is very satisfactory; indeed, as satisfactory as that found by Vening Meinesz (1951) on the basis of an empirically founded theory of convection in spherical shells.

In concluding this paper I wish to record my indebtedness to Miss Donna Elbert but for whose assistance with the numerical work this paper might not have been written. My thanks are also due to Professor G. P. Kuiper for drawing my attention to the geophysical interest attached to the problem considered in this paper.

REFERENCES

CARSLAW, H. S., and JAEGER, J. C., 1947, *Conduction of Heat in Solids* (Oxford: Clarendon Press).
CHANDRASEKHAR, S., 1952, *Phil Mag.* [7], **43,** 1317.
CHANDRASEKHAR, S., and ELBERT, D., 1953 (in the press).
GRAY, A., and MATHEWS, G. B., 1922, *A Treatise on Bessel Functions* (2nd edition) (London: Macmillan).
JEFFREYS, H., 1952, *Mon. Not. R. Astr. Soc., Geophys. Suppl.*, **6,** 272.
PREY, A., 1922, *Abh. Ges. der Wissenschaften Math. Phys. Klasse* (Göttingen), **11,** 1.
VENING MEINESZ, F. A., 1951, *Kon. Ned. Akad. Wetenschappen* (Amsterdam), Series B, 54, 212, 220.

XXVI. *The Mean Life of Charged V-Particles*

By J. P. Astbury, J. S. Buchanan, P. Chippindale, D. D. Millar, J. A. Newth, D. I. Page, A. Rytz and A. B. Sahiar
The Physical Laboratories, The University, Manchester*

[Received November 6, 1952]

Abstract

Eight hundred tracks of slow particles have been photographed during a cloud chamber experiment on penetrating showers. Measurements of tracks produced by ten heavy, negative, non-decaying particles are presented. The total observed time of flight of these particles is $1{\cdot}6\times 10^{-8}$ sec. After combining this time with the number of slow *V*-particles observed to decay in the cloud chamber, it is concluded that at least one type of heavy meson must have a mean life greater than 4×10^{-9} sec.

§ 1. Introduction

The photographs discussed here were obtained in an experiment on penetrating showers at the Jungfraujoch (3580 metres above sea level). A description of the experimental arrangement has been given already (Astbury *et al.* 1952). The cloud chamber had an illuminated volume of $54\times 54\times 9$ cm^3 and was operated in a magnetic field of 5800 gauss. All the photographs considered below were selected from 10 000 taken in the first 26 weeks of operation. They were obtained with selection systems which are illustrated in figs. 1 (*a*) and (*b*) of our previous paper.

The photographs showing the decay of $V^{\pm}$-particles were discussed in our previous paper and it was concluded there that the mean life of the particles was at least of the order of 10^{-9} sec. More valuable information can be obtained from an estimate of the number of charged *V*-particles that have been observed to traverse the cloud chamber without decaying. The present paper shows how such an estimate has been made for the slow, heavily-ionizing particles.

Mesons with masses of about $1200m_e$ can be distinguished by their ionization from π-mesons if their momenta are between 3×10^7 ev/c and 6×10^8 ev/c. However, visual estimates of the ionization density in a cloud chamber track are so unreliable that it is difficult to distinguish tracks due to particles of mass $1200m_e$ from those due to protons. For this reason in the following analysis an attempt has been made to identify only negatively charged heavy mesons.

§ 2. Measurements and Results

Tracks of 800 slow particles were selected for analysis ; the criteria for selection were that the particles should be associated with showers

---

* Communicated by Professor P. M. S. Blackett, F.R.S.

and that their tracks in the cloud chamber should be at least 10 cm long. The curvatures of 600 tracks were measured by comparison with standard curves. The remaining 200 tracks, including those with smallest curvature, were measured with a travelling microscope. The errors in these measurements were always less than the probable spurious curvatures introduced by convection in the cloud chamber or by multiple scattering of the slow particle.

The specific ionizations of the 800 tracks were estimated by a single observer. 200 tracks were then excluded from the analysis because their estimated ionizations were greater than 10. A further 180 tracks were excluded because either the technical quality of the photograph or the position of the track in the cloud chamber made a reliable estimate of ionization impossible. Finally, tracks of twenty apparently negative particles were rejected because their direction of flight was not certain. Event CC 17 (Plate 11 (*b*)) shows an example of a particle in this last category.

Fig. 1

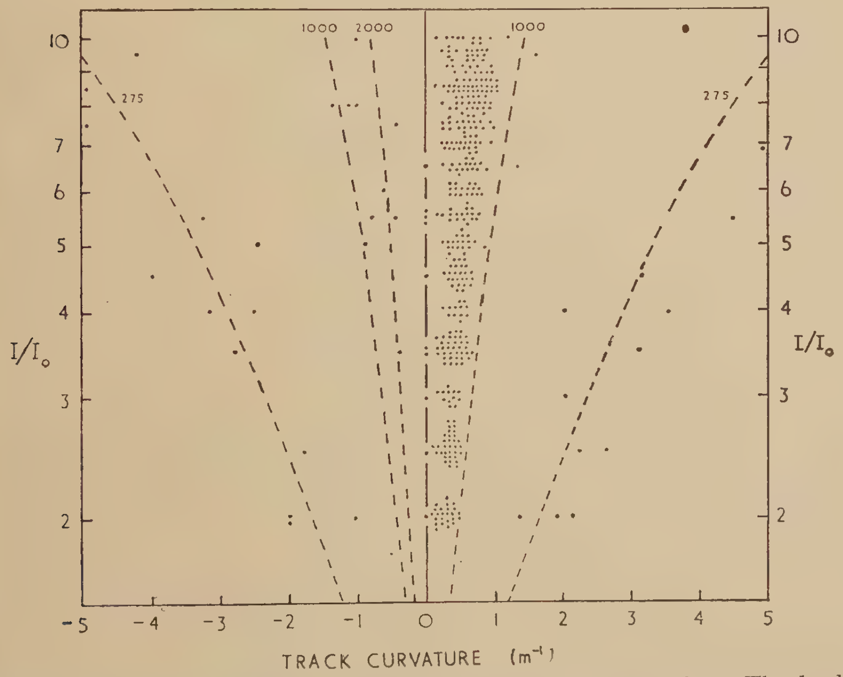

The curvatures and estimated ionizations of 400 slow particles. The broken lines give the expected values for particles of mass $275m_e$, $1000m_e$ and $2000m_e$.

In fig. 1 the estimated ionization densities of the remaining 400 tracks are plotted against curvature. To avoid confusion no probable errors have been indicated on the figure. The actual estimates of ionization were made by setting upper and lower limits which differed, in general, by a factor of nearly two. The mean value of these limits for each track has been used in plotting the figure.

Figure 1 also shows the theoretically predicted values of ionization and curvature for singly charged particles of mass $275m_e$, $1000m_e$ and $2000m_e$.

The measurements made on ten tracks apparently due to negatively charged heavy particles are presented in table 1. These tracks were all measured with a travelling microscope and their ionization densities were estimated independently by three observers. The errors in the momenta given in column 2 are probable errors including errors of measurement, distortion due to gas motion in the cloud chamber, and spurious curvature due to multiple coulomb scattering of the particles. The ionization values given are the extreme limits of the estimates made by the three observers. The limits given in column 4 to the mass of each particle have been calculated by combining the lower and upper limits of momentum and ionization from the previous columns. Column 5 gives the length of each track visible in the cloud chamber, and column 6 the observed time of flight of each particle. The times of flight (T) are measured in the rest systems of the particles, and have been calculated from the relation $L=(P/M)T$, where P is the measured momentum and M the mass of the particle. In calculating the values of T the masses of all the particles in table 1 have been taken to be $1200m_e$. The photographs of three events listed in the table are reproduced in Plate 10 (*a* and *b*) and Plate 11 (*a*).

Table 1. Negative Heavy Particles

Event	$P(10^8$ev/c)	Ionization (I/I_0)	Mass (m_e)	Track length (cm)	Time of flight (10^{-9} sec)
P31	$1{\cdot}7 \pm 0{\cdot}2$	>8	>1100	20	2·4
JM41	$1{\cdot}6 \pm 0{\cdot}2$	>8	>1030	22	2·8
JV76	$4{\cdot}1 \pm 0{\cdot}8$	3 to 8	1230 to 3600	15	0·7
DN20	$4{\cdot}3 \pm 1{\cdot}3$	5 to 10	1580 to 4600	14	0·7
KD79	$1{\cdot}9 \pm 0{\cdot}2$	3 to 7	630 to 1400	28	3·0
JC3	$2{\cdot}3 \pm 0{\cdot}3$	3 to 8	700 to 1900	14	1·2
JY82	$5{\cdot}0 \pm 1{\cdot}5$	2 to 5	950 to 3400	20	0·8
DP22	$1{\cdot}3 \pm 0{\cdot}4$	>8	>660	13	2·1
CH19	$2{\cdot}9 \pm 0{\cdot}9$	4 to 8	910 to 2800	15	1·1
FK24	$1{\cdot}7 \pm 0{\cdot}5$	>10	>1000	14	1·7
				Total	16·5

§ 3. Discussion

Bearing in mind the size of the errors discussed above, the main features of the results shown in fig. 1 can be readily explained. Most of the tracks measured were produced by heavy positive particles. The majority of these are certainly due to protons, but deuteron and α-particle tracks probably broaden the distribution of points on the figure. The number of heavy positive mesons is discussed in § 4.

The tracks of positive and negative light particles occur in roughly equal numbers and can all be interpreted as due to π- or μ-mesons. Since they are all associated with nuclear interactions these light mesons are probably π-mesons, but this could not be deduced with certainty from our measurements.

The points in fig. 1 apparently due to heavy negative particles are the most interesting feature of the analysis. We show below that few of these points can result from errors of measurements or interpretation ; the majority represent non-decaying heavy mesons. If this is so, the measurements in table 1 can be used to give a lower limit to the mean life of the particles.

There are two possible causes of erroneous classification of tracks in this group. First, gross distortion in the cloud chamber could have resulted in a negative π-meson appearing to have a very small curvature or in a proton track having its curvature reversed and appearing to be negative. Second, and more important, a positive particle travelling towards an interaction could have been mistaken for a negative particle coming from the interaction. No imaginable error in the ionization estimates could cause any light meson to have been included among the particles listed in table 1.

The figures in table 1 allow the likelihood of gross distortion to be estimated. The probable errors in the momenta are statistical in the sense that they are derived from the known performance of the cloud chamber. In every case the measured curvature of the tracks is more than three times the probable error in curvature. Further, a distortion of more than five times this probable error would be required before a proton track of the same ionization would have the measured curvature. The distortion necessary to make a π-meson appear heavy is still greater and this source of error need not be considered. Since the total number of tracks included in our analysis is 400, it is unlikely that even one of the group in table 1 has been misinterpreted as a result of distortions.

The probability of a proton moving towards a nuclear interaction and being interpreted as a negative particle produced in the interaction can only be calculated approximately. This is because no satisfactory criterion of ‘ association ’ can be laid down which is applicable to all events. A nuclear interaction near the cloud chamber has to be located by projecting backwards the visible tracks in the chamber. The precision with which the site of the interaction can be determined depends upon its distance from the chamber, the number of secondary fast particles that cross the sensitive volume and the angular spread of these particles. In addition, when a slow particle is emitted from the interaction, its probable scattering in the material above the cloud chamber may be several degrees and its association with the interaction may be obscured.

A loose criterion of association can be used to give an upper limit to the number of spurious association among the ten events. For this purpose any track is assumed to come from a shower if it meets the chamber wall (or the lead inside the chamber) at a point less than one centimetre from the shower axis. This condition is generally less stringent than those applied to the tracks in table 1 since it ignores the direction of the track. However, event KD79 (Plate 11 (*a*)) does not satisfy the condition—magnetic deflection alone would account for the spread of the particles in this event.

Using this criterion and making the additional assumption that all heavily-ionizing particles are randomly orientated in space, the probability of a chance association between *any* single track and a *given* interaction is found to be $\sim 0{\cdot}002$. A spurious association cannot arise, however, unless more than one nuclear interaction occurs near the chamber in the same event. If n is the average number of interactions producing tracks in the chamber in each event, the geometrical probability (0·002) must be multiplied by $(n-1)$ to find the probability of a spurious association of *any* proton track with *any* nuclear interaction. The value of n is between 1·5 and 2 so that the final probability, with these assumptions, for a proton being interpreted as a heavy negative particle is $\sim 0{\cdot}002$.

Among the original 800 tracks analysed there were 600 where this misinterpretation might have occurred. Multiplying this number by the calculated probability, we find the expected number of spurious events in table 1 to be rather greater than one.

All the particles listed in table 1 are travelling downwards in the cloud chamber. A rather more refined geometrical argument based on the number of upward moving protons (84 in all) and the precision with which each of the ten nuclear interactions can be located leads to a result similar to that given above.

From these considerations it is likely that at least seven of the particles in table 1 are negatively charged and heavy (mass $> 700 m_e$). In § 4 only the total time of flight of these particles is used; this is taken to be 11×10^{-9} sec to allow for errors in interpretation. It is worth emphasizing that the particles with the longest times of flight are those whose tracks are longest and most curved. Therefore they are the most accurately measured and the least liable to misinterpretation. Thus the total time of flight has probably been under-estimated.

§ 4. The Mean Life of Charged *V*-Particles

From the discussion in § 3 we conclude that negative, non-decaying, heavy mesons have been observed for a total time of $\sim 11 \times 10^{-9}$ sec. In our earlier paper (Astbury *et al.* 1952) we reported measurements on two heavily-ionizing charged *V*-particles which decayed inside the cloud chamber. Table 2 reproduces the relevant measurements.

If we assume that all the non-decaying particles discussed above are of the same type as the decaying *V*-particles an estimate of their mean life can be made.

No positive heavy mesons have been identified directly because of the uncertainty attached to ionization estimates. It is known, however, that decaying positive and negative *V*-particles occur in nearly equal numbers (Armenteros *et al.* 1952, Astbury *et al.* 1952). The best estimate of the time for which positive non-decaying particles have been observed is therefore assumed to be 11×10^{-9} sec also.

Table 2. Slow Charged *V*-Particle Decays

Event	Track length (cm)	*P/M*	Time of flight (10^{-9} sec)
JB127	13	0·47	0·9
JK23	10	0·40	0·8

These figures refer to the primary particle before decay.
These events are events 2 and 3 in table 4 given in Astbury *et al.* (1952).

Combining this figure with those in table 2 we find that slow particles of both signs have been observed for a total time of 24×10^{-9} sec. During this time two particles have been observed to decay. This leads directly to an estimate of the mean life $\tau\sim12\times10^{-9}$ sec. The statistical error in this estimate is very large but, if the mean life were as short as 4×10^{-9} sec, the probability of our observing as few as two decays would be less than 10%.

It is possible that the decaying and non-decaying particles are not all of the same type. Three distinct types of heavy charged meson have been identified in the photographic emulsion. These are the κ-, χ-, and τ-mesons, all of which have masses between $950m_e$ and $1500m_e$. These mesons decay according to the following schemes (Powell 1952):

$$\kappa^{\pm}\rightarrow\mu^{\pm}+2 \text{ neutrals},$$

$$\chi^{\pm}\rightarrow\pi^{\pm}+1 \text{ neutral},$$

$$\tau^{\pm}\rightarrow\pi^{\pm}+\pi^{+}+\pi^{-}.$$

The ζ-meson is excluded from the discussion because its mass (500 to $570m_e$) is outside the mass limits for any of the particles in table 1.

The non-decaying heavy mesons could, from our measurements, be identified with any of the three types listed above. The decaying *V*-particles cannot, from their mode of decay, be τ-mesons but could be κ-mesons, χ-mesons or a mixture of the two. If there were no information about the relative abundance of the three different types of meson, we could only conclude that at least one type must have a mean life of the order of 10^{-8} sec to account for our non-decaying particles. However, if a large fraction of these particles were τ-mesons, it would imply that τ-mesons had a long mean life (since none are observed to decay) and that they were abundant. If this were so, they would be expected to decay at rest in the photographic emulsion relatively frequently. What evidence there is (Menon 1951) suggests that this is not so; τ-meson decays appear to be much less frequent than those of other heavy mesons. It follows that most of our non-decaying particles are probably κ- or χ-mesons, and that at least one of these mesons must have a mean life greater than 4×10^{-9} sec.

§ 5. THE MEAN LIFE OF π-MESONS

For interest, the same method of analysis has been used to estimate the mean life of the π-meson. Thirty-three tracks due to slow, light mesons of both signs were identified among the original 800 tracks. The sum of the observed times of flight of these particles is $5{\cdot}3 \times 10^{-8}$ sec and three examples of $\pi \rightarrow \mu$ decay can be identified. The assumption that all the light mesons are π-mesons leads to a most probable mean life of $1{\cdot}8 \times 10^{-8}$ sec. This result is in good agreement with the accepted value of $2{\cdot}5 \times 10^{-8}$ sec.

§ 6. CONCLUSIONS

An analysis of 800 tracks due to slow particles has shown the presence of a small group due to heavy negative mesons which cross the cloud chamber without decaying. The total time of flight of these mesons is about 10^{-8} sec. Assuming that similar positive particles are equally numerous, it can be concluded that at least one type of heavy meson has a mean life of the order of 10^{-8} sec. It is most probable that the mesons observed are the κ- or χ-mesons which have been identified in the photographic emulsion. Whether the charged V-particles are κ- or χ-mesons or a mixture of the two remains uncertain.

ACKNOWLEDGMENTS

Our work has received generous financial support from the Department of Scientific and Industrial Research, which has also given maintenance grants to J. S. Buchanan, P. Chippindale and D. I. Page. A. B. Sahiar and A. Rytz have received fellowships from the Indian Atomic Energy Commission and the Jungfraujoch Research Foundation respectively. We are very grateful to the Foundation for their considerate hospitality and to Herr H. Wiederkehr, the curator of the station, for the invaluable help which he has given us.

We have had the benefit of many useful discussions with Professor J. G. Wilson and with our colleagues at Manchester. We thank Professor P. M. S. Blackett for the facilities he has provided for us, and for the time which he has devoted to the direction of our work.

REFERENCES

ARMENTEROS, R., BARKER, K. H., BUTLER, C. C., CACHON, A., and YORK, C. M., 1952, *Phil. Mag.*, **43**, 597.

ASTBURY, J. P., CHIPPINDALE, P., MILLAR, D. D., NEWTH, J. A., PAGE, D. I., RYTZ, A., and SAHIAR, A. B., 1952, *Phil. Mag.*, **43**, 1283.

MENON, M. G. K., 1951, *Report of Bristol Conference*, December 1951.

POWELL, C. F., 1952, *Report of Copenhagen Conference*, June 1952.

XXVII. *On the Statistical Estimation of Mean Life-times*

By M. S. Bartlett
University of Manchester*

[Received January 1, 1953]

Abstract

Statistical methods of estimation of the mean life-times of unstable particles from cloud chamber photographs are discussed (i) for decaying particles only, (ii) when non-decaying particles can be recognized.

Some discussion is also given of the effect of momentum errors, and of estimation and discrimination problems for mixtures of particles.

§ 1. Introductory Remarks

In view of recent interest (see, for example, references at end of paper) in estimating the mean life-times of unstable particles from cloud chamber photographs, some notes on purely statistical aspects of this estimation problem are recorded below. They were initially stimulated by conversations with research physicists at Manchester and it is hoped will be of use to other workers confronted with this type of statistical problem.

It is well-known that there are many difficulties (see Wilson and Butler 1952) in isolating unambiguous and accurate observations from the photographic material, quite apart from the usually sparse total amount of statistical information on the true mean life-times contained in such observations even if extracted free from error. The main purpose of these notes is, however, to discuss the estimation problem after the observations have been extracted, although a few remarks have been included (§ 3) on the effect of errors in the assessment of the momenta of the particles. How far some of the more ‘ precise ’ methods of estimation (more precise in the sense of relying on fewer approximations) will be justified on particular data will of course depend partly on the latter's overall reliability, but it will be shown that the more precise methods are not much more complicated (and sometimes simpler) than the more usual ones available in the case of larger samples of data, and are much less liable to mislead. Some brief comments on the possibility of discrimination and estimation in the case of mixtures of more than one type of particle are also added.

§ 2. One Type of Particle, with no Record of Undecayed Particles

We consider first the case of n observations for one type of particle, the time to decay from the (effective) edge of the chamber being, after conversion from the corresponding measured length, denoted by t_r for

---

* Communicated by the Author.

the rth observation. The associated total time available for decay is denoted by T_r. The variation of T_r from one observation to another slightly complicates the estimation problem; otherwise this is similar to one discussed many years ago in connection with problems of artificial radioactivity (see, for example, Peierls 1935, Bartlett 1936). For completeness, however, the maximum likelihood equation of estimation is summarized, especially as its use in this context calls for special comment and extension.

The life-time probability distribution for all the particles is

$$\prod_{r=1}^{n} f(t_r)\,dt_r = \prod_{r=1}^{n} \frac{e^{-t_r/\theta}\,dt_r/\theta}{1-e^{-T_r/\theta}}, \qquad (0 \leqslant t_r \leqslant T_r), \quad . \quad . \quad . \quad (1)$$

given that $t_r \leqslant T_r$, where θ is the unknown mean life-time, or equivalently, $\lambda = 1/\theta$ is the average rate of decay. It should be noticed that t_r may be measured from any previously chosen zero, provided T_r is also (thus permitting a choice of origin which avoids, as far as possible, edge effects in the chamber). From (1), we obtain the estimation equation

$$\sum_{r=1}^{n} \frac{\partial L_r}{\partial \theta} \equiv \frac{1}{\theta} \sum_{r=1}^{n} (u_r - 1 + U_r Q_r / P_r) = 0, \quad . \quad . \quad . \quad . \quad (2)$$

where $L_r \equiv \log f(t_r)$, $u_r \equiv t_r/\theta$, $U_r \equiv T_r/\theta$, and $P_r = 1 - Q_r$ is the chance of decay $1 - e^{-U_r}$ in the time interval $(0, T_r)$. Equation (2) may be solved by iteration or interpolation; the latter method is recommended in conjunction with the further extensions below, and its use will be illustrated presently.

The 'information function'

$$\sum_{r=1}^{n} E\left(-\frac{\partial^2 L_r}{\partial \theta^2}\right) = \frac{1}{\theta^2} \sum_{r=1}^{n} \left(1 - \frac{U_r{}^2 Q_r}{P_r{}^2}\right) = \frac{1}{\theta^2} \sum_{r=1}^{n} (I_1)_r, \quad . \quad . \quad (3)$$

say, where E denotes statistical averaging, in this case over the probability distribution (1), is best known as providing the reciprocal of the asymptotic error variance in large samples of the estimate $\hat{\theta}$ from eqn. (2), but it is also important in providing the *exact* variance of $\Sigma \partial L_r / \partial \theta$ in (2), whose true mean value $\Sigma E(\partial L_r / \partial \theta)$ is moreover exactly zero.

There are two limitations in the use of (3) to provide a standard error for $\hat{\theta}$: firstly, it is an approximation valid only for small standard errors, and secondly, it depends on the unknown quantity θ. The dependence of (3) is mainly on $1/\theta^2$ for large U_r; $\log \hat{\theta}$ will have an asymptotic error variance obtained from the same expression (3) with the $1/\theta^2$ removed, and thus under such conditions the second limitation can be largely removed by working on the $\log \theta$ scale. However, in most cases the U_r are not large, and even this change of scale may be inadequate.

An alternative method of indicating the statistical accuracy of $\hat{\theta}$ is to give a 'confidence interval' for θ, which assigns statistical limits to θ such that the chance of θ being outside these limits is equal to some chosen value 0·05, 0·10, etc. It is hardly practicable in the present context to obtain these limits exactly; it is, however, quite possible to obtain much more valid limits than indicated by the crude standard error of $\hat{\theta}$. We may consider directly the standardized quantity

$$S(\theta)\equiv\sum_{r=1}^{n}\left(u_r-1+\frac{U_rQ_r}{P_r}\right)\Big/\sqrt{\sum_{r=1}^{n}(I_1)_r}, \quad . \; . \; . \; . \; (4)$$

which has zero mean and unit variance. The only approximation now involved is to treat $S(\theta)$ as normal (Gaussian), so that from a graph of $S(\theta)$ against θ the confidence limits corresponding to any probability level may be read off by equating $S(\theta)$ to the associated value μ. Thus for $P=0{\cdot}05$ (sum of *both* distribution 'tails') $\mu=\pm1{\cdot}96$, for $P=0{\cdot}05$ (one tail only, or $0{\cdot}10$ for both tails), $\mu=1{\cdot}645$, etc.

An interesting feature of $S(\theta)$ is that its value as $\lambda\equiv1/\theta\to0$ is

$$\frac{\Sigma(t_r-\frac{1}{2}T_r)}{\sqrt{(\Sigma T_r^2/12)}}+\frac{1}{\theta}\sqrt{\left(\frac{\Sigma T_r^2}{12}\right)}+O\left(\frac{1}{\theta^2}\right). \quad . \; . \; . \; . \; (5)$$

Workers in this field have realized that unless $\Sigma t_r<\frac{1}{2}\Sigma T_r$ no finite estimate $\hat{\theta}$ is possible, but (5) provides a rapid method of making more 'precise' statements about θ in other conditions for which $\theta=\infty$ is a possible value. From it we see that *in the neighbourhood of* $1/\theta=0$ the use of $S(\theta)$ (which is invariant to any change of scale for θ) is approximately equivalent to the estimate

$$\frac{1}{\theta}\sim\frac{\Sigma(t_r-\frac{1}{2}T_r)}{\Sigma T_r^2/12}, \text{ with standard error } \frac{1}{\sqrt{\Sigma T_r^2/12}}. \quad . \; . \; (6)$$

The use of the $1/\theta$ scale is also most convenient with the more exact eqn. (4), as in addition to $1/\theta=0$, values of $S(\theta)$ may be computed for convenient values of $1/\theta$ such as $1/\theta=0{\cdot}1$, $0{\cdot}2$, etc. To facilitate this computation a table of the quantities

$$1-UQ/P, \qquad I_1\equiv1-U^2Q/P$$

has been prepared (table 1).

Finally, it is noted that the remaining approximation, that $S(\theta)$ is normal, may be improved if desired (for further theoretical details, see Bartlett 1953). Thus the sampling distribution of $S(\theta)$ always has a positive skewness, and if this is corrected, the resulting quantity will be more nearly normal. A general formula for the third moment $E\{(\partial L_r/\partial\theta)^3\}$ of $\partial L_r/\partial\theta$ is

$$2E\left(\frac{\partial^3L_r}{\partial\theta^3}\right)+3\frac{\partial}{\partial\theta}E\left(-\frac{\partial^2L_r}{\partial\theta^2}\right), \quad . \; . \; . \; . \; . \; . \; (7)$$

whence in this case we find

$$(\kappa_3)_r\equiv E\left\{\left(\frac{\partial L_r}{\partial\theta}\right)^3\right\}=\frac{1}{\theta^3}\left\{2-\frac{U_r^3Q_r(1+Q_r)}{P_r^3}\right\}. \quad . \; . \; . \; . \; (8)$$

In place of $S(\theta)$ in (4), we may as a refinement when calculating confidence limits for θ, use the amended quantity

$$S-\tfrac{1}{6}\gamma(S^2-1), \quad . \; . \; . \; . \; . \; . \; . \; . \; . \; (9)$$

Table 1

U	$P(=I_2)$	$1-UQ/P$	I_1	$[\kappa_3]_1$	$[\kappa_3]_2$
0·0	0	0	0	0	0
0·1	0·0952	0·0492	0·0008	0·000	−0·081
0·2	0·1813	0·0967	0·0033	0·000	−0·129
0·3	0·2592	0·1425	0·0075	0·000	−0·148
0·4	0·3297	0·1867	0·0132	0·000	−0·145
0·5	0·3935	0·2293	0·0206	0·001	−0·123
0·6	0·4512	0·2702	0·0295	0·001	−0·085
0·7	0·5034	0·3095	0·0399	0·002	−0·036
0·8	0·5507	0·3472	0·0517	0·003	0·023
0·9	0·5934	0·3834	0·0649	0·005	0·089
1·0	0·6321	0·4180	0·0793	0·008	0·161
1·1	0·6671	0·4511	0·0950	0·011	0·236
1·2	0·6988	0·4828	0·1118	0·015	0·313
1·3	0·7275	0·5130	0·1297	0·021	0·392
1·4	0·7534	0·5418	0·1485	0·028	0·471
1·5	0·7769	0·5692	0·1682	0·035	0·550
1·6	0·7981	0·5952	0·1886	0·045	0·627
1·7	0·8173	0·6200	0·2097	0·056	0·703
1·8	0·8347	0·6435	0·2313	0·068	0·777
1·9	0·8504	0·6658	0·2534	0·083	0·848
2·0	0·8647	0·6870	0·2759	0·099	0·917
2·1	0·8775	0·7070	0·2987	0·116	0·984
2·2	0·8892	0·7259	0·3217	0·136	1·047
2·3	0·8997	0·7437	0·3448	0·157	1·108
2·4	0·9093	0·7606	0·3680	0·181	1·165
2·5	0·9179	0·7764	0·3911	0·206	1·220
2·6	0·9257	0·7914	0·4141	0·232	1·272
2·7	0·9328	0·8055	0·4369	0·261	1·321
2·8	0·9392	0·8187	0·4595	0·291	1·368
2·9	0·9450	0·8311	0·4818	0·322	1·411
3·0	0·9502	0·8428	0·5037	0·355	1·452
3·1	0·9550	0·8538	0·5253	0·389	1·491
3·2	0·9592	0·8640	0·5464	0·425	1·527
3·3	0·9631	0·8736	0·5670	0·462	1·561
3·4	0·9666	0·8826	0·5871	0·499	1·593
3·5	0·9698	0·8910	0·6067	0·538	1·623
3·6	0·9727	0·8989	0·6257	0·577	1·650
3·7	0·9753	0·9062	0·6442	0·617	1·676
3·8	0·9776	0·9130	0·6620	0·657	1·700
3·9	0·9798	0·9194	0·6793	0·697	1·723

Table 1 (*cont.*)

U	$P(=I_2)$	$1-UQ/P$	I_1	$[\kappa_3]_1$	$[\kappa_3]_2$
4·0	0·9817	0·9254	0·6959	0·738	1·744
4·1	0·9834	0·9309	0·7119	0·779	1·763
4·2	0·9850	0·9361	0·7274	0·820	1·781
4·3	0·9864	0·9409	0·7422	0·861	1·798
4·4	0·9877	0·9453	0·7564	0·901	1·813
4·5	0·9889	0·9494	0·7700	0·942	1·828
4·6	0·9899	0·9533	0·7830	0·981	1·841
4·7	0·9909	0·9569	0·7954	1·021	1·854
4·8	0·9918	0·9602	0·8072	1·059	1·865
4·9	0·9926	0·9632	0·8185	1·097	1·876
5·0	0·9933	0·9661	0·8293	1·135	1·885
5·1	0·9939	0·9687	0·8395	1·171	1·895
5·2	0·9945	0·9712	0·8492	1·207	1·903
5·3	0·9950	0·9734	0·8584	1·242	1·911
5·4	0·9955	0·9755	0·8671	1·276	1·918
5·5	0·9959	0·9774	0·8754	1·309	1·924
5·6	0·9963	0·9792	0·8832	1·341	1·930
5·7	0·9967	0·9809	0·8906	1·372	1·936
5·8	0·9970	0·9824	0·8975	1·402	1·941
5·9	0·9973	0·9838	0·9041	1·431	1·946
6·0	0·9975	0·9851	0·9103	1·459	1·950
6·1	0·9978	0·9863	0·9162	1·486	1·954
6·2	0·9980	0·9874	0·9217	1·512	1·958
6·3	0·9982	0·9884	0·9268	1·537	1·962
6·4	0·9983	0·9893	0·9317	1·562	1·965
6·5	0·9985	0·9902	0·9363	1·585	1·968
6·6	0·9986	0·9910	0·9406	1·607	1·970
6·7	0·9988	0·9917	0·9446	1·628	1·973
6·8	0·9989	0·9924	0·9484	1·648	1·975
6·9	0·9990	0·9930	0·9519	1·668	1·977
7·0	0·9991	0·9936	0·9552	1·686	1·979
7·1	0·9992	0·9941	0·9583	1·704	1·981
7·2	0·9993	0·9946	0·9612	1·721	1·982
7·3	0·9993	0·9951	0·9640	1·736	1·984
7·4	0·9994	0·9955	0·9665	1·752	1·985
7·5	0·9994	0·9958	0·9689	1·766	1·986
7·6	0·9995	0·9962	0·9711	1·780	1·988
7·7	0·9995	0·9965	0·9731	1·793	1·989
7·8	0·9996	0·9968	0·9751	1·805	1·990
7·9	0·9996	0·9971	0·9768	1·817	1·990
8·0	0·9997	0·9973	0·9785	1·828	1·991

where the skewness coefficient γ is given by

$$\gamma = \sum_{r=1}^{n} \theta^3(\kappa_3)_r \bigg/ \left[\sum_{r=1}^{n} (I_1)_r\right]^{3/2}. \qquad (10)$$

To facilitate the computation of γ, the values of the dimensionless quantity

$$\theta^3\kappa_3 = 2 - U^3Q(1+Q)/P^3$$

are also tabulated in table 1 (as $[\kappa_3]_1$, $[\kappa_3]_2$ being defined in § 4). To the same order of approximation, since $S = \pm\mu$ to the first approximation, the equation for the limits may be alternatively written

$$S - \tfrac{1}{6}\gamma(\mu^2 - 1) = \pm\mu. \qquad (11)$$

The expression (9) has the advantage of being available for any μ; (11) has the advantage that if interpolation for S is approximately linear, e.g. on the $1/\theta$ scale, the left-hand side of (11) will probably be rather more so than (9).

To illustrate the use of these various methods, the data of Fretter *et al.* (1953) on neutral V-particles have been used. These authors give for their second type of particle $V_2{}^0$ an estimated mean life-time of $4 \pm 3 \times 10^{-10}$ sec (based on eleven observations), their estimation being in effect based on the eqns. (2) and (3) above. We find, however, from the crude but simple method (6) that

$$\frac{1}{\theta} \sim 0{\cdot}21 \pm 0{\cdot}15 \times 10^{10}\ \text{sec}^{-1}, \qquad (12)$$

indicating that a value $1/\theta = 0$ is quite consistent with these data (a conclusion not apparent from the standard form of maximum likelihood estimate used by the authors). A more exact use of (4), using the $1/\theta$ scale, shows that interpolation on this scale is nearly linear (see fig. 1). We are therefore more justified in quoting the maximum likelihood estimate for $1/\theta$, this being $0{\cdot}256 \pm 0{\cdot}198$. Since the value of $\Sigma(t_r - \frac{1}{2}T_r)/\sqrt{(\Sigma T_r{}^2/12)}$ is only $-1{\cdot}39$, a finite upper 0·05 confidence limit for θ is not possible; for the lower 0·05 limit we obtain

$$\left[\frac{1}{\theta}\right]_{0\cdot05} \sim 0{\cdot}587 \times 10^{10}, \qquad (13)$$

(compare the approximate value $0{\cdot}582 = 0{\cdot}256 + 1{\cdot}645 \times 0{\cdot}198$). With the skewness correction (the use of both the alternative corrections (9) and (11) is shown in fig. 1), this is modified to

$$\left[\frac{1}{\theta}\right]_{0\cdot05} \sim 0{\cdot}621 \times 10^{10}. \qquad (14)$$

It may be of interest to note that the crude method (8) gives for the data on $V_1{}^0$ (23 observations, with θ estimated by Fretter *et al.* to be $10 \pm 7 \times 10^{-10}$ sec) the estimate similar to (12),

$$\frac{1}{\theta} \sim 0{\cdot}094 \pm 0{\cdot}066 \times 10^{10}\ \text{sec}^{-1}, \qquad (15)$$

again compatible with $1/\theta = 0$. With such data it is quite evident that often only lower bounds to θ can be given.

§ 3. THE EFFECT OF MOMENTUM ERRORS

One of the main sources of actual error in the measurements t_r and T_r is in the conversion factor from the corresponding length measurements d_r and D_r, say. As the conversion factor is the same for both measurements, it has been wondered whether a more accurate method of estimation might be obtainable by working as far as possible with the ratios $d_r/D_r = t_r/T_r$. This question is examined briefly here, with reference to the type of problem discussed in § 2. The nature of the momentum errors will of course differ in different circumstances, for example, with charged particles in a magnetic field more direct determinations are possible than with uncharged particles; we shall merely consider first-order effects when the error in T_r is assumed to be of the fairly general form

Fig. 1

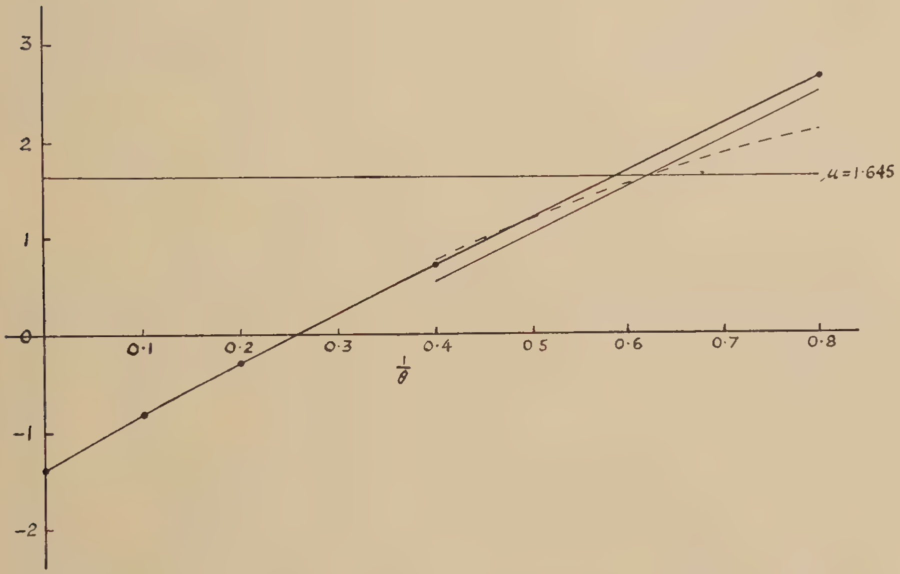

Example of $S(\theta)$ plotted against $1/\theta$ (eqn. (4); the lower continuous line corresponds to the skewness correction of eqn. (11), the dotted line to the alternative use of eqn. (9)).

$$\delta T_r = \nu T_r^{\alpha} + \epsilon T_r^{\beta}, \qquad (16)$$

where the first component is a bias or systematic error, and ϵ in the second component is purely random with mean zero and variance σ_{ϵ}^2.

In the eqn. (2), we see that each $\partial L_r/\partial\theta$ is weighted equally in the complete equation. The use of t_r/T_r in place of t_r will still permit (in the absence of momentum errors) an asymptotically unbiased estimate of θ if we write alternatively, corresponding to weights $1/T_r$,

$$\frac{1}{\theta}\sum_{r=1}^{n}\left[\frac{u_r-1}{U_r}+\frac{Q_r}{P_r}\right]=0. \qquad (2\,a)$$

We denote the expression to the left of eqn. (2) by A and the corresponding expression in (2 *a*) by B. Then we find

$$\delta A \sim \sum_{r=1}^{n} \left(\frac{u_r}{U_r} + \frac{Q_r}{P_r} - \frac{U_r Q_r}{P_r^2} \right) \delta U_r ,$$

$$\delta B \sim \frac{1}{\theta} \sum_{r=1}^{n} \left(\frac{1}{U_r^2} - \frac{Q_r}{P_r^2} \right) \delta U_r .$$

Consider first the resulting bias in the estimate of θ. Since

$$E(\delta A) = \sum_{r=1}^{n} \nu T_r^{\alpha-1} (I_1)_r ,$$

$$E(\delta B) = \sum_{r=1}^{n} \nu T_r^{\alpha-2} (I_1)_r ,$$

we find that the *proportionate* bias in our estimate of θ (or to the same order, of $1/\theta$, etc.) is $\nu \Sigma T_r^{\alpha-1}(I_1)_r / \Sigma (I_1)_r$ for $\hat{\theta}$ and $\nu \Sigma T_r^{\alpha-2}(I_1)_r / \Sigma[(I_1)_r/T_r]$ for the estimate obtained from (2 *a*). If we put $\alpha=1$, this gives the trivial but correct answer ν in both cases, for all measurements are then wrongly scaled and the final estimate must also be. A more relevant assumption in many cases is that $\alpha=0$. This corresponds to the approximate relations

$$T_r \propto d_r/p_r, \qquad \delta p_r \propto p_r^2,$$

where p_r is the estimated momentum and δp_r its error, the second relation $\delta p_r \propto p_r^2$ being probably representative at least of the errors in momentum determinations from the track curvatures of charged particles. In such situations we should have $\alpha=\beta=0$. This gives biases by the two methods of

$$\frac{\nu \Sigma T_r^{-1}(I_1)_r}{\Sigma (I_1)_r}, \qquad \frac{\nu \Sigma T_r^{-2}(I_1)_r}{\Sigma T_r^{-1}(I_1)_r}. \quad . \quad . \quad . \quad . \quad . \quad (17)$$

By Schwarz's inequality, the first is always less than the second, so that eqn. (2 *a*) appears in this respect at least to be inferior to (2). For example, if we consider the same range of T_r as in the sample of eleven observations referred to in § 2, we obtain biases $0{\cdot}136\nu$, $0{\cdot}249\nu$ respectively.

In the case of the random error component, the position is not quite so clear-cut. The total error variance of our estimate will be made up of two parts, one due to the smallness of the sample and the other to the random momentum errors. By the usual approximate methods of evaluating these errors we find for the overall error variances of our two estimates

$$\frac{\Sigma (I_1)_r + \sigma^2(\delta A)}{[\Sigma (I_1)_r]^2}, \qquad \frac{\Sigma T_r^{-2}(I_1)_r + \sigma^2(\delta B)}{[\Sigma T_r^{-1}(I_1)_r]^2}, \quad . \quad . \quad . \quad (18)$$

where

$$\sigma^2(\delta A) \sim \sigma_\epsilon^2 \Sigma T_r^{2\beta-2}[(I_1)(I_1+1)]_r ,$$

$$\sigma^2(\delta B) \sim \sigma_\epsilon^2 \Sigma T_r^{2\beta-4}[I_1^2]_r .$$

When σ_ϵ^2 is zero, the second method is of course inferior to the use of the maximum likelihood equation. For non-zero σ_ϵ^2, however, it is possible that in some cases the second overall error variance would be less than the first, though this seems rather unlikely. For instance, for the range of T_r in our previous example and $\beta=0$, we obtain as our two approximate error variances

$$0{\cdot}629(1+0{\cdot}0375\,\sigma_\varepsilon^2), \qquad 0{\cdot}629(1{\cdot}83+0{\cdot}00935\,\sigma_\varepsilon^2),$$

where 10^{-10} sec is our unit time interval. The second error variance is only less than the first if $\sigma_\varepsilon>5\frac{1}{2}$, which for T_r ranging from 1 to 20 represents a very large random error.

§ 4. ONE TYPE OF PARTICLE, WITH A RECORD OF UNDECAYED PARTICLES

It may sometimes be possible to take into account tracks of charged particles which have not decayed. For such data we thus assume particles $1 \ldots n$ as before, with $n+1 \ldots N$ further undecayed particles. As the probability for the sth undecayed particles is $Q_s=\mathrm{e}^{-T_s/\theta}$, and the probability for the rth decaying particle with decay in the range t_r, t_r+dt_r is $\mathrm{e}^{-t_r/\theta}\,dt_r/\theta$, we now have for the total data a probability p such that

$$\frac{\partial \log p}{\partial\theta}=-\frac{n}{\theta}+\frac{1}{\theta^2}\left[\sum_{r=1}^{n} t_r+\sum_{s=n+1}^{N} T_s\right], \quad . \quad . \quad . \quad . \quad . \quad (19)$$

so that the maximum likelihood estimate now becomes

$$\hat{\theta}=\frac{1}{n}\left[\sum_{r=1}^{n} t_r+\sum_{s=n+1}^{N} T_s\right]. \quad . \quad . \quad . \quad . \quad . \quad . \quad (20)$$

It may at first sight appear a little surprising that this estimate is simpler than that for decayed particles only, but it will be seen that the more complete records permit a direct estimate of the mean life-time to be made (cf. Astbury *et al.* 1953). The information function corresponding to (19) and (20) is

$$\frac{1}{\theta^2}\sum_{q=1}^{N}(1-\mathrm{e}^{-U_q/\theta})=\frac{1}{\theta^2}\sum_{q=1}^{N} P_q=\frac{1}{\theta^2}\sum_{q=1}^{N}(I_2)_q, \quad . \quad . \quad . \quad (21)$$

say.

A graph of $P=I_2$, the information (apart from the factor $1/\theta^2$) per particle, is plotted against U in fig. 2; it represents the fraction of the information $1/\theta^2$ available per particle in a chamber of unlimited size. For comparison, the fraction PI_1, expected if undecayed particles cannot be recorded, is also shown. For small U, it will be seen that the ratio $PI_1/I_2=I_1$ is very small, so that there is then a large gain in information if the more complete records are obtainable.

From (19), we have

$$\frac{\partial \log p}{\partial\theta}=\frac{n}{\theta}\left(\frac{\hat{\theta}}{\theta}-1\right), \quad . \quad . \quad . \quad . \quad . \quad . \quad . \quad . \quad (22)$$

with mean zero and variance $\Sigma(I_2)_q$. Hence a confidence interval may be obtained, on the assumption that $\partial \log p/\partial\theta$ is approximately normal, from the equation

$$n\left(\frac{\hat{\theta}}{\theta}-1\right)\bigg/\sqrt{\sum_{q=1}^{N}(I_2)_q}=\pm\mu. \quad . \quad . \quad . \quad . \quad . \quad (23)$$

As a further approximation we might substitute within the square root the estimate n, giving confidence limits for θ of

$$\hat{\theta}/(1\pm\mu/\sqrt{n}), \quad . \quad . \quad . \quad . \quad . \quad . \quad . \quad . \quad . \quad (24)$$

though this will not be advisable if n is too small. It is interesting to notice from (24) that here also $1/\theta$ is a more useful scale to use than θ.

If a correction for skewness is required, we find from the general formula (7)

$$\sum_{q=1}^{N}(\kappa_3)_q=\frac{1}{\theta^3}\sum_{q=1}^{N}(2P_q-3Q_qU_q), \quad . \quad . \quad . \quad . \quad . \quad . \quad (25)$$

and make use of a modified equation similar to (9) or (11). The dimensionless quantity $\theta^3\kappa_3$ is tabulated in the table (as $[\kappa_3]_2$); while negative for a small range of U, it is in general positive. Of course in this type of problem n is one of the random quantities, and, being discrete, will make precise approximation impracticable for very small n.

Fig. 2

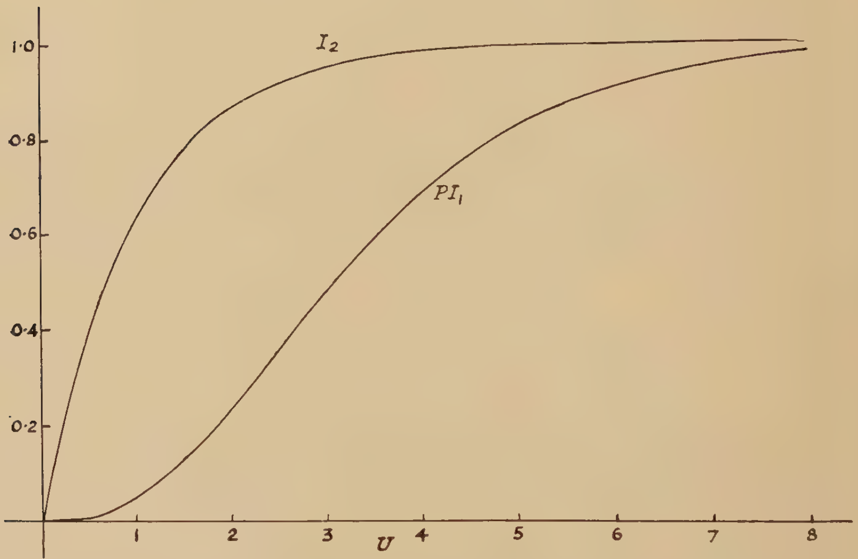

The expected information for decaying particles, and the information for all particles, expressed as ratios of the information available as $T\to\infty$.

If mixed data are available, some being of the type considered in § 2 and some of the present type, we merely add the eqns. (2) and (22), and the total information function will be the sum of the separate ones; similarly, if required, for the third moment.

§ 5. Two Types of Particle

There is no difficulty in principle in extending these methods to two types of particle in unknown proportions, but a general investigation of accuracy divorced from actual data becomes laborious and it seems preferable to proceed directly in any problem, using if necessary such approximations as

$$-\frac{\partial^2 \log p}{\partial\alpha\partial\beta} \sim E\left(-\frac{\partial^2 \log p}{\partial\alpha\partial\beta}\right) \equiv I_{\alpha\beta},$$

where p denotes the probability of the entire data. Thus for data of the type considered in § 4 we have

$$p = \Pi\{p_a p_\alpha + q_a p_\beta\}, \quad . \quad . \quad . \quad . \quad . \quad . \quad . \quad (26)$$

where $p_a = 1 - q_a$, assumed constant for all particles, is the probability that a particle is of type a with decay constant α; β is the other decay constant. (Notice that p_a can only be constant relative to the observational conditions, and will depend on α, β and the distributional origin of the particles relative to the (effective) initial boundary of the chamber.) p_α (p_β) denotes the probability of the observation given that the particle is of type a (b) and is of the mixed type given in § 4 (i.e. it is an infinitesimal probability only if decay occurs, in which case the infinitesimal element dt_r is dropped). Π denotes multiplication over all particles, the distinguishing suffices for which have for convenience been omitted. The maximum likelihood equations for p_a, α and β are

$$\left.\begin{aligned} \frac{\partial \log p}{\partial p_a} &= \Sigma \frac{p_\alpha - p_\beta}{p_a p_\alpha + q_a p_\beta} = 0, \\ \frac{\partial \log p}{\partial \alpha} &= \Sigma \frac{p_a p_\alpha}{p_a p_\alpha + q_a p_\beta} \frac{\partial \log p_\alpha}{\partial \alpha} = 0, \\ \frac{\partial \log p}{\partial \beta} &= \Sigma \frac{q_a p_\beta}{p_a p_\alpha + q_a p_\beta} \frac{\partial \log p_\beta}{\partial \beta} = 0, \end{aligned}\right\} \quad . \quad . \quad . \quad (27)$$

where $\partial \log p_\alpha/\partial\alpha$, $\partial \log p_\beta/\partial\beta$ are as in eqn. (19). The approximate standard error of any estimate is the square root of the corresponding diagonal term in the *inverse* of the matrix of terms $I_{\alpha\beta}$, $I_{\alpha\alpha}$, etc. with respect to the *three* unknowns α, β and p_a (see, for example, Kendall 1946, ch. 17). It is likely to be large in most cases, unless the data are very extensive.

In the particular case where one decay constant, say β, becomes large, a simpler procedure becomes available. The chance of decay in the chamber of the second type of particle is now negligible, so that (unless p_a is nearly zero) the problem reduces to the estimation of α by the method of § 1, and then the estimate of p_a from a knowledge of the chance of decay P_r for each of these particles, the ratio of decayed to undecayed particles being equated to

$$p_a \sum_{q=1}^{N} P_q \Big/ \left(p_a \sum_{q=1}^{N} Q_q + N q_a\right). \quad . \quad . \quad . \quad . \quad . \quad (28)$$

In the case where only decayed particles are available, the form of eqns. (27) is modified, because the chance of such a *decayed* particle being of type a is no longer p_a, but

$$p_a' = p_a P_r(\alpha)/[p_a P_r(\alpha) + q_a P_r(\beta)], \quad . \quad . \quad . \quad . \quad . \quad (29)$$

depending in a *variable* way on α and β. Equation (26) now holds with p_a' in place of p_a, $f(t_r; \alpha)$, defined as in eqn. (1), for p_α and $f(t_r; \beta)$ for

p_β.* In the particular case where β is large, we must assume that p_a' is not near unity for typical T_r (otherwise no estimation problem involving more than one unknown occurs), and this now implies that p_a must be small. Equation (26) becomes replaced by

$$p=\Pi\{p_a'(f(t_r\,;\ \alpha)-1/T_r)+1/T_r\},$$

where

$$p_a'=\frac{p_aP_r(\alpha)}{p_a(P_r(\alpha)-T_r/\beta)+T_r/\beta}\sim\frac{\rho P_r(\alpha)}{\rho P_r(\alpha)+T_r}, \quad . \quad . \quad . \quad (30)$$

where $\rho\equiv p_a\beta$ is assumed the new unknown parameter. Hence

$$p=\Pi\{[\rho P_r(\alpha)f(t_r\,;\ \alpha)+1]/[\rho P_r(\alpha)+T_r]\},$$

or

$$\log p=\Sigma\{\log(\rho f_r+1)-\log(\rho P_r+T_r)\}, \quad . \quad . \quad . \quad . \quad (31)$$

where $f_r=(\mathrm{e}^{-t_r/\alpha})/\alpha$, $P_r=1-\mathrm{e}^{-T_r/\alpha}$.

In view of the difficulty even with only one type of particle in rejecting $\theta=\infty$ from records only of decaying particles it seems very doubtful whether for such data we should feel justified in going beyond (31) to the full equation involving three unknowns. Even with (31), unless, in spite of the further unknown ρ, we obtain an estimate of α clearly distinct from ∞, it is evident that the simpler hypothesis of only one mean life-time is adequate. In any case the interpretation needs a little care, for the assumption of β large gives a uniform distribution of decays from this type of particle over the chamber, and could be simulated by some mis-identifications or general ‘ noise ’ effect in the chamber.

From (31) we obtain the estimation equations

$$\left.\begin{aligned}\frac{\partial\log p}{\partial\rho}&=\Sigma\frac{T_rf_r-P_r}{(\rho f_r+1)(pP_r+T_r)}=0,\\ \frac{\partial\log p}{\partial\alpha}&=\frac{\rho}{\alpha}\Sigma\left\{\frac{(u_r-1)f_r}{\rho f_r+1}+\frac{U_rQ_r}{\rho P_r+T_r}\right\}=0.\end{aligned}\right\} \quad . \quad . \quad . \quad (32)$$

Instead of using maximum likelihood estimates obtained from (32) with approximate standard errors (in which case it would seem advisable to use the $1/\alpha$ scale), we could extend the method of confidence limits to give a confidence region for ρ and α simultaneously. This would consist of constructing a region of values of ρ and α such that

$$J_{\alpha\alpha}D_\alpha^2+2J_{\alpha\varrho}D_\alpha D_\varrho+J_{pp}D_\varrho^2\leqslant\chi_0^2, \quad . \quad . \quad . \quad . \quad . \quad (33)$$

where

$$\begin{pmatrix}J_{\alpha\alpha} & J_{\alpha\varrho}\\ J_{\alpha\varrho} & J_{\varrho\varrho}\end{pmatrix}=\begin{pmatrix}I_{\alpha\alpha} & I_{\alpha\varrho}\\ I_{\alpha\varrho} & I_{\alpha\alpha}\end{pmatrix}^{-1},$$

---

* Other modifications may be required in particular circumstances, depending on further relevant information from the track records. For example, $P_r(\alpha)$ may be interpreted somewhat more generally as the chance of the *observed* decay in the chamber (apart from the value of t_r), given that the particle is of type a, and similarly for $P_r(\beta)$, (in this case the later eqns. (30), (31), (32) will need reconsideration). If, further, the conversion factor depends on the type of particle, then t_r, T_r will no longer have the same values in $f(t_r\,;\ \alpha)$ and $f(t_r\,;\ \beta)$.

the suffix ρ being used in connection with the unknown ρ, $D_\alpha \equiv \partial \log p/\partial\alpha$, $D_\varrho \equiv \partial \log p/\partial\rho$, and $\chi_0{}^2$ is the critical value of a 'χ^2 quantity' with two degrees of freedom, e.g. 4·6 for the 0·10 significance level (see, for example, Fisher and Yates 1938). As the quantities D_α, D_ϱ are squared in (33), it is less necessary here to consider any skewness corrections. Of course, if this region 'explodes' with respect to large α for all ρ, the hypothesis of two distinct life-times is again hardly justified.

§ 6. DISCRIMINATION TESTS

The difficulty of separating a mixture of two types of particle implies that a complete statistical analysis is hardly worth while unless the data are rather extensive. In this and other cases a comparison of the fit obtained by two different hypotheses may often be useful, and this is usually more conveniently performed on the L functions (log. probabilities) directly rather than on their derivatives or on the estimated constants. Thus let $L = \log p$ be the probability of (26) (with any infinitesimal elements omitted), and $L' = \log p'$ the probability on the hypothesis that only one type of particle (in regard to life-times) is involved. Then we may take very approximately

$$-2(L_{\max} - L'_{\max}),$$

as a χ^2 quantity with two degrees of freedom (cf. for example, Kendall 1946, § 21.20), where the maxima are with respect to variation in the unknown constant(s). Unless we can find values of p_a, α and β to make the quantity in (34) greater than, say, 4·6 (the 0·10 significance level of χ^2 for two degrees of freedom), the more complicated hypothesis would hardly be justified. (In such a test it is essential that the most efficient estimate of the decay constant in L' be used.)

For an equation like (31), the corresponding approximate χ^2 would have only one degree of freedom.

Another possible application of the χ^2 procedure is for testing the compatibility of two or more sets of data. Thus for two sets supposedly referring to one and the same type of particle we should have

$$-2([L_1]_{\max} + [L_2]_{\max} - [L_1 + L_2]_{\max}), \quad . \quad . \quad . \quad . \quad (34)$$

as a χ^2 with one degree of freedom, where L_1 and L_2 refer to the two sets of data. Subdivision of the *same* data, not involving selection of t_r, e.g. with regard to values of T_r, might also sometimes be useful for testing internal consistency.

ACKNOWLEDGMENTS

I am indebted to J. P. Astbury, J. Maddox, J. E. Moyal, and other physicists at Manchester, from conversations with whom these notes developed. I am also indebted to Mrs. A. Linnert for assistance with the computations and figures, and in particular, for the preparation of the table.

REFERENCES

ASTBURY, J. P., *et al.*, 1952, " On the Decay of Charged *V*-particles ", *Phil. Mag.* [7], **43,** 1283 ; 1953, "The Mean Life of Charged *V*-particles" *Ibid.* (in the press).

BARKER, K. H., *et al.*, 1952, " The Mean Life-time and Frequency of Production of Charged *V*-particles ", *Phil. Mag.* [7], **43,** 1201.

BARTLETT, M. S., 1936, " Statistical Information and Properties of Sufficiency ", *Proc. Roy. Soc.* A, **154,** 124 ; 1953, " Approximate Confidence Intervals ", *Biometrika* (in the press).

FISHER, R. A., and YATES, F., 1938, *Statistical Tables for Biological, Agricultural and Medical Research* (Edinburgh : Oliver and Boyd).

FRETTER, W. B., *et al.*, 1953, " A study of Neutral *V*-particles ", *Phys. Rev.* (in the press).

KENDALL, M. G., 1946, *Advanced Theory of Statistics*, Vol. 2 (London : Griffin, 1st ed.).

PEIERLS, R., 1935, " Statistical Errors in Counting Experiments ", *Proc. Roy. Soc.* A, **149,** 467.

WILSON, J. G., and BUTLER, C. C., 1952, " A Note on the Measurement of Lifetime of Unstable Particles ", *Phil. Mag.* [7], **43,** 993.

XXVIII. *The Decay in Fluorescence Efficiency of Organic Materials on Irradiation by Particles and Photons*

By F. A. Black
Department of Natural Philosophy, University of Glasgow*

[Received December 15, 1952]

Summary

Measurements have been made of the damage caused by α-particle irradiation of several materials; some results are given for electron and ultra-violet irradiation. A comparison of the fluorescence efficiency for α-particle and electron excitation for these materials is made. The implication of the results is discussed in some detail, and analysis leads to a new understanding of the abnormally low α-particle fluorescence yield in organic materials.

It is known (Birks and Black 1951) that the fluorescence efficiency of an anthracene crystal decays during the exposure of the crystal to a strong α-particle beam. Investigations extending to other materials and other forms of bombardment are described briefly below and shown to lead to a new view of the mechanism of fluorescence.

The six organic materials used were in crystalline form and had, whenever possible, freshly cleaved surfaces. Sources of ^{210}P and ^{35}S were employed to provide beams of α-particles and electrons. The decay in the fluorescence intensity during the bombardment was found directly from measurements of the output current of a photomultiplier, changes of 3% being detectable.

The variation of the fluorescent intensity L under constant excitation, with the number N of α-particles absorbed per cm^2 was found to be similar for different organic materials, being expressed over a range depending on the extent of variation in energy and direction of the α-particles striking the crystal, by the equation

$$L=(1+AN)^{-1}. \qquad (1)$$

A is a constant, characteristic of the material. Small variations in the value of A for anthracene were found when different faces of a cubic crystal were presented to the α-particle beam. This effect might have been more marked had the beam been collimated.

Some of the experimental results for α-particle bombardment are shown in fig. 1 and in the table. $E_{1/2}$ is the energy dissipation per cm^3 required to reduce the fluorescence efficiency to half its initial value. No figures are given for $CaWO_4$ or ZnS–Ag. Experiments with these materials failed to reveal any perceptible change in fluorescence for $N=4\times10^{11}$.

---

* Communicated by Professor P. I. Dee, F.R.S.

Experiments with electrons as the bombarding particles were confined to anthracene. No change in fluorescence was detected, whether measured by α-particles or electrons, during a period in which the crystal absorbed 10^{13} electrons/cm^2 of average energy 40 kv. This was equivalent to an energy dissipation near the surface of $1{\cdot}5\times10^8$ erg/cm^3. Irradiation with electrons thus appeared to have no effect upon the fluorescence comparable with that produced by α-particles.

Fig. 1

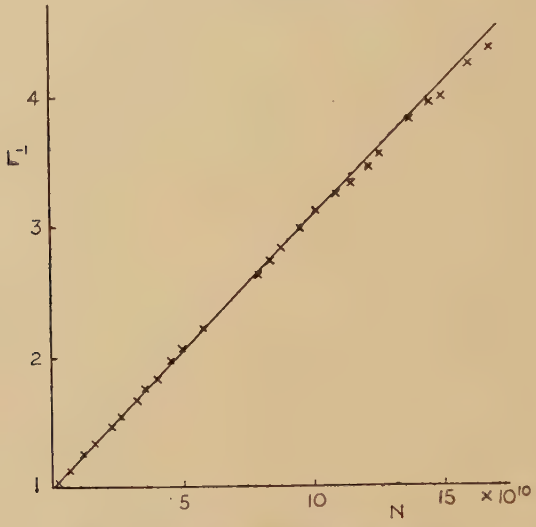

The variation of L^{-1} with N for anthracene bombarded by 3 MEV α-particles.

Relative figures for various materials were obtained for the ratio, R, of the fluorescence efficiency for excitation by 3 MEV α-particles to that for excitation by electrons of average energy 40 kv. Values of R, relative to that for anthracene, are shown in the table.

Table

	Anthracene	Naphthalene	Terphenyl	Stilbene	Pyrene	Diphenyl acetylene	ZnS–Ag powder	$CaWO_4$ crystal
$E_{1/2}\times10^{-8}$ erg/cm^3	1·3	1·7	5·5	7·0	13	32	—	—
$A\times10^{12}$	20	15	4·7	3·7	2 ?	0·8	<0·1	<0·1
R	1·0	0·9	0·8	0·8	0·5 ?	0·7	24	3·2

Irradiation by light of wavelength 3650 Å was found to reduce the fluorescence efficiencies of anthracene, naphthalene and stilbene. The values of $E_{1/2}$ in erg/cm^3 were very approximately 8×10^{11} for anthracene and less than 4×10^{10} for naphthalene. For naphthalene and stilbene the decay was only temporary and the efficiency increased again when the crystal was left unexposed. Anthracene did not recover even when heated to 100° c for some hours. The fluorescence efficiencies were measured by means of a standard weak ^{210}P source. A preliminary experiment had shown that when an extremely thin anthracene crystal is damaged by α-particles, the efficiency of the crystal for various forms of excitation (electron, light and α-particle) all decrease by approximately the same factor if this factor is small.

The relationship between L and N holding for α-particle bombardment and expressed in eqn. (1) was found for anthracene by another method by Birks and Black (1951). It also seems to hold for several inorganic phosphors according to calculations made from data given by Marsden (1910) for α-particle bombardment and by Grotheer (1939) for electron bombardment. This fact was not noted in the papers concerned.

The results for the inorganic phosphors, however, were complicated by loss in transparency of the crystal during bombardment and by a recovery of the efficiency. These effects for the organic materials were too small in most cases appreciably to affect the values of L over the ranges of N for which the experiments were conducted. Hence for the organic materials the efficiency W could be expressed, relative to its initial value by

$$W=(1+C[D])^{-1}, \quad . \quad . \quad . \quad . \quad . \quad . \quad . \quad . \quad . \quad (2)$$

where $[D]$, assumed proportional to N, is the concentration of damaged molecules in the bombardment layer and C is a constant which for anthracene cannot possibly be less than 400.

As was noted by Birks and Black (1951) this result is to be expected if some form of intramolecular energy transport occurs, the excitation energy moving through the crystal until it is converted into fluorescent light or, on meeting a damaged molecule, into heat. If the energy spends on the average a time θ on each molecule of a material of decay time τ, containing a concentration $[D]$ of damaged molecules, where one damaged molecule captures the energy with a probability k relative to that for an undamaged molecule, then the efficiency W is given by

$$W=1-k[D]\int_0^\infty \theta^{-1}y\,dt, \quad . \quad . \quad . \quad . \quad . \quad . \quad . \quad (3)$$

where y, the fraction of the energy initially created which survives for a time t, is determined by the equation

$$\frac{dy}{dt}=-y(\tau^{-1}+k\theta^{-1}[D]). \quad . \quad . \quad . \quad . \quad . \quad . \quad . \quad (4)$$

When θ is independent of t, eqn. (3) reduces immediately to eqn. (2) with $C=k\tau\theta^{-1}$.

The table reveals that the power of prolonged α-particle bombardment to produce a reduction in the fluorescence efficiency varies widely between different materials. Yet it shows also that the fluorescence efficiency for excitation by α-particles is smaller than that for excitation by β-particles by a factor which is approximately constant for all the organic materials. This suggests that the saturation of the specific fluorescence for α-particle excitation found by Birks (1950, 1951) may not be caused by those damaging or fluorescence inhibiting effects which a single α-particle produces locally and permanently and which, when caused by large numbers of α-particles, become measurable as macroscopic reductions in the fluorescence efficiency.

We are therefore forced to look for some other explanation of the abnormally low fluorescence yields of organic materials under α-particle excitation. Furst and Kallmann (1952) have suggested that in the α-particle track interaction between two neighbouring excited molecules may lead to non-radiative dissipation of the energy. It is known (Franck and Livingstone 1949) that energy can be transferred between molecules for distances of up to 60 Å. This part of the process generally described as sensitized fluorescence will be most probable when the fluorescence spectrum of the donor molecule coincides with the absorption spectrum of the acceptor. This increased probability is more readily achieved for two excited molecules than for molecules only one of which is excited.

The result of energy migration between two excited molecules is that one is reduced to its ground state while the other is raised to a higher excited state. A direct radiative transition from this state to ground does not seem to occur for anthracene (Pringsheim 1949). Instead the high excitation energy will probably lead to various photo-chemical processes such as dissociation, the net result being failure of the molecule to emit except in the infra-red. This process of double de-excitation furnishes a basis for the understanding of the behaviour of the specific fluorescence of organic materials when excited by ionizing particles.

Let an ionizing particle raise n_0 molecules per unit length into their first excited state. The number n of these excited molecules remaining in the track at a time t after the particle has passed will be given by

$$\frac{dn}{dt} = -\gamma n - \alpha n^2 - \mu n - \mu n(1-e^{-\lambda n}). \quad . \quad . \quad . \quad . \quad . \quad (5)$$

The first three terms on the right-hand side represent respectively the probabilities of fluorescence, double de-excitation and energy migration outwards from the track. Not all the energy which proceeds from the track will lead to fluorescence as a fraction of it will, before it can escape, be lost by double de-excitation with the main group of excited molecules. It can be shown that this fraction is $(1-e^{-\lambda n})$ where λ is a constant less than α. The fourth term accordingly must be included. The specific fluorescence F is then given by

$$F = \int_0^\infty \{\gamma n + \mu n - \mu n(1-e^{-\lambda n})\}\, dt. \quad . \quad . \quad . \quad . \quad . \quad (6)$$

Briefly,
$$\frac{dF}{dt} = \frac{dF}{dn_0}\frac{dn_0}{dt} = -(\gamma n_0 + \mu n_0 e^{-\lambda n_0}),$$

whence we obtain from (5) on the assumption, almost certainly true, that $\gamma \ll \mu$,

$$\frac{dF}{dn_0} = \{(2+az)e^z - 1\}^{-1}, \qquad (7)$$

where $z = \lambda n_0$ and $a = \alpha/\lambda\mu$.

Equation (7) was integrated graphically and λF as a function of z is shown in fig. 2 for various values of a. The scales were adjusted so that in each case the maximum value of λF was the same. The shape of the curve is independent of the value of a when this is less than 1. The points representing the experimental results of Taylor *et al.* (1951) for two kinds of heavily ionizing particles all lie within 20% of the curve for $a = 10$. From a figure of 5% for the efficiency of anthracene for electron excitation, n_0 can be calculated to be about 2×10^7 cm for a 5 Mev α-particle. This with $a = 10$ gives $\lambda = 7 \times 10^{-8}$ and $\alpha = 7 \times 10^{-7} \mu$. This is for anthracene. Other materials will have different values of λ and μ and consequently the shape of the F curve will vary slightly. Taylor *et al.* have shown that this is so for anthracene and stilbene.

Fig. 2

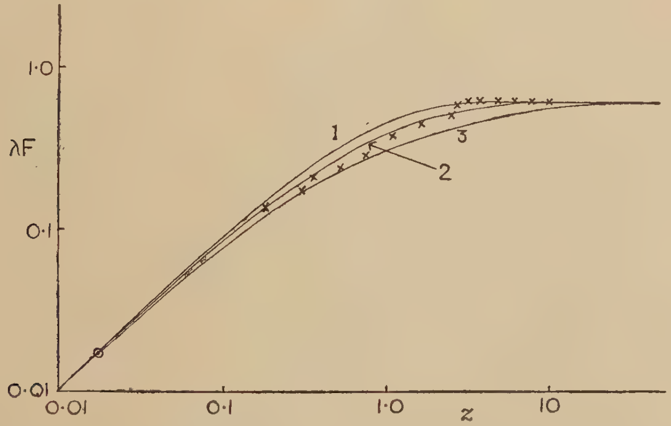

The variation of F with Z. Curve 1 : $a \leqslant 1$; curve 2 : $a = 10$; curve 3 : $a = 100$. The scale exhibited is for $a = 0$. The crosses represent data given by Taylor for two kinds of heavy ionizing particles in anthracene, on the assumption that n_0 is proportional to the specific energy loss. The circle is for electrons of 120 kv.

I am indebted to Dr. S. C. Curran for many helpful discussions on the work and to Mr. G. M. Lewis for his advice and encouragement.

References

Birks, J. B., 1950, *Proc. Phys. Soc.* A, **63,** 1294 ; 1951, *Ibid.*, **64,** 874.
Birks, J. B., and Black, F. A., 1951, *Proc. Phys. Soc.* A, **64,** 511.
Franck, J., and Livingstone, R., 1949, *Rev. Mod. Phys.*, **21,** 505.
Furst, M., and Kallmann, H., 1952, *Phys. Rev.*, **85,** 816.
Grotheer, W., 1939, *Z. Phys.*, **112,** 541.
Marsden, E., 1910, *Proc. Roy. Soc.* A, **83,** 548.
Pringsheim, P., 1949, *Fluorescence and Phosphorescence* (Interscience Publishers Inc. : New York and London).
Taylor, Jentschke, Remley, Eby and Kruger, 1951, *Phys. Rev.*, **84,** 1034.

XXIX. *Photo-Electric Determination of the Mass of the Bristol κ_1-Meson*

By Krister Kristiansson
Department of Physics, University of Lund, Sweden*

[Received October 20, 1952]

Summary

The track-density of the Bristol κ_1-meson has been determined photo-electrically. The measurements have been accurately corrected for uneven development and transparency of the emulsion. The mass has been calculated by comparison with tracks which have roughly the same slope as the meson-track and also by comparison with a proton track which crosses that of the meson. The result of the mass-determination is $m\kappa_1=1518\pm70$ electron masses.

§ 1. Introduction

A hitherto unobserved phenomenon was recorded in a nuclear research plate which the Bristol group exposed on the Jungfraujoch under 30 cm lead (O'Ceallaigh 1951). A particle whose track is reminiscent of that of a proton, as far as grain-density and scattering are concerned stops in the emulsion and decays with the production of one charged and one or more neutral particles. Small-angle scattering measurements on the track of the charged secondary give $p\beta c=250$ Mev, while the grain density is the same as that for particles at minimum ionization. These facts set an upper limit of *ca.* 400 m_e to the mass of the secondary particle, which, if it is of known type, must thus be an electron, a μ- or a π-meson.

The range of the primary in the 400 μ thick Ilford G5 emulsion employed is more than 4000 μ, long enough to allow of a satisfactory mass-determination. Two estimates made by O'Ceallaigh, the first depending on combined range and scattering measurements and the other on a combination of gap-counting and range observations, gave the results (1260 ± 290) and $(1385\pm200)\,m_e$, respectively. Though the agreement is satisfactory, it nevertheless seemed desirable to make a third estimate by photo-electric measurement of the track density.

§ 2. The Measurement of the Density

The photo-electric apparatus has been fully described by von Friesen and Kristiansson, and it has not been altered in the present work (von Friesen *et al.* 1950, 1952). All measurements were made with the same slit, its dimensions in the focal plane of the objective being $1{\cdot}98\times30$ microns. Density observations were begun 20 μ from the end of the track and continued to the point where it left the emulsion. The density at a given point on the track was taken to be the mean of the densities in two equal intervals one slit-length long, one at each side of the point, that is, the density was determined at points 30 μ apart.

---

* Communicated by Professor Sten von Friesen.

In fig. 1, where the κ_1-meson is compared with one μ-meson and three protons, the integrated density is shown as a function of the range. Particle No. 1 is especially interesting since it is a recoil particle, and hence it can be assumed with very great probability to be a proton.

Fig. 1

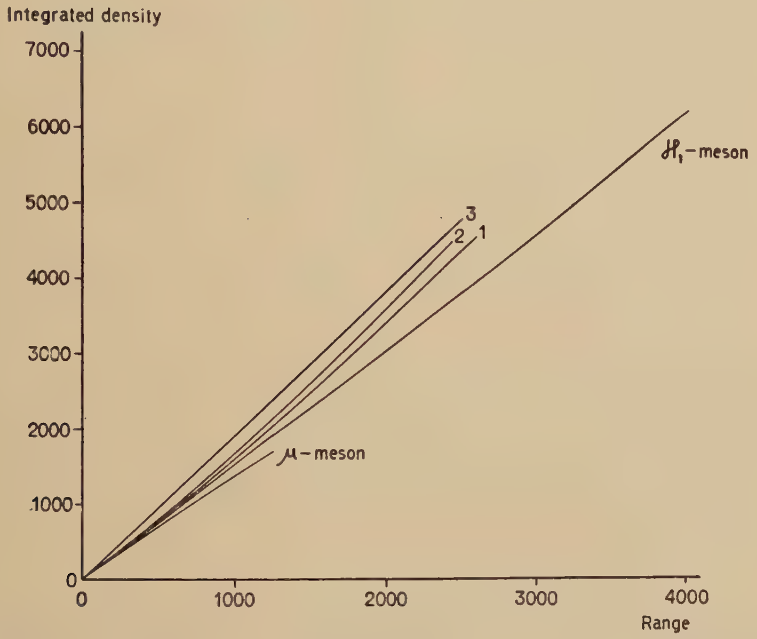

Integrated density versus residual range for the κ_1-meson, three protons and a μ-meson.

It is situated at approximately the same place as the κ_1-meson track, with which it is roughly parallel. Thus it is conveniently used as a standard of comparison in determining the κ_1-meson mass. Particles Nos. 2 and 3 are also protons, as will be shown later, and their directions are not very different from that of the κ_1-meson. Figure 2 is a vertical section through the emulsion showing the position of the particles.

When diagrams Nos. 1 and 2 are compared one sees that the values obtained for the integrated density is bigger the higher up the particle lies in the emulsion. Hence one cannot exclude the possibility that the different densities exhibited by the particles (fig. 1) depend more on the position of the particles in the emulsion than on possible differences in mass. To find out if this is the case the density was determined for a number of tracks which lie at different depths in the emulsion. In this way a correction factor has been computed for each depth, and by multiplication with this factor each density measured has been reduced to the middle depth in the emulsion.

Fig. 2

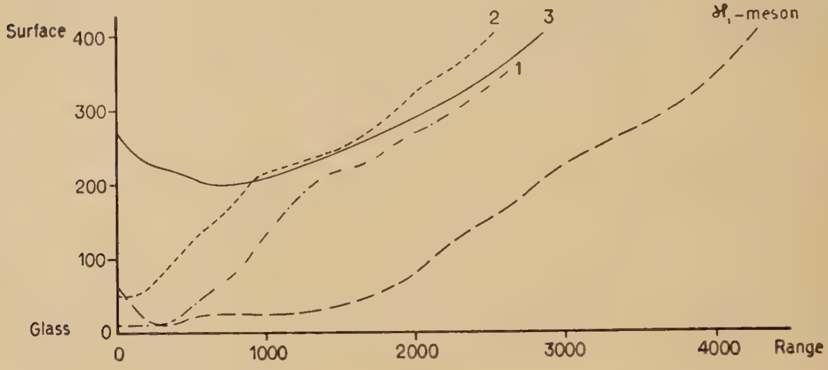

Vertical section through the emulsion showing the position of the κ_1-meson and of the three comparison protons.

§ 3. DETERMINATION OF THE DEPTH-CORRECTION FOR AN EMULSION

If particles with the same velocity and charge traverse a thick emulsion at different depths their tracks will not have the same appearance although the ionization is the same. The projected track area registered by the photo-electric apparatus is found to be a function also of the position of the track in the emulsion. This variation depends principally on three effects.

Development

It is practically impossible to produce absolutely even development throughout the whole of a thick emulsion. Irregularities are chiefly of two kinds: firstly the number of grains is variable, and secondly the average size of the developed grains can be different. Only the first factor comes into play in grain-counting, while both are of importance in photo-electric recording and gap-measurements. In the emulsion containing the κ_1-meson an additional fixing effect occurs. During the fixing process precipitated silver was dissolved, especially in the tracks nearest to the surface of the emulsion, and the area of the tracks was diminished.

Fog

Tracks which are not completely black are observed in thick emulsions. This is especially so for tracks which are situated deep in the emulsion. The effect occurs because the light is diffracted both by very small background grains formed during development and by grains in tracks which lie higher up in the emulsion. The result is that the track also appears to have a certain luminosity and light which apparently originates in the grains measured. In these circumstances the calculated track-area becomes less than the true area.

The Microscopic Effect

The microscope probably introduces an effect also. The appearance of the imaged light-beam varies somewhat with the position of the track in the emulsion because the distance between the objective and the condenser is different when tracks at different depths are studied. The effect is undoubtedly small and possibly totally negligible.

The degree of development, the fog, and the microscope effect are all functions of how deep the track lies in the emulsion and of that only. Hence the correction which will eliminate them and reduce all track-densities to a common depth must also be a function of the depth only.

Fog and the microscope-effect depend on the emulsion and the microscope, respectively, while the variation in the degree of development is directly connected with the track under investigation. It is therefore not inconceivable that the degree of development might be a function also of the track density. The total correction would then be different for tracks of different densities. I have therefore determined the correction factor for three different densities.

Protons, deuterons and tritons have been employed for the best determination of the correction factor. Their tracks have been studied in the range $R=0$ to $R=1000\,\mu$, in which interval the density can to a good approximation be considered constant and identical for all three types of particles with the degree of development used. In fig. 3 the observed densities are set out as a function of depth in the emulsion. By dividing up the emulsion into equally thick layers and calculating the average density in each, a best-fit curve for the given degree of development has been drawn. The errors indicated in the diagram are standard errors.

Eight μ–mesons have been employed in determining the development correction for less dense tracks. In these μ–meson tracks the region $R=0$ to $R=600\,\mu$ has been used in part, as has also the interval $R=600$–$1200\,\mu$, to calculate two correction curves. In these cases it is impossible to plot the points directly in the same way as before because the density varies in the interval. Instead, the correction has been found by successive approximations. Figure 4 shows the relation between density and depth for the ionization densities in question. In certain regions the corrections are less exact than the proton correction because of the smaller number of points used in determining them. (The curves are dashed in these regions.)

The calculated correction factor for the different ionization densities is given in fig. 5 as a function of depth in the emulsion. This correction factor is defined as that factor by which the measured density must be multiplied in order to reduce it to half-depth in the emulsion. One sees that there is a little difference in the correction for the different

Fig. 3

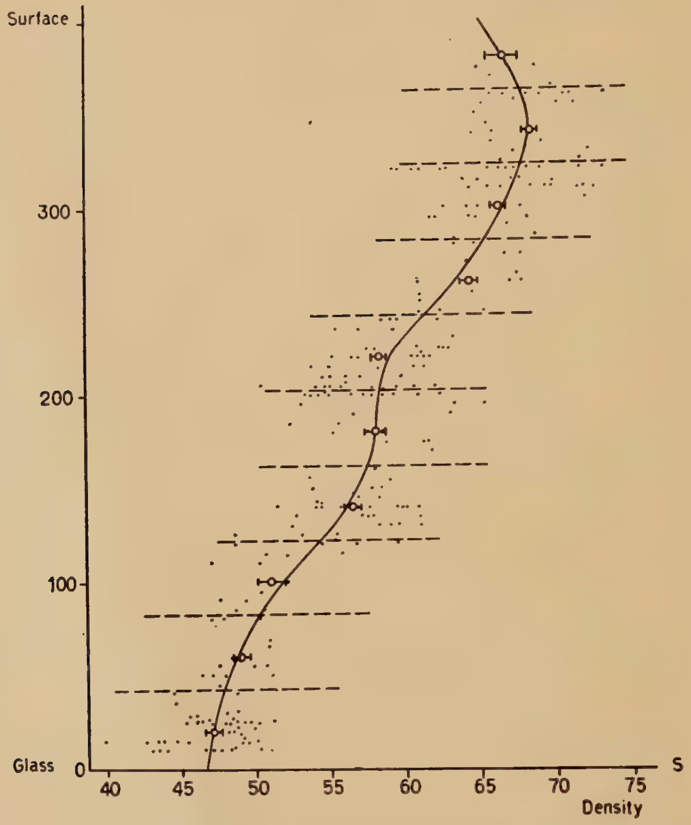

Density of proton-, deutron- and triton-tracks versus distance from the glass.

Fig. 4

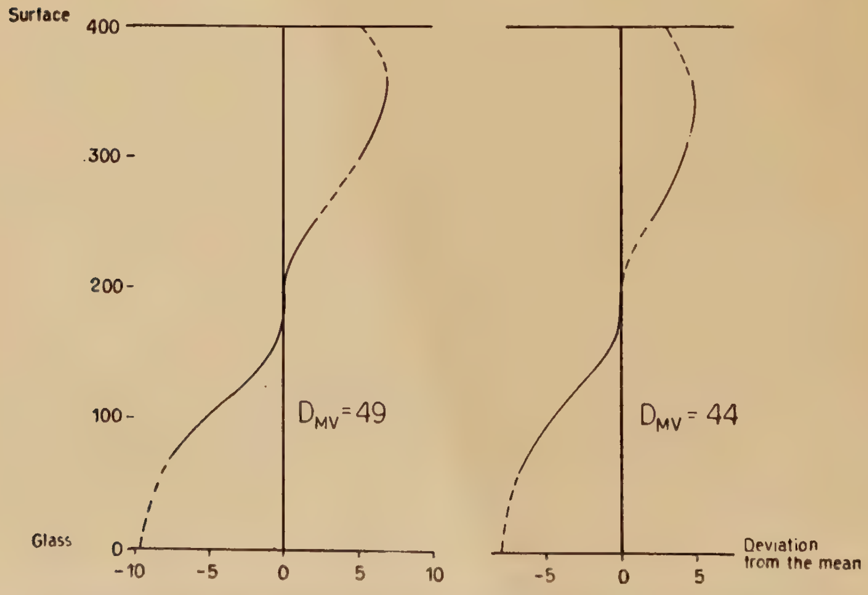

Development curves for low densities computed from μ-meson tracks.

ionization-densities. It is not possible to tell from the measurements made whether or not this difference depends on the ionization or whether its origin is purely statistical.

Fig. 5

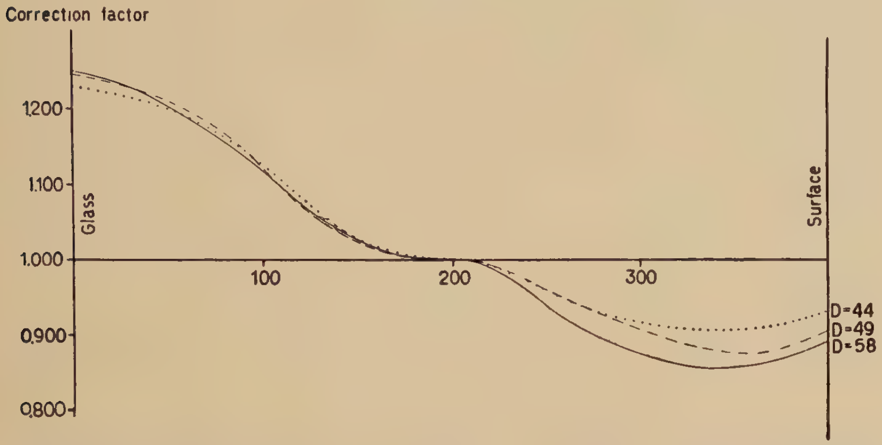

Calculated development-correction factor versus distance between track and glass.

Fig. 6

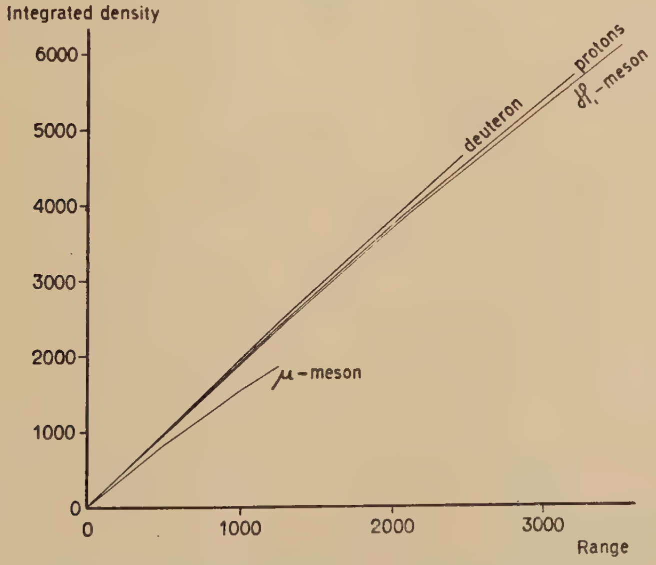

Corrected integrated density versus residual range.

All the tracks employed in determining the mass of the κ_1-meson have been reduced to the centre of the emulsion. The integrated densities, after correction, are given as a function of the range in fig. 6. This is to be compared with fig. 1, in which the density before correction is plotted. The proton-group in fig. 6 is an average derived from four protons. The separate particles lie so close together that it is not possible to resolve the individual particles in the diagram.

Fig. 7

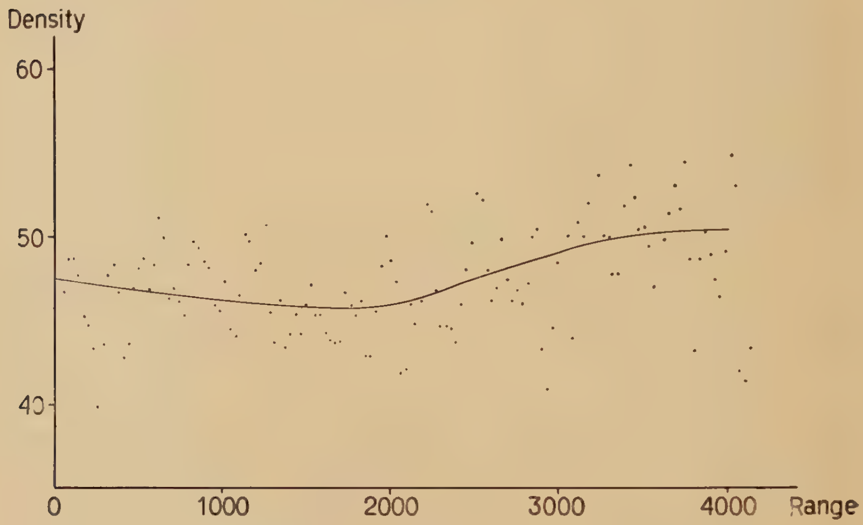

κ_1-meson density, before correction, versus residual range.

Fig. 8

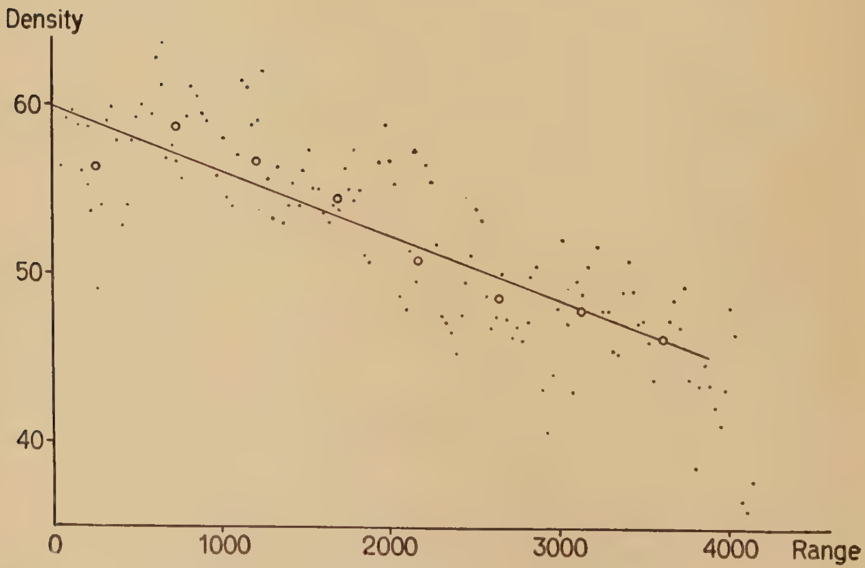

Corrected κ_1-meson density versus residual range.

Figures 7 and 8 demonstrate how important the correction is for a single particle. The κ_1-meson is chosen as an example. In fig. 7 its density before correction is shown as a function of range, while the corrected densities are given in fig. 8. It is seen that the measured values have a large spread. The following method has been used to obtain best results in drawing the density-range curve, which can be approximated by a straight line. The track is divided up into intervals for each of which an average density value is calculated and inserted in the diagram. These points are then used in calculating the constants of the straight line, according to the method of least squares. The portion of the track closest to the point at which the particle enters the emulsion is not employed in the calculation since the density there may have been influenced by unconsidered effects in the surface of the emulsion. The density-range curves were drawn for the other particles in the same way.

Fig. 9

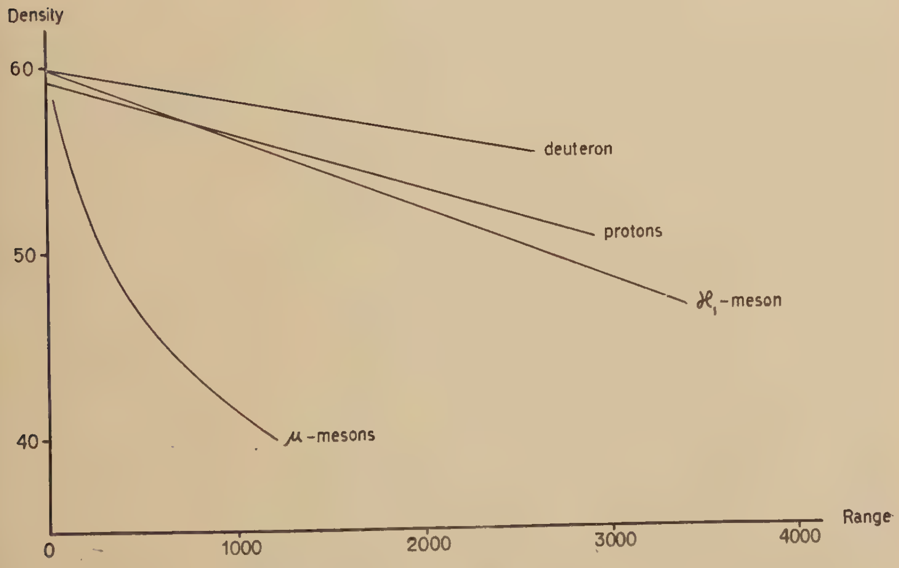

Range-density diagram for the κ_1-meson and the comparison particles.

§ 4. DETERMINATION OF THE MASS

In the density-range diagram of fig. 9 curves are shown both for the κ_1-meson and for the particles with which it is compared in finding the mass. The proton curve is a median curve of four protons of which three travel approximately parallel with the κ_1-meson, the fourth being a particle which goes from the glass towards the surface, where it stops. The μ–meson curve is a median of the eight particles used in calibrating the plate.

In table 1 the data will be found for those straight lines which approximate the density as a function of range. The slopes and their intercepts on the axis $R=0$ are given. The figures give an indication of the accuracy with which a density measurement can be carried out.

Table 1

Particle	Density at R=0	Slope
κ_1-meson	59·9	3·8
Proton 1	59·5	3·1
,, 2	58·0	2·5
,, 3	59·7	3·1
,, 4	59·1	2·8
Deuteron	59·9	1·8

A relation $R=(m/Z^2)f(v)$ obtains between the residual range, mass, charge and velocity of a particle. Consequently if two particles of equal charge are compared with one another the ratio of their masses is that of their residual ranges provided that the comparison is made at points where their velocities are equal. Two particles with the same velocity and charge produce the same ionization, and therefore their track-densities should be the same also. In order to obtain the relation between the masses of two particles it is thus sufficient to determine the relation between their residual ranges beyond points of equal density.

The mass of the κ_1-meson can thus be found by comparing the proton- and κ_1-curves in fig. 9. When the comparison is made for a density of 52 units the result is $m\kappa_1=1550$ electron masses. This value is not, however, independent of which density is chosen in making the comparison, since the proton- and meson- curves intersect. The statistical fluctuations in the densities of the individual tracks are so great that such an intersection is not improbable. The comparison is made at as great a range as possible because the relative error in the range-determination is there least.

However, it is possible to eliminate the crossing of the proton- and meson-curves. The mass determination is then independent of the density chosen for the comparison. The average value of the intercepts of the curves on $R=0$ has been found and all the curves are made to pass through this point. The slopes are found by a new least-squares calculation, this time under the proviso that all curves should cut the line $R=0$ at this point. It is theoretically correct that all the curves should cut the axis of ordinates at the same point since all density-range curves for singly-charged particles are similar in shape, with their R-axis elongated in a degree proportional to the mass. The intercept on the line $R=0$ is 59·4 units. The slopes are shown in table 2, which also gives the value of the κ_1-meson mass calculated from each individual comparison particle. The mass-relation is easily found since the mass is inversely proportional to the slope.

Table 2

Particle	Slope	Mass of the κ_1-meson
κ_1-meson	3·64	
Proton 1	3·07	1549 m_e
,, 2	3·04	1533 ,,
,, 3	2·98	1503 ,,
,, 4	2·99	1509 ,,
Deuteron	1·50	1512 ,,
Mean value	. .	1521 ,,

When all four protons and the deuteron are employed, the average mass of the κ_1-meson is found to be $(1521 \pm 75)m_e$. The error is a probable error determined from the spread of the points which have been used in the calculation of the density-range curves. The error in the slope Δk has been calculated from the formula :

$$\Delta k = \sqrt{\left[\frac{\Sigma_i w_i (\Delta D_i / R_i)^2}{(n-1)\Sigma_i w_i}\right]},$$

where w_i is the statistical weight of the different points, ΔD_i is the difference between the density measured and the density determined from the density-range curve for the range R_i. The statistical weight of the points has been put proportional to the range.

§ 5. SYSTEMATIC ERRORS IN THE MASS-DETERMINATION

When the μ-meson mass is calculated from that of the proton by comparing ranges a result *ca.* 20% too small is obtained. The same observation was made in earlier measurements with the photo-electric apparatus (von Friesen *et al.* 1951), and if the effect is the result of some systematic error peculiar to the method of measurement then one must assume that the same systematic error arises in determining the mass of the κ_1-meson. The correct masses of the particles are shown as abscissae in fig. 10, the ordinates being the measured masses. The departure from the correct value (represented by the dashed line) is large in the case of the μ-meson but should approach zero asymptotically, and is, therefore, vanishingly small for the calculated κ_1-meson-mass.

In determining the meson-mass given in table 2 the density curves have been approximated by straight lines. This introduces a systematic error in so far as the measured ranges are not proportional to the masses. If such a proportionality did occur, the curves with their approximating straight lines would have been of similar shape, and the approximation would have been of no importance in the mass-determination. An attempt to estimate the order of magnitude of the error was made by computing second degree range-density curves using measurements on protons and mesons. The curvature obtained, however, is so small that the standard error in it is of the same order as the curvature itself. Thus a reliable determination of the systematic error introduced by the approximation is impossible. An estimate has, however, been made which shows that it must be small in comparison with the probable error calculated from the spread of the density-measurements.

Fig. 10

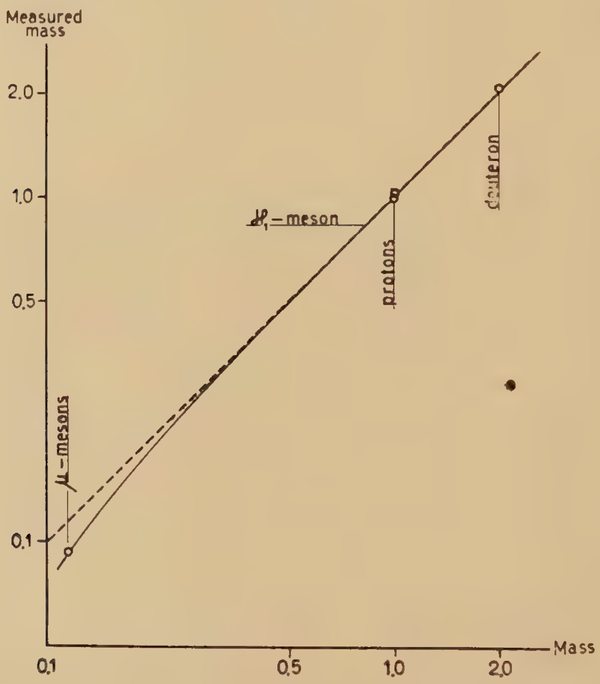

Comparison between the measured and actual masses of the comparison particles.

It is not possible to decide what kind of systematic error is brought in by irregularities in the emulsion, though there is no reason to assume that any error arises because the κ_1-meson is quite far from the edges of the plate. Further, as already has been pointed out, proton No. 1 is at the same place in the emulsion, and it shows no sign of anomalous density.

§ 6. Mass-Determination by Comparison with Crossing Proton Tracks

The κ_1-meson mass-determination just described was carried out following an appreciable correction of the density, and the accuracy therefore depends to a high degree on how good the correction is. It is possible, however, to find approximately the relation between the masses of two particles without considering exactly how uneven the development is, provided that it is a function only of the distance from the glass. Instead of comparing tracks which coincide as nearly as possible with one another in a vertical section of the emulsion. tracks which cross each other are employed. The κ_1-meson travels from the surface through the emulsion and stops near the glass. It is compared with a proton which comes from the glass, goes upward in the emulsion and stops near the surface (see fig. 11). There is a point at which the tracks are at the same distance from the glass, and in that point the degree of development is the same if it is a function only of the distance from the glass. Measurements on both tracks have shown that the crossing point is 2575 μ from the ends of both tracks. The density of the proton track at that point is 49·6 units and in the meson track it is 47·7 units. Thus the density difference at the point of intersection is 1·9 units. The mass-difference to which this density difference is equivalent can be found from fig. 9, where the density curves for different masses can be constructed from the proton curve. A particle

Fig. 11

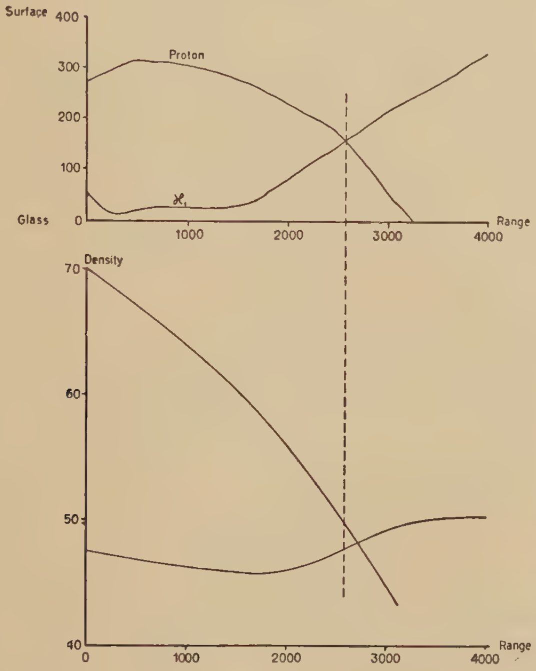

Mass-determination by means of crossing tracks.
Above : vertical section showing the tracks.
Below : density versus range for the same tracks.

with mass $1500\,m_e$ has a density difference of 1·9 units at a range of $2575\,\mu$.

The error in the estimates made in this way are large, for several reasons. The greatest error is a consequence of statistical density-variations along the track. Furthermore, the curve cannot be drawn with as great certainty as it can after correction because the curve form is not simple. In a rough way the error in density has been found to be about 0·8 unit for each curve corresponding with a probable error in mass of $200\,m_e$.

Thus the result of the present κ_1-meson mass determination is $(1500 \pm 200)\,m_e$.

§ 7. THE MASS OF THE κ_1-MESON

The mass of the κ_1-meson has thus been calculated in two ways from the measurements of the projected area of the track. In the first determination the mass has been calculated after corrections of the density. Taking account of the errors of the method the mass was found to be $(1521 \pm 75)\,m_e$. The second method, where crossing tracks were used, gave the result $(1500 \pm 200)\,m_e$.

The mean value of the two determinations has been calculated to $(1518 \pm 70)\,m_e$.

ACKNOWLEDGMENTS

I have pleasure in thanking Professor Sten von Friesen and Professor Bengt Edlén for their continued interest and encouragement. I wish to thank Professor C. F. Powell, University of Bristol, and Dr. C. O'Ceallaigh, University of Cork, for their kindness in lending me the plate in which the κ_1-particle was found.

REFERENCES

O'CEALLAIGH, C., 1951, *Phil. Mag.*, **42,** 1032.

VON FRIESEN, S., and KRISTIANSSON, K., 1950, *Nature, Lond.*, **166,** 686 ; 1951, *Ibid.*, **168,** 377 ; 1952, *Arkiv f. Fysik*, **4,** 505.

XXX. *The Exchange Energy of Nearly Free Electrons in Metals*

By E. P. Wohlfarth
Department of Mathematics, Imperial College, London*

[Received November 20, 1952]

Summary

The paper describes calculations of the exchange energy of an assembly of nearly free electrons of low density (§ 2). Two differing one-electron wave functions are used, given by relations (2.7) and (2.22), both concerning a nearly empty Brillouin zone. It is found in both cases that the total exchange energy is much less sensitive to changes of the effective mass of the electrons than is the Fermi energy. Previous related work is referred to (§ 1) and the bearing of the results on some physical properties of metals is indicated (§ 3).

§ 1. Introduction

The calculation of the exchange energy of an assembly of perfectly free electrons constituted one of the early advances of the modern electron theory of metals (see, for example, Sommerfeld and Bethe 1933). Use of one-electron wave functions of the form

$$\psi_m(\mathbf{r}_i)=V^{-1/2}\exp(i\mathbf{k}_m\,.\,\mathbf{r}_i), \quad . \quad . \quad . \quad . \quad . \quad (1.1)$$

where $\mathbf{k}_m$, $\mathbf{r}_i$ represent position vectors in reciprocal and real space respectively and V is the volume of the metal, gives for the exchange energy for two electrons with parallel spins and wave vectors $\mathbf{k}_m$, $\mathbf{k}_n$ (Bloch 1929)

$$\left.\begin{aligned} J_{mn}&=e^2\iint\frac{1}{r_{12}}\psi_m(\mathbf{r}_1)\psi_n{}^*(\mathbf{r}_1)\psi_m{}^*(\mathbf{r}_2)\psi_n(\mathbf{r}_2)\,d\tau(\mathbf{r}_1,\mathbf{r}_2)\\ &=\frac{4\pi e^2}{V}\frac{1}{|\mathbf{k}_m-\mathbf{k}_n|^2}.\end{aligned}\right\} \quad (1.2)$$

The total exchange energy of the metal in this approximation is given by

$$J=J_{\text{f.e.}}=\sum_{m}\sum_{n}J_{mn}=\tfrac{3}{4}Ne^2\left(\frac{3N}{\pi V}\right)^{1/3}, \quad . \quad . \quad . \quad . \quad (1.3)$$

if the metal is non-ferromagnetic, N being the number of electrons in volume V.

The relation (1.2) may be used in discussing such properties of the free electron gas as the temperature variation of the electronic specific heat (Wohlfarth 1950) and of the spontaneous magnetization for a ferromagnetic metal (Lidiard 1951). In such discussions it appears that, because of the rapid variation of J_{mn} as $|\mathbf{k}_m-\mathbf{k}_n|\rightarrow 0$, results are obtained which differ widely from observation. It is thought at present that these deviations may be partly removed by taking some account of the effects of correlation forces between electrons with antiparallel spins. On the other hand, the relation for J_{mn} based on one-electron functions of the tight binding type is of an entirely different form from (1.2) (Wohlfarth 1953) and more reasonable thermal and magnetic results may be derived. The present calculation, based on nearly free electron functions, makes an attempt to interpolate between the behaviour of the perfectly free electron gas and of an assembly of tightly bound electrons.

---

* Communicated by the Author.

Again, relation (1.3) may be used immediately in calculations of the cohesive energy of metals in the free electron approximation (Wigner and Seitz 1934) and in deriving the condition under which the metal is ferromagnetic (Bloch 1929). The present calculation of J, using nearly free electron functions, gives some information on such questions as the effect on the total exchange energy of an effective electronic mass different from the actual mass, of the presence of Brillouin zone boundaries and of the shape of the Fermi surface (cf. § 3).

The problem of calculating the exchange energy for anything but the free electron gas is one of enormous difficulty and in this paper calculations are carried out for two limiting cases only (cf. § 2). Other attempts along somewhat similar lines have been made previously. In a calculation of the cohesive energy of lithium Seitz (1935, 1940) expresses the wave function in the form

$$\psi_m(\mathbf{r}_i)=(\alpha+i\gamma\mathbf{k}_m\cdot\mathbf{r}_i)\exp(i\mathbf{k}_m\cdot\mathbf{r}_i), \quad . \quad . \quad . \quad . \quad (1.4)$$

where α and γ, strictly functions of position inside each atomic cell, were taken to be constants. The calculated exchange energy does not differ appreciably from the free electron value (1.3), the correction being such as to increase J numerically. Herring (1951) has, however, recently found that the sign of this correction should be opposite to that obtained by Seitz, whose calculation is stated to involve a computational error. Herring and Hill (1940) carried out a rough calculation of this correction in their work on beryllium. This calculation applies to the limit of low electron density and thus bears some formal resemblance to the present calculation, although the wave functions used in the two cases are different. With q the number of electrons per atom ($q\ll 1$) Herring and Hill's formula is of the form

$$J=J_{\text{f.e.}}\{1+\epsilon q^{2/3}+O(q^{4/3})\}, \quad . \quad . \quad . \quad . \quad . \quad (1.5)$$

where $J_{\text{f.e.}}$ is given by (1.3) and ϵ, a function of the radius of the atomic sphere, was obtained by numerical calculation for beryllium. Here ϵ is negative and small, in qualitative agreement with the present results.

§ 2. CALCULATION OF THE EXCHANGE ENERGY

A general relation for J_{mn} based on the nearly free electron approximation had been given in an earlier paper (Wohlfarth 1949, relation (4.8)) and it was stated that, owing to the complexity of this relation and of the shape of the Fermi surface, the summation process to give J as in (1.3) would be prohibitively difficult. It is, therefore, proposed to delimit the problem considerably. Two cases will be considered :

(i) *Interaction between electrons overlapping into the second Brillouin zone.* It is assumed that the first zone is full and that overlap occurs in the neighbourhood of $\mathbf{k}=(\pm\pi/a, 0, 0)$, where a is the lattice parameter. With q, the number of electrons per atom in the second zone, small compared with unity, this situation is best visualized by reference to fig. 1.

Fig. 1

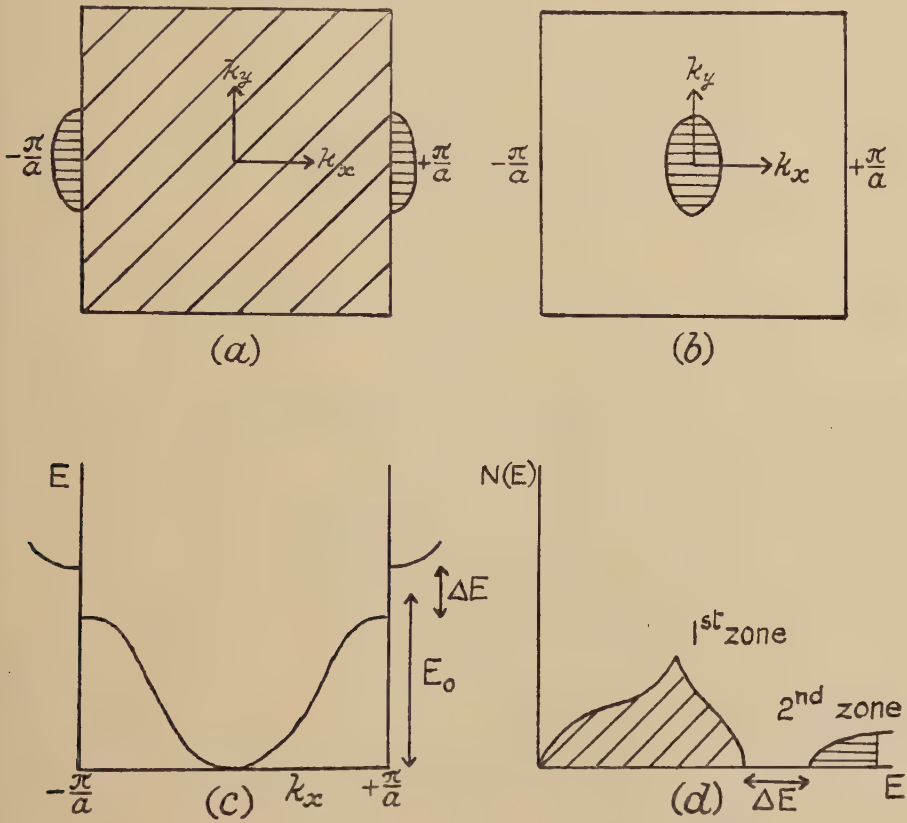

(*a*) Electron distribution in $\mathbf{k}$ space, $k_z=0$; extended zone scheme. (*b*) Reduced zone scheme. (*c*) Variation of energy with k_x, $k_y=k_z=0$; ΔE, energy gap ; $E_0=(\hbar^2/2m)(\pi/a)^2$. (*d*) Density of states curve. All figures are schematic.

Figure 1 (*a*) shows the overlap, the two parts of the Fermi surface being such as to combine to form an oblate ellipsoid of revolution, since the states $\mathbf{k}=(\pm\pi/a, 0, 0)$ are effectively identical. This ellipsoid may conveniently be regarded as lying at the centre of the zone shown in 1 (*b*), which is that of 1 (*a*) displaced by $\pm\pi/a$. 1 (*c*) shows the variation of the energy with k_x and 1 (*d*) the density of states curve, all the figures being schematic. The calculation to be described is concerned with the few electrons distributed in the ellipsoid in 1 (*b*) or, alternatively, in the parabolic part of the $N(E)$ curve in 1 (*d*) above the energy gap.

As is well known (Mott and Jones 1936, p. 65) the energy is here given by

$$E=\frac{\hbar^2}{2m}(\alpha k_x^2+k_y^2+k_z^2), \quad . \quad . \quad . \quad . \quad . \quad . \quad . \qquad (2.1)$$

where $\alpha=1+4E_0/\Delta E$, $E_0=(\hbar^2/2m)(\pi/a)^2$. In (2.1) k_x is measured relative to the centre of the zone in 1 (*b*) and relative to $k_x=\pm\pi/a$ in 1 (*a*). The ellipsoid has semi-axes *a*, *b*, *b* (this *a* should not be confused with the lattice parameter), where

$$a=\alpha^{-1/3}k_0, \qquad b=\alpha^{1/6}k_0, \qquad k_0=(3\pi^2N/V)^{1/3}. \quad . \quad . \quad . \qquad (2.2)$$

Strictly the effective electronic mass m^* has to be expressed in the tensor form

$$m/m^*=\begin{Bmatrix} \alpha & 0 & 0 \\ 0 & 1 & 0 \\ 0 & 0 & 1 \end{Bmatrix}. \quad . \quad . \quad . \quad . \quad . \quad . \quad . \qquad (2.3)$$

The Fermi energy, obtained by summing *E* in (2.1) over the occupied states, may, however, be written in the form

$$E_F=\tfrac{3}{5}N\frac{\hbar^2}{2m}\alpha^{1/3}k_0^2, \quad . \quad . \quad . \quad . \quad . \quad . \quad . \quad . \qquad (2.4)$$

which is identical with the expression for quasi-free electrons with an effective mass equal to

$$m^*=\alpha^{-1/3}m. \quad . \quad . \quad . \quad . \quad . \quad . \quad . \quad . \quad . \qquad (2.5)$$

Since α may be large, say ~ 10, the Fermi energy of the overlapping electrons may be 2–3 times larger than that of the same number of perfectly free electrons. The problem is to calculate the corresponding change in the exchange energy.

The one-electron wave functions may be written as

$$\psi_m(\mathbf{r}_i)=\{A_{0m}+A_{1m}\exp(-2\pi i x_i/a)\}\exp(i\mathbf{k}_m\,.\,\mathbf{r}_i). \quad .. \qquad (2.6)$$

A simple transformation gives the alternative expression

$$\psi_m(\mathbf{r}_i)=\{2/V(1+\beta^2k_{xm}^2)\}^{1/2}\{\sin(\pi x_i/a)+i\beta k_{xm}\cos(\pi x_i/a)\}\exp(i\mathbf{k}_m\,.\,\mathbf{r}_i), \quad . \quad . \quad . \qquad (2.7)$$

correct to the second power of k_{xm}, where $\mathbf{k}_m$ is measured relative to the bottom of the second zone as in 1 (*a*) and

$$\beta=a(\alpha-1)/2\pi. \quad . \quad . \quad . \quad . \quad . \quad . \quad . \quad . \qquad (2.8)$$

For $k_{xm}=0$, (2.7) represents a standing wave in the *x* direction (cf. Mott and Jones 1936, p. 62).

The calculation of J_{mn} proceeds by standard methods. It is noted that J_{mn} may be written in the form

$$\left.\begin{aligned} J_{mn}&=e\int U(\mathbf{r}_2)\psi_m^*(\mathbf{r}_2)\psi_n(\mathbf{r}_2)\,d\tau(\mathbf{r}_2), \\ \text{where} \quad \nabla^2U(\mathbf{r}_2)&=-4\pi e\psi_m(\mathbf{r}_2)\psi_n^*(\mathbf{r}_2), \end{aligned}\right\} \quad . \quad . \quad . \qquad (2.9)$$

and it is found that

$$\begin{aligned} J_{mn}=\frac{4\pi e^2}{V}[(1+\beta^2k_{xm}^2)(1+\beta^2k_{xn}^2)]^{-1}\Bigg[&\frac{(1+\beta^2k_{xm}k_{xn})^2}{K^2} \\ &+\frac{1/2}{(K^2+p^2)^2-4p^2K_1^2}\{(K^2+p^2)((1-\beta^2k_{xm}k_{xn})^2+\beta^2K_1^2) \\ &+4\beta pK_1^2(1-\beta^2k_{xm}k_{xn})\}\Bigg], \quad . \quad . \quad . \quad . \quad . \quad . \quad . \quad . \quad . \qquad (2.10) \end{aligned}$$

where $p=2\pi/a$, $\mathbf{K}=(\mathbf{k}_m-\mathbf{k}_n)=(K_1, K_2, K_3)$. For $K \ll \pi/a$ (2.10) may be expanded up to K^2 and J_{mn} becomes

$$J_{mn}=\frac{4\pi e^2}{V}\left[\frac{1}{K^2}-\beta^2\frac{K_1{}^2}{K^2}+\frac{1}{2p^2}-\frac{K^2}{2p^4}+\frac{2}{p^4}\{(k_{xm}{}^2+k_{xn}{}^2)(p\beta+1)\right.$$
$$\left.-k_{xm}k_{xn}(2+2p\beta+p^2\beta^2)\}\right]. \quad . \quad . \quad . \quad . \quad (2.11)$$

The problem is now to sum J_{mn} over the ellipsoid defined by (2.2). Only the first two terms in (2.11) present any difficulty and a brief outline is given of the method adopted of integrating the first term. It is required to evaluate

$$I=\iint_M \frac{d\tau\,(\mathbf{R}_1, \mathbf{R}_2)}{|\mathbf{R}_1-\mathbf{R}_2|^2}, \qquad M\equiv\frac{X^2}{a^2}+\frac{Y^2+Z^2}{b^2}=1. \quad . \quad . \quad (2.12)$$

By use of Poisson's equation it may be shown that

$$I=\frac{1}{4\pi}\int_\infty \frac{d\tau(\mathbf{r})}{r}\iint_M \exp\{i(\mathbf{R}_1-\mathbf{R}_2)\,.\,\mathbf{r}\}\,d\tau(\mathbf{R}_1, \mathbf{R}_2).$$

Consider the integral

$$I_1=\int_M \exp(i\mathbf{R}\,.\,\mathbf{r})\,d\tau(\mathbf{R}).$$

Put $X=au$, $Y=bv$, $Z=bw$, then $d\tau(\mathbf{R})=ab^2\,d\tau(\boldsymbol{\rho})$, where $\boldsymbol{\rho}=(u, v, w)$. The domain of integration is now the unit sphere $M'\equiv u^2+v^2+w^2=1$. Also $\mathbf{R}\,.\,\mathbf{r}=\boldsymbol{\rho}\,.\,\mathbf{r}'$, where $\mathbf{r}'=(ax, by, bz)$. Hence

$$I_1=ab^2\int_{M'} \exp(i\boldsymbol{\rho}\,.\,\mathbf{r}')\,d\tau(\boldsymbol{\rho})=4\pi ab^2\left(\frac{\sin r'-r'\cos r'}{r'^3}\right),$$

and

$$I=4\pi a^2b^4\int_\infty \frac{d\tau(\mathbf{r})}{r}\left(\frac{\sin r'-r'\cos r'}{r'^3}\right)^2,$$

or, transforming $\mathbf{r}=(x, y, z)$ to $\mathbf{r}'=(ax, by, bz)\equiv(x', y', z')$,

$$I=4\pi ab^2\int_\infty d\tau(\mathbf{r}')\left(\frac{x'^2}{a^2}+\frac{y'^2+z'^2}{b^2}\right)^{-1/2}\left(\frac{\sin r'-r'\cos r'}{r'^3}\right)^2.$$

The integrations are elementary and finally give

$$I=2\pi^2a^2b^2(1-\eta^2)^{-1/2}\ln\frac{1+(1-\eta^2)^{1/2}}{1-(1-\eta^2)^{1/2}}, \quad . \quad . \quad . \quad (2.13)$$

where $\eta=a/b$. Hence, using (2.2),

$$I=4\pi^2k_0{}^4f_1(\alpha), \qquad f_1(\alpha)=\alpha^{1/6}(\alpha-1)^{-1/2}\cosh^{-1}\alpha^{1/2}. \quad . \quad (2.14)$$

Since $f_1(1)=1$ the corresponding free electron expression is obtained correctly for $\alpha=1$. The limiting expressions are

$$\left.\begin{aligned}\alpha\to 1, \qquad & f_1(\alpha)=1-\tfrac{1}{45}(\alpha-1)^2+O((\alpha-1)^4),\\ \alpha\to\infty, \qquad & f_1(\alpha)=\tfrac{1}{2}\alpha^{-1/3}\ln 4\alpha.\end{aligned}\right\} \quad . \quad . \quad (2.15)$$

It follows from (2.14), (2.15) that $f_1(\alpha)$ is a very slowly varying function. Even for $\alpha^{1/3}=m/m^*$ as large as 3, $f_1(\alpha)\doteq 0{\cdot}79$, so that a change of 300% in the Fermi energy produces a change of only about 20% in the leading term in the exchange energy, compared with the corresponding free electron values.

The integration of the second term in (2.11) proceeds by similar means and only the final expression for J need be given. It is convenient to express J as a power series in $q^{2/3}$, where q is the number of electrons per atom. This is achieved by noting that for the simple cubic lattice the lattice parameter a is given by $a=(qV/N)^{1/3}$, where N is the total number of electrons, slightly modified relations applying to other lattice types. Then, from (2.8), $\beta=(qV/N)^{1/3}(\alpha-1)/2\pi$. The final expression then becomes, with $J_{\text{f.e.}}$ given by (1.3),

$$J=J_{\text{f.e.}}\left\{f_1(\alpha)+\left(\frac{\pi}{3}\right)^{1/3}\frac{1}{6\pi}q^{2/3}f_2(\alpha)+\left(\frac{3}{\pi}\right)^{1/3}\frac{1}{60\pi}q^{4/3}f_3(\alpha)+O(q^2)\right\}. \quad (2.16)$$

Here $f_1(\alpha)$ has already been defined in (2.14) and (2.15). Also

$$\left.\begin{array}{ll} & f_2(\alpha)=1-2(\alpha-1)(\alpha^{1/3}f_1(\alpha)-1), \\ \alpha\to 1, & f_2(\alpha)=1-\frac{2}{3}(\alpha-1)^2+O((\alpha-1)^4), \\ \alpha\to\infty, & f_2(\alpha)=1+2\alpha-\alpha\ln 4\alpha, \end{array}\right\} \quad . \quad . \quad (2.17)$$

so that $f_2(\alpha)$ varies much more rapidly than $f_1(\alpha)$, soon becoming negative. Finally

$$f_3(\alpha)=\alpha^{-2/3}(2\alpha-1), \quad . \quad . \quad . \quad . \quad . \quad . \quad . \quad (2.18)$$

again a fairly rapidly varying function. Since, however, the numerical coefficients in (2.16) become rapidly very small for increasing powers of $q^{2/3}$ the total exchange energy differs only slightly from the free electron value, since the effective mass has little influence on the leading term and the convergence of the series is rapid, especially if $q\ll 1$ as is assumed in the calculation.

(ii) *Interaction between electrons near the centre of the first Brillouin zone.* Here, if $q\ll 1$, the electrons are, to a first approximation, described correctly by free electron functions (1.1). To a second approximation, if only the perturbation arising from the first zone boundary is important, the energy in the one-dimensional case becomes (Mott and Jones 1936, p. 61)

$$E=\frac{\hbar^2}{2m}k^2-\frac{2m}{\hbar^2}\frac{(\Delta E/2)^2}{(k-2\pi/a)^2-k^2}. \quad . \quad . \quad . \quad . \quad (2.19)$$

Here, since $q\ll 1$ implies $k\ll\pi/a$, expansion gives

$$E'=E+\delta^2E_0=(\hbar^2/2m)(k^2(1-\delta^2)-\pi\delta^2k/a+\ldots),$$

where $\delta=\Delta E/4E_0$, cf. fig. 1. The energy has to be measured relative to the lowest state, $k=0$, i.e. relative to $E'=0$. The effective mass is given by

$$\frac{m}{m^*}=\frac{m}{\hbar^2}\frac{d^2E'}{dk^2}=1-\delta^2-\delta^2O(q^{1/3}). \quad . \quad . \quad . \quad . \quad (2.20)$$

In the three-dimensional case, unless $\delta=0$, the Fermi surface is no longer spherical. For the purpose of the calculation of exchange energy the deviations may, however, be neglected, since the above calculation shows how insensitive is the exchange energy to even quite large deviations of the Fermi surface from a sphere. With this approximation the effective mass near the centre of the zone is isotropic, in contrast to the above case, and it is given by (2.20). The wave function is

$$\psi_m(\mathbf{r}_i)=(A_{0m}+2A_{1m}\,(\cos px_i+\cos py_i+\cos pz_i))\exp\,(i\mathbf{k}_m\,.\,\mathbf{r}_i), \qquad (2.21)$$

where $p=2\pi/a$. It is required to calculate the exchange energy correct to $q^{2/3}$. To this approximation (2.21) becomes

$$\psi_m(\mathbf{r}_i)=V^{-1/2}(1-\tfrac{3}{4}\gamma_m{}^2)\{1+\gamma_m\,(\cos px_i+\cos py_i+\cos pz_i)\}\exp\,(i\mathbf{k}_m\,.\,\mathbf{r}_i),$$

where

$$\gamma_m=(a\delta/\pi)(k_{xm}+k_{ym}+k_{zm}). \quad . \quad . \quad . \quad . \quad . \quad . \quad (2.22)$$

The relation for J_{mn} is obtained as before and after expansion to terms in $(a\delta/\pi)^2$, i.e. in $\delta^2q^{2/3}$, it is found that

$$J_{mn}=\frac{4\pi e^2}{V}\,\frac{1}{|\mathbf{k}_m-\mathbf{k}_n|^2}\{1-\tfrac{3}{2}(\gamma_m{}^2+\gamma_n{}^2-\gamma_m\gamma_n)\}. \quad . \quad . \quad (2.23)$$

The total exchange energy J is obtained by integrating (2.23) over the occupied states, the Fermi surface being here taken to be spherical as discussed above. The integrations are elementary and the final expression is

$$J=J_{\text{f.e.}}\left\{1-\frac{7}{2\pi}\left(\frac{\pi}{3}\right)^{1/3}\delta^2q^{2/3}+\delta^2O(q^{4/3})\right\}, \quad . \quad . \quad . \quad (2.24)$$

where $J_{f.e.}$ is given by (1.3). Comparison of (2.20) and (2.24) shows that the ratio of the relative changes of the exchange and Fermi energies on changing the effective mass is given by

$$\frac{(J-J_{\text{f.e.}})/J_{\text{f.e.}}}{(m-m^*)/m^*}=1{\cdot}132q^{2/3}+O(q). \quad . \quad . \quad . \quad . \quad (2.25)$$

Since $q \ll 1$ it appears again that the exchange energy depends much less sensitively on changes of the effective mass than does the Fermi energy. As already noted relation (2.24) bears some formal resemblance to Herring and Hill's relation (1940) given by (1.5). In the present calculation the correction term is closely connected with the magnitude of the energy gap at the first zone boundary.

§ 3. DISCUSSION

The present calculation is based on an approximate treatment of the metallic state whose validity in describing any particular metal is doubtful since the potential energy of the electrons is not everywhere small compared with their kinetic energy. Further, the results obtained in § 2 are strictly applicable only in the limit of low electron density. The two calculations described above are, however, based on two entirely different types of one-electron wave functions, (2.7) representing a slightly perturbed standing wave and (2.22) a slightly perturbed plane wave, both for electrons in a nearly empty zone, but with differing effective electronic masses. The fact that qualitatively similar results are obtained in both cases indicates that conclusions drawn from these calculations may have a wider validity than is justified by the premises underlying the calculations.

(i) Relations (2.11) and (2.23) show that the leading term in J_{mn} is in both cases equal to the value (1.2) for perfectly free electrons. Hence the present calculation still predicts an anomalous temperature variation of electronic specific heat and spontaneous magnetization (cf. § 1). The calculation has, in fact, failed to provide an intermediate case between free electron and tightly bound electron behaviour.

(ii) Relations (2.16) and (2.24) show that the calculated exchange energy varies much less rapidly on changing the effective mass of the electrons than does the Fermi energy. This conclusion may provide some explanation of the fact that in calculations of the cohesive energy of many metals good agreement with experiment is usually attained by assuming the exchange energy to have the free electron value $J_{\mathrm{f.e.}}$ although great care is often necessary to correct the Fermi energy if m/m^* differs appreciably from 1 (see, for example, the discussion of beryllium by Raimes 1952). In particular, relations (2.14)–(2.16) show how insensitive is the exchange energy to deviations of the Fermi surface from spherical shape. This result may have some bearing on the problem of the contribution of exchange forces to the elastic constants of metals (Leigh 1951).

(iii) The condition for ferromagnetism of a perfectly free electron gas is that the ratio of exchange energy J to Fermi energy E_F given by (1.3) and (2.4) ($\alpha=1$) be larger than 2·5 (Bloch 1929). The second calculation in § 2 shows that for nearly free electrons, to the second approximation, the Fermi energy is reduced by a factor $(1-\delta^2)$ (cf. eqn. (2.20)), while to the same approximation (2.24) shows that the exchange energy is practically unchanged. Decrease of the Fermi energy, i.e. increase of the tightness of binding and narrowing of the energy band, thus increases the ratio J/E_F and therefore the tendency towards ferromagnetism, a well known result.

It gives me great pleasure to acknowledge the help I have had from Dr. A. N. Gordon in carrying out the evaluation of some of the integrals used in the calculations.

REFERENCES

Bloch, F., 1929, *Z. Phys.*, **57**, 545.
Herring, C., 1951, *Phys. Rev.*, **82**, 282.
Herring, C., and Hill, A. G., 1940, *Phys. Rev.*, **58**, 132.
Leigh, R. S., 1951, *Phil. Mag.*, **42**, 139.
Lidiard, A. B., 1951, *Proc. Phys. Soc.* A, **64**, 814.
Mott, N. F., and Jones, H., 1936, *Theory of the Properties of Metals and Alloys* (Oxford : Clarendon Press).
Raimes, S., 1952, *Phil. Mag.*, **43**, 327.
Seitz, F., 1935, *Phys. Rev.*, **47**, 400 ; 1940, *Modern Theory of Solids* (New York : McGraw-Hill).
Sommerfeld, A., and Bethe, H., 1933, *Handbuch der Physik* (2nd ed.), 24/2, 333.
Wigner, E., and Seitz, F., 1934, *Phys. Rev.*, **46**, 509.
Wohlfarth, E. P., 1949, *Phil. Mag.*, **40**, 703 ; 1950, *Ibid.*, **41**, 534 ; 1953, *Rev. Mod. Phys.* (in the press).

XXXI. *The Electrical Resistivity of Gold at Very Low Temperatures*

By A. J. Croft, E. A. Faulkner, J. Hatton and E. F. W. Seymour
Clarendon Laboratory, Oxford University *

[Received December 27, 1952]

Abstract

The experiments were made (i) with a new apparatus in which a bath of liquid helium can be cooled to 0·2° K and (ii) with a two-stage demagnetization apparatus in which temperatures of 0·006° K can be reached.

The results showed that (i) for specimens in different states of physical strain down to 0·2° K and (ii) for a specimen down to 0·006° K the resistance is linear with log $1/T$. This is in contrast to the relationship to be expected from Slater's theory, i.e. R proportional to exp θ/T.

The anomalous increase in the resistivity of certain 'pure' metals with falling temperature which occurs at temperatures below about 6° K is now well established experimentally, especially in the case of gold (for references see Mendoza and Thomas 1951). Slater (1951) has suggested that this behaviour may be due to a rearrangement of the gold lattice such that an energy gap occurs in the occupied Brillouin zone just at the top of the distribution of the conduction electrons. The metal would then behave like an intrinsic semi-conductor and a rapid rise in the resistivity with falling temperature would be expected. Some limitations of Slater's theory have been discussed by Katz (1952).

This paper reports the results of measurements of the electrical resistivity of gold made

(I) in a new apparatus in which a bath of liquid helium can be cooled to 0·2° K, and

(II) in the two-stage demagnetization apparatus described by Darby *et al.* (1951), in which measurements have been made down to 0·006° K.

Part I. *Experiments with the Liquid Helium Demagnetization Cryostat*

(A. J. Croft and E. A. Faulkner)

The main difficulty in measuring electrical resistivities at temperatures below 1° K is to get satisfactory thermal contact between the specimen and the paramagnetic salt which is used for achieving the cooling and measuring the temperature. The usual methods, such as compressing the salt round the wire, are liable to strain it. A better course is to submerge both in a bath of liquid helium, for this still has a useful thermal conductivity at 0·1° K. This is made possible in this apparatus by the use of the method of Hudson, Hunt and Kurti (1949) for reducing the heat influx due to recondensation of helium transported by the film

---

* Communicated by Professor F. E. Simon, F.R.S.

to the warmer regions. A container with the metal specimen, the paramagnetic salt and liquid helium inside it is suspended on a capillary tube (0·2 mm i. d. and 100 mm long) which limits the amount of vapour able to recondense and yet provides a way for getting the helium in and out.

The complete apparatus is shown in fig. 1. The inner bath is suspended inside an evacuable space which is at the bottom of a liquid helium dewar attached to the pumping line by a copper/glass seal. This outer bath holds sufficient liquid helium when it is full at 4° K to leave enough for an experiment several hours long after it has been pumped down to 1·1° K and has cooled down the inner bath as well. (The use of glass has many advantages, but even though Monax glass is used, the dewar has to be repumped after a few experiments.)

Of the paramagnetic salts for which the absolute temperature scale has been determined, the most suitable is gadolinium sulphate ; it gives a relatively large entropy change/unit volume on magnetization and has a very large specific heat between 0·2 and 0·7° K. Using a 100 kw water-cooled magnet which gives 11 kG, and demagnetizing from 1·1° K, we reach a temperature just below 0·2° K. The ballistic method of measuring the magnetic moment of the salt is used. To deduce the absolute temperatures from these measurements we have applied the corrections given by van Dijk (1946). As cylindrical samples were used in both his work and ours, it is difficult to allow for the differences between the sample and secondary coil shapes in the two cases. For this reason the values of the absolute temperature are probably not very accurate at the lower temperatures.

The experiments so far done in the cryostat have been measurements of electrical resistance for which we have used the galvanometer amplifier circuit developed by other workers in this laboratory (MacDonald 1947). The leads are brought into the inner bath through holes sealed with Araldite, a thermo-setting plastic ; a tungsten pinch sealed to a small copper/glass seal is used to bring them through the top of the vacuum space. The cryostat has proved easy to use ; the normal rate of warming up is about 0·15° K/hr at 0·3° K. If one wanted to go to lower temperatures than 0·2° K by using, for example, iron ammonium alum, the heat input would have to be cut down ; this could be done by using an extra liquid helium bath at the top of the capillary tube.

The gold wire was 0·1 mm in diameter and had been drawn by Messrs. Johnson, Matthey (their no. 3459), using first a tungsten carbide die and then a diamond one.

Their analysis is

Chemical :	Fe Ni	Less than 0·001% each.
Spectrographic :	Fe, Ni	All sensitive lines.
	Ag, Cu, Mn	Faintly visible.
	Sn, Na	Very faintly visible.
	Zn	Barely visible.

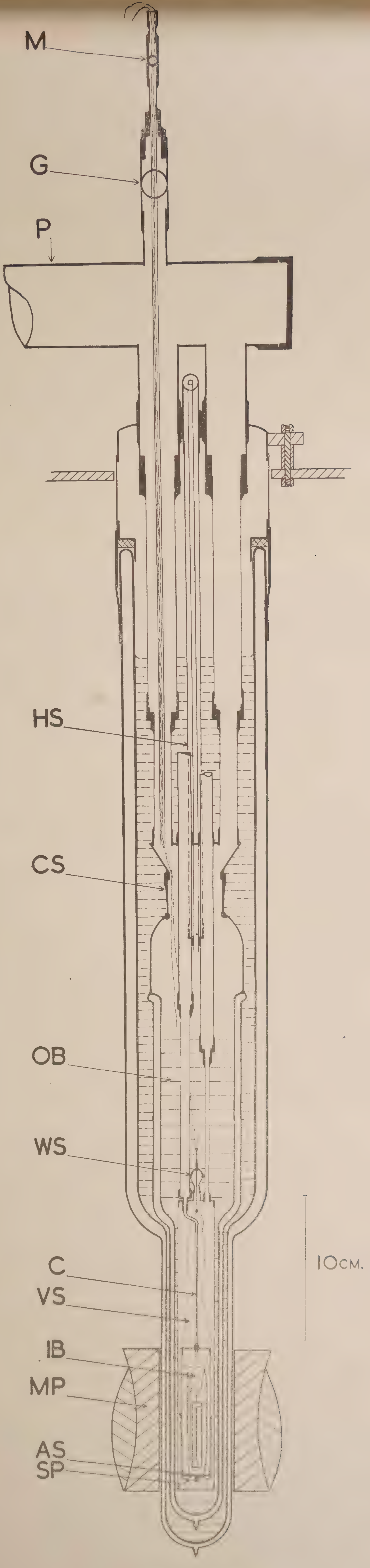

Section of Cryostat.

M, connection to manometer; G, connection to gasholder; P. connection to pump; HS, liquid helium siphon; CS, copper/glass seal on top of dewar; OB, outer bath dewar; WS, tungsten-pinch seal; C, capillary; VS, vacuum space; IB. inner bath; MP, magnet pole-piece; AS, Araldite seal, SP, spacer.

A length of 1·25 m was loosely wound on a former; the ends were soft-soldered to connecting lugs. Experiment I was made with the wire taken straight from the reel. Experiment II was done on the same length after it had been annealed in a vacuum at red heat for three hours. Before Experiment III it was annealed again, but at a higher temperature. In each case the measuring current was 5 mA.

Results

The results of these experiments are shown in fig. 2; above 1° K each point represents the mean of several resistance measurements made at a constant temperature; below 1° K each point represents one reading of temperature and resistance.

Fig. 2

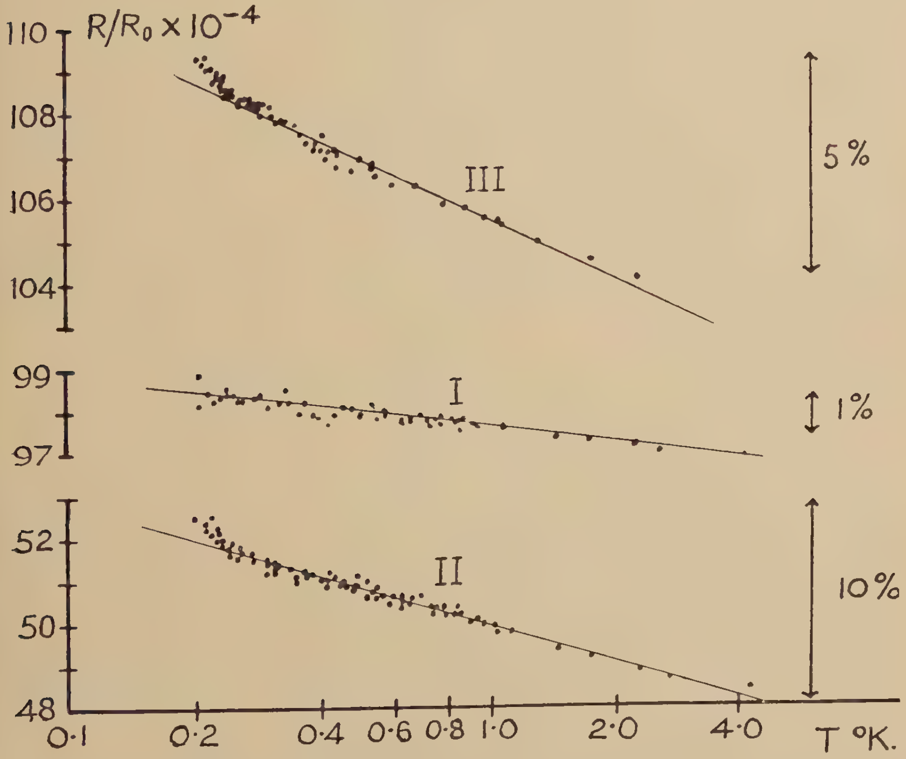

The straight lines conform to

$$R/R_0 = \text{const.} - a \log T,$$

where R_0 is the value of the resistance at 0° C.

The magnitude of the increase can be expressed by a coefficient α which is defined by

$$\alpha = -\frac{10^3}{R_{1^\circ\mathrm{K}}} \frac{dR}{d(\log T)}.$$

The following table shows the residual resistance ratio and the value of α found in the three experiments :—

Experiment I:	$R/R_0 = 97\times10^{-4}$ at 4° K	$\alpha=11$
Experiment II:	$= 48$	$\alpha=58$
Experiment III:	$=103$	$\alpha=23$

Comment

(1) The experimental points lie quite close to the $-a \log T$ line between 0·25° K and 2° K. The deviations from the straight line below this temperature which appear in II and III are probably due to the uncertainty in the corrections to the absolute temperature scale which has already been mentioned. It does not show up in I because of the lesser slope and greater scatter. (Similar unexpected deviations have been found in other work not yet published.)

(2) The first annealing reduced R/R_0, as one would expect, and increased α. The wire seems to have become contaminated during the second annealing because R/R_0 became larger than it was originally ; it is interesting to note that the value of α is between the values found in the first two experiments.

(3) The purity of the wire in Experiment II as indicated by the value of R/R_0 is between that of Mendoza and Thomas (1951) ($R/R_0=83\times10^{-4}$) and that of de Haas, Casimir and van den Berg (1938) ($R/R_0=22\times10^{-4}$).

Part II. *Experiments with the Two-Stage Demagnetization Apparatus*

(J. Hatton and E. F. W. Seymour)

In the measurement of electrical resistance at temperatures too low for the specimen to be immersed in liquid helium, special attention must be paid to the thermal contact between the metal and the paramagnetic salt used to produce the low temperature. In the experiment described here, the gold wire was embedded in the paramagnetic salt. It was decided that a potential difference of about six microvolts across the specimen could be measured with sufficient accuracy (about 0·3%). With the expected resistance of the gold at the low temperatures, this potential difference was calculated to produce a power dissipation of only a few ergs per minute. Further, since the measuring current would be on for only short periods, it was considered that the heating due to it would not be too high. Unfortunately it is not possible to make any quantitative estimate of the tolerable power dissipation in the wire since neither the thermal conductivity of the paramagnetic salt nor the efficacy of the contact between it and the wire is known at the temperature involved.

The gold wire used was from the same reel as that used in the experiments described in Part I of this paper.

Fig. 3

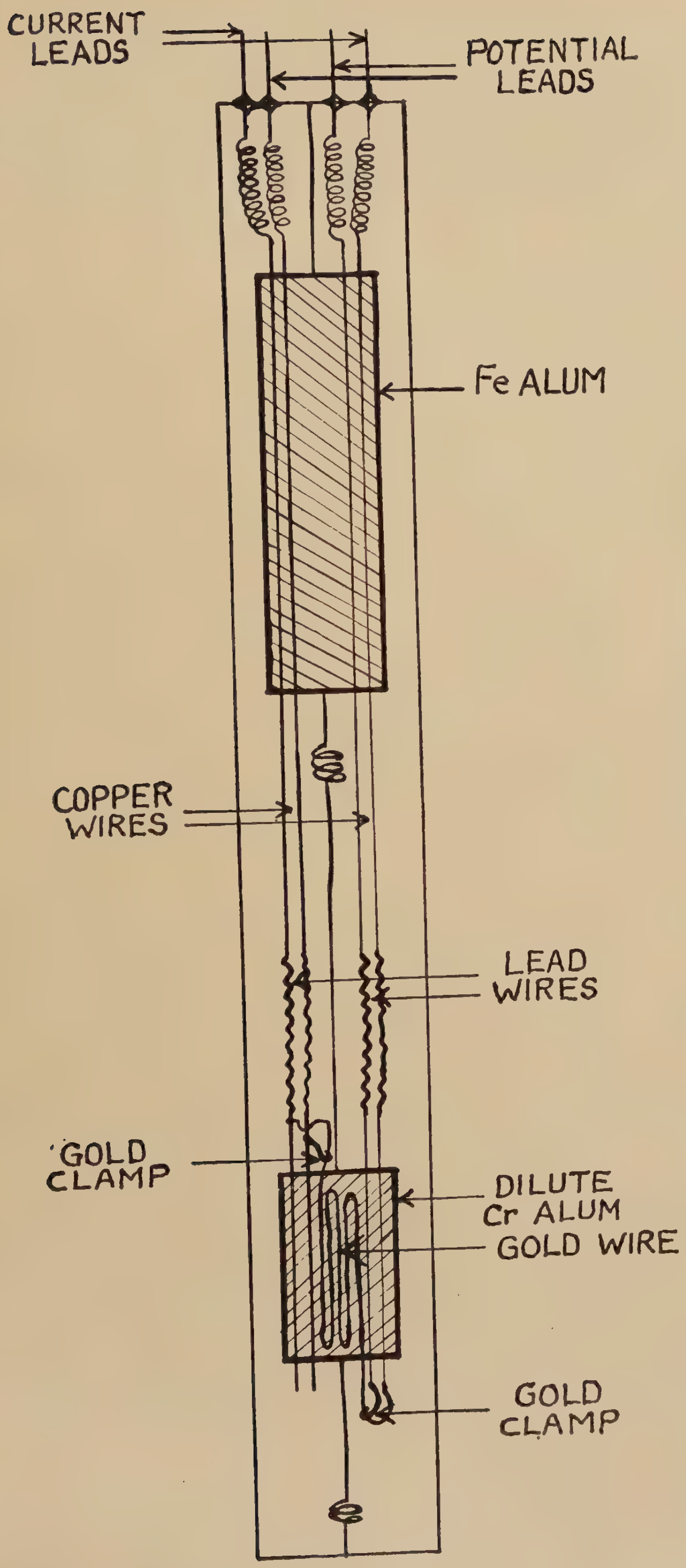
CURRENT LEADS
POTENTIAL LEADS
Fe ALUM
COPPER WIRES
LEAD WIRES
GOLD CLAMP
DILUTE Cr ALUM
GOLD WIRE
GOLD CLAMP

The first stage of the demagnetization apparatus shown in fig. 3 was a cylinder pressed from powdered iron alum. The second stage consisted of crystals of a mixed salt of potassium aluminium alum and 5% potassium chrome alum. The crystals were powdered and compressed around the gold wire in such a way that there was no contact between different parts of the gold wire or between the gold and the various copper wires which were also embedded in the salt.

Fig. 4

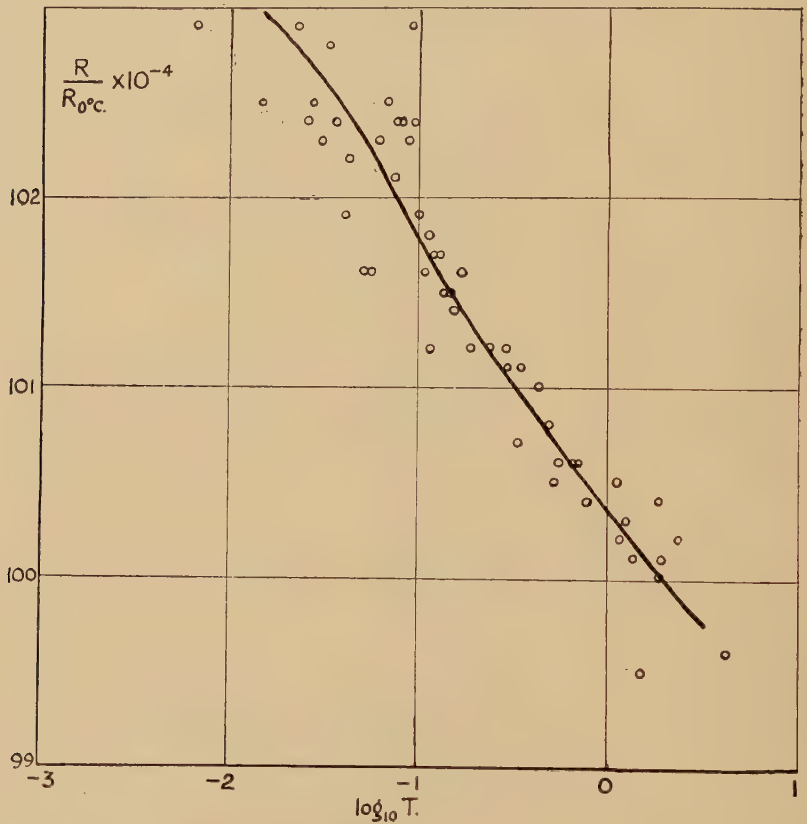

Current and potential leads passed through the first stage and then to the second stage via the lead wires which provided the heat switch between the stages. Each of the four leads was soldered to copper wires embedded in the second stage to increase the thermal contact. The ends of the gold wire were soldered directly to the current leads, but the potential connections were made by small gold strips clamped on to the gold wire and then soldered to the potential leads. This precaution was adopted to avoid the possibility of disturbing effects which alloying of the gold and solder might have.

The demagnetization procedure and the temperature measurement of the paramagnetic salts were as described in Darby *et al.* 1951.

The resistance measurements were made in a conventional manner. A current of 0·88 mA was passed through the specimen. The voltage across a standard 1 ohm resistance in the current circuit, measured with a potentiometer, enabled accurate measurements of the current to be made. The voltage across the gold specimen due to this current was measured by means of a feedback galvanometer amplifier of similar design to the one mentioned in Part I.

Results

The resistance of the gold wire at room temperature was approximately 0·75 ohm and at liquid helium temperatures 0·0075 ohm.

The lowest temperature at which resistance measurements were made was approximately $6{\cdot}5 \times 10^{-3}$ deg K. As the specimen warmed up, temperature and resistance measurements were made each minute to begin with, and later on at longer intervals. The results are shown in fig. 4. The value of α as defined above is approximately 10, which is in good agreement with the results of Experiment I of Part I of this paper.

The total heat inflow to the second stage from all causes was 25 erg/min. The electrical power dissipation in the gold wire during measurements was approximately 3·5 erg/min, but the measuring current was on for only about 10 seconds per measurement. It seems reasonable to suppose, therefore, that the temperature of the gold wire would not be appreciably different from that of the surrounding paramagnetic salt. This conclusion is supported by the fact that the measured value of the resistance at a given temperature was independent of whether the measuring current was on for only a few seconds or for periods of about thirty seconds.

Conclusions

The results of these two series of measurements show that the electrical resistivity of gold at low temperatures increases with falling temperature approximately according to

$$R \propto \log\,(\text{const.}/T)$$

down to about 0·006° K. If the increase were due to behaviour similar to that of a semi-conductor, a much more rapid rise would be expected, that is

$$R \propto \exp \theta/T$$

with θ of the order of magnitude of 1° K. The resistance at the lowest temperature would then be orders of magnitude greater than its value at the minimum, whereas the observed increase is only about 3%.

The results for wires subjected to different annealing procedures show no clear correlation between the magnitude of the resistance increase and the physical state of the metal. Unfortunately it is not possible to decide whether the effect is a property of perfectly pure gold or is determined by the presence of impurities (see, however, MacDonald 1952).

ACKNOWLEDGMENTS

Dr. Croft and Mr. Seymour are grateful to the D.S.I.R. for maintenance grants and Dr. Hatton to the Pressed Steel Co. Ltd., Cowley, for a Fellowship. The authors thank Professor Simon for his interest in the work, and Dr. B. V. Rollin for his assistance with the experiments described in Part II.

REFERENCES

DARBY, J., HATTON, J., ROLLIN, B. V., SEYMOUR, E. F. W., and SILSBEE, H. B., 1951, *Proc. Phys. Soc.* A, **64**, 861.
DE HAAS, W. J., CASIMIR, H. B. G., and VAN DEN BERG, G. J., 1938, *Physica*, **5**, 225.
HUDSON, R. P., HUNT, B., and KURTI, N., 1949, *Proc. Phys. Soc.* A, **62**, 392.
KATZ, E., 1952, *Phys. Rev.*, **85**, 495.
MACDONALD, D. K. C., 1947, *J. Sci. Instrum.*, **24**, 232 ; 1952, *Phys. Rev.*, **88**, 148.
MENDOZA, E., and THOMAS, J. G., 1951, *Phil. Mag.*, **42**, 291.
SLATER, J. C., 1951, *Phys. Rev.*, **84**, 179.

XXXII. *A Study of the Reaction* $^{11}B(d, n)^{12}C$ *by an Improved Photographic Method*

By W. M. GIBSON
H. H. Wills Physical Laboratory, University of Bristol*

[Received January 12, 1953]

SUMMARY

A way of simplifying the microscope measurements and the resulting calculations, in the photographic emulsion method of studying neutron spectra, is described. The energy distribution of neutrons from the reaction $^{10}B(d, n)^{11}C$ has been measured, to show that the saving in time is accompanied by no appreciable loss of accuracy.

The method has been used in a study of the angular distribution of neutrons from the reaction $^{11}B(d, n)^{12}C$ at 8·1 MEV. The results are consistent with the theory of the stripping process and confirm that the 4·47 MEV level in ^{12}C, like the ground state, has even parity.

§ 1. INTRODUCTION

THE use of photographic plates for measuring neutron energies has been described by many authors (e.g. Powell 1940, 1942; Richards 1941). Measurements are made on the tracks of protons which have moved forwards, after neutron collision, in directions making small angles with that of the neutron flux. The energy of each neutron, E_n, is then deduced from the proton energy, E_p; the angle between the directions of motion of the neutron and the proton, ϕ, is obtained from the relation

$$E_n = E_p \sec^2 \phi.$$

The usual procedure has been to allow the neutrons to enter the plate parallel to the surface of the emulsion, and on each track to measure the following: the length, a; the angle between the direction of the neutrons and the horizontal projection of the initial direction of the proton, θ; and the vertical component of the first portion of the track, h. h gives the angle of dip δ, a correction being made for the shrinkage of the emulsion in the vertical direction during processing; the range of the proton, R, is equal to $a \sec \delta$. The angle ϕ is determined from the equation

$$\cos \phi = \cos \theta \cos \delta.$$

The range–energy relation gives E_p when R is known, and E_n is calculated from E_p and ϕ.

This method has proved satisfactory in many studies of neutron energy distributions. However, the microscope work is slow, and each track requires several calculations; these facts have limited the number of tracks which it has been practicable to measure in any particular plate; consequently, the statistical accuracy of the value of the neutron flux, obtained from the number of tracks found in a known volume of emulsion, has not usually been great.

---

*Communicated by Professor C. F. Powell, F.R.S.

A new technique has therefore been developed to reduce the time used in measuring and calculating. It is hoped that the measurement of neutron fluxes, and the comparison of fluxes to obtain angular distributions of neutrons from nuclear reactions, will be made less arduous by this technique.

§ 2. The Improved Method

Suppose that the beginning of a track is in focus at a fixed point in the field of view, and that the objective lens or the plate is moved through a small vertical distance F. The part of the track then in focus is defined by its intersection, as it was formed in the unprocessed emulsion, with a plane SF above or below the beginning of the track; S is the factor by which the thickness of the emulsion is reduced during processing, and is about 2·1 for Ilford Nuclear Research emulsions. A track with a given ϕ will appear somewhere on the hyperbola formed by the intersection with this plane of a cone with semi-angle ϕ, apex at the fixed point where the beginning of the track was set, and axis parallel to the neutron direction. A special graticule carrying a series of these hyperbolae could therefore be made and used in a microscope eyepiece for the determination of ϕ in a single operation.

It is possible, however, to reduce the labour of calculation still further: for protons of energy about 10 Mev, the range in Ilford C2 emulsion varies as $E^{1\cdot70}$. Since $E_n = E_p \sec^2\phi$ the range which would have been observed for a proton with the whole of the energy E_n is

$$R_0 = R(\sec\phi)^{3\cdot40},$$

R being the range observed for a track at an angle ϕ. R is not usually measured directly, since it is easier to measure L, the component of the length in the direction of the neutrons; R is then equal to $L \sec\phi$, and

$$R_0 = L(\sec\phi)^{4\cdot40}.$$

Hence it is best to use a graticule with hyperbolae plotted at equal intervals of $(\sec\phi)^{4\cdot40}$, since with such a graticule we need measure only L and $(\sec\phi)^{4\cdot40}$. The product R_0 may then be plotted, and the distribution of ranges re-plotted as a distribution in energy if this is required.

It has been assumed throughout that the tracks are straight: in fact there is some scattering, and it is difficult to estimate the inaccuracy this introduces. The results show, however, that the errors are no greater than in the older method.

The appearance of the graticule used in Bristol is shown in fig. 1; it was constructed by two-stage photographic reduction of an ordinary drawing, onto a plate of very high resolution. The outer hyperbola has $(\sec\phi)^{4\cdot4} = 1\cdot30$; this corresponds to $\phi = 19\cdot5°$. The overall size of the graticule, and its position in the field of view, are chosen so that no appreciable error can be caused by the curvature of the microscope field. It must be confirmed that there is no excessive curvature of the field of any microscope which is to be used for this work, but no difficulty of this sort has yet been encountered.

The known vertical movement is provided by a special attachment on the fine-focussing adjustment. The ordinary control knob (I) is connected to a second knob (II) on the same axis, in such a way that there is free relative movement through a small angle. Because of the presence of backlash in the microscope mechanism, the setting of the start of the track on the origin is done by moving II in one direction and pushing I with it ; the known further movement is made by moving I in the same direction through the whole of the interval of free relative motion. This interval defines F, and its exact magnitude is adjusted to suit the particular objective and graticule in use. Since the scale of each hyperbola is proportional to the magnification, to the vertical distance F, and to the shrinkage factor S, a given graticule can be used with any objective provided that F is suitable adjusted. For the graticule shown in fig. 1, used with a ×45 objective, F is $2{\cdot}9\,\mu$ for plates with $S=2{\cdot}1$.

Fig. 1

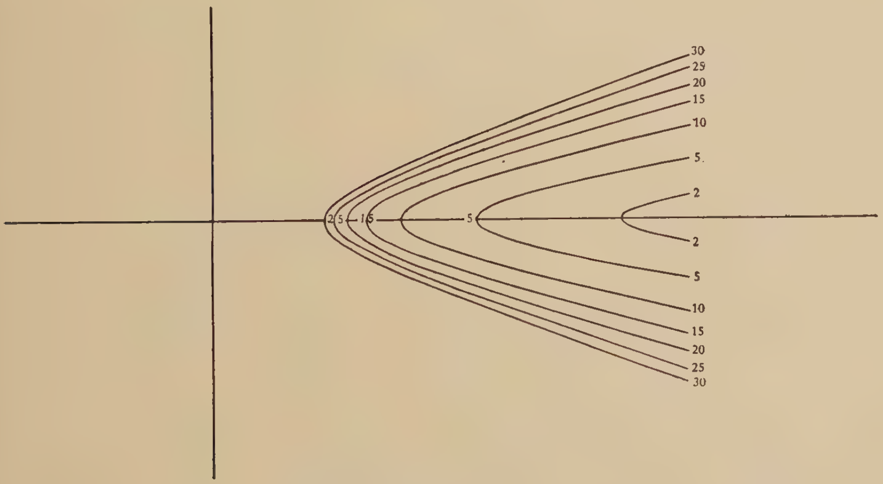

Special graticule for measuring the factor (sec ϕ)$^{4{\cdot}4}$ for tracks of recoil protons. The numbers are % corrections, i.e. $100\{(\sec\phi)^{4{\cdot}4}-1\}$.

The length, L, is measured on the micrometer head of the stage adjustment, modified by the addition of a ratchet device ; the zero is set when the beginning of the track is moved up to the vertical line in the graticule, and the length is read directly when the end of the track is on the same line.

The accurate measurement of dip is always difficult, and in this procedure it is the measurement of dip implicit in the estimation of the factor (see ϕ)$^{4\cdot 4}$ which leads to the chief inaccuracy. However, it is found that the mean error in this factor is about 1%, and this is not excessive. The assumption of a simple power law for the range–energy relation can lead to error if widely differing neutron energies are being measured: calculation shows that the angle 19·5° for which the outside hyperbola is drawn and which corresponds to a factor 1·30 at 10 Mev, gives factors 1·305 at 16 Mev, 1·290 at 6 Mev and 1·282 at 3 Mev; the difference is correspondingly less for the other hyperbolae. This graticule can therefore be used without appreciable systematic error between about 6 Mev and 20 Mev; at lower, or much higher, energies it would be necessary to use slightly different graticules if the greatest possible accuracy were to be obtained.

Fig. 2

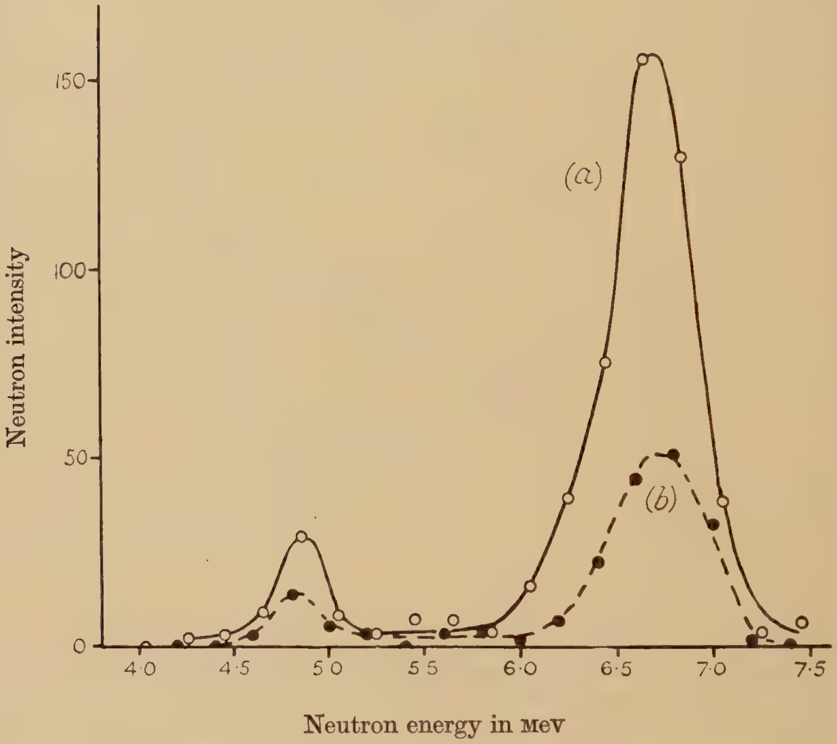

Neutron energy distributions from the reaction $^{10}B(d, n)^{11}C$. Curve (*a*) shows the new results, curve (*b*) those obtained in 1949. Each ordinate is proportional to the number of neutrons in a 0·2 Mev interval. The factor by which the number of proton tracks observed was multiplied to give the neutron intensity, in the arbitrary units used, varied from 1·0 at 7 Mev to 0·6 at 4·5 Mev.

The method was tested with plates exposed to the neutrons emitted at 90° from a ^{10}B target bombarded with 930 kev deuterons. Similar plates had been made the basis of an earlier investigation (Gibson 1949). In fig. 2 the new results are compared with those obtained in 1949 ; the resolution and the accuracy of the new method are at least equal to those of the older and more laborious technique.

Fig. 3

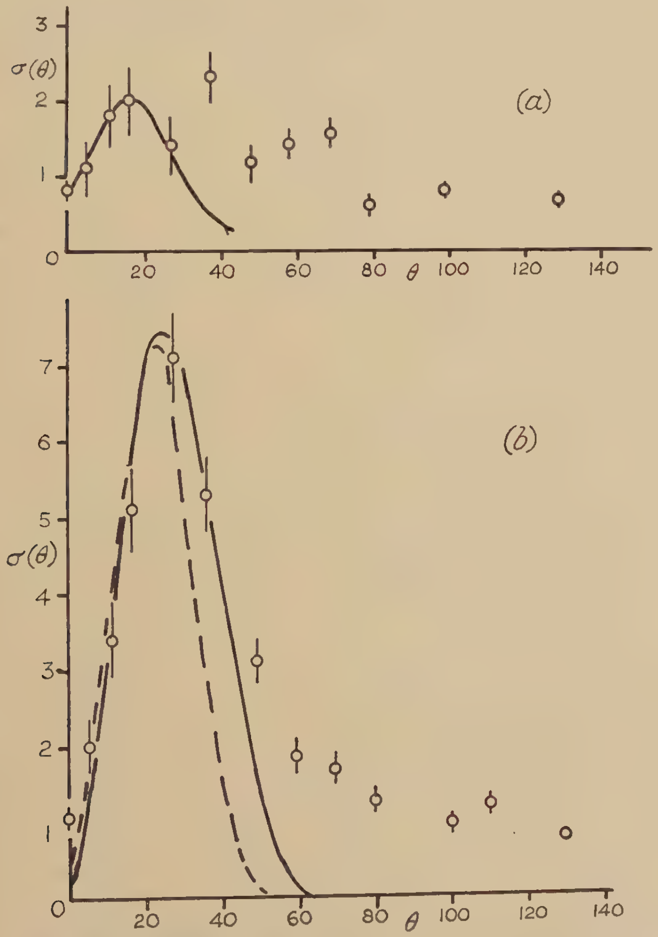

C–m–s angular distributions for neutrons from the reaction ^{11}B(d, n)^{12}C. (*a*) ^{12}C formed in its ground state, (*b*) ^{12}C formed in 4·47 Mev excited state. Full lines are the curves given by Butler's theory, with $l_p=1$, and $r=4{\cdot}4\times10^{-13}$ cm ; broken lines are given by the Born-approximation theory with $l_p=1$ and $r=6{\cdot}4\times10^{-13}$ cm.

The number of tracks in the group attributed to the formation of ^{11}C in an excited state at 2·02 Mev was not great in the original results. The new figures confirm the existence of this level ; since the groups appear at the same energies as before, the energy of the excited state may still be taken as 2·02 MeV.

§ 3. $^{11}B(d, n)^{12}C$

The method, having been tested and found satisfactory, was used in a study of plates exposed to neutrons from the reaction $^{11}B(d, n)^{12}C$; in this case the deuterons were accelerated to an energy of 8·1 MeV in the University of Liverpool cyclotron. The experimental arrangements were the same as those described by Middleton, El-Bedewi and Tai (1953), who have discussed fully the importance of the angular distributions of neutrons from this and similar reactions.

Two groups of neutrons were clearly resolved, and the energies indicated that they were emitted when ^{12}C was formed in its ground state and in the excited state at 4·47 MeV (Gibson 1949). Measurements were made on these two groups at a number of angles, and the differential cross-sections were calculated. The calculations included allowances for the loss of proton tracks through the surfaces of the emulsion and for the variation of n, p scattering cross-section with energy, and the conversion to the centre-of-mass system. The angular distributions obtained are shown in fig. 3.

The results for neutrons from formation of ^{12}C in its excited state fit well with theory, if it is assumed that an angular momentum $l_p=1$ is transferred to the nucleus by the proton which it absorbs. Two theoretical curves are shown in fig. 3: the one with which agreement is closer is based on Butler's theory of the stripping process (Butler 1951), with a radius of $4{\cdot}4\times10^{-13}$ cm (the Gamow radius); the second curve is obtained from the Born-approximation theory (Bhatia *et al.* 1952) with a radius of $6{\cdot}4\times10^{-13}$ cm^2. Both theories, however, show quite definitely that the angular momentum transferred is $l_p=1$. If the ground state of ^{11}B is assumed to have spin 3/2 and odd parity, the 4·47 MeV level in ^{12}C must then have even parity; the results give no information about the spin, except that it must be 0, 1, 2 or 3. Ajzenberg and Lauritsen (1952) suggest spin 2 and even parity.

Theory suggests that formation of ^{12}C in its ground state, by a stripping process, is less likely than formation in the first excited state (W. M. Fairbairn, private communication). This is confirmed by the results shown in fig. 3: the differential cross-sections are lower, and it is probable that competing reactions partly mask the characteristic form which the stripping process gives to an angular distribution. The behaviour below 30°, however, is consistent with the value $l_p=1$; this value is expected, since the ground state of ^{12}C has even parity and spin 0.

ACKNOWLEDGMENTS

The author wishes to express his thanks to Mr. A. R. Gattiker for help in preparing the graticules, to Dr. R. Middleton and other members of the Physics Department of the University of Liverpool, for making the ^{11}B exposure, to Mrs. J. M. Juritz and Mrs. B. M. Herman for much of the microscope work, and to Dr. Middleton and Mr. W. M. Fairbairn for discussions of the stripping theory of the reaction ^{11}B(d, n)^{12}C. He is grateful also to Professors C. F. Powell and H. W. B. Skinner for their continued interest and assistance.

REFERENCES

AJZENBERG and LAURITSEN, 1952, *Rev. Mod. Phys.*, **24**, 321.
BHATIA, HUENG, HUBY and NEWNS, 1952, *Phil. Mag.*, **43**, 485.
BUTLER, 1951, *Proc. Roy. Soc.* A, **208**, 559.
GIBSON, 1949, *Proc. Phys. Soc.* A, **62**, 586.
MIDDLETON, EL-BEDEWI and TAI, 1953, *Proc. Phys. Soc.* A, **66**, 95.
POWELL, 1940, *Nature, Lond.*, **145**, 155 ; *Proc. Roy. Soc.* A, **181**, 344.
RICHARDS, 1941, *Phys. Rev.*, **59**, 796.

XXXIII. *The Cross Section for Star Production in Nuclear Emulsions by* 130 MeV *Protons*

By C. F. LEES, G. C. MORRISON, H. MUIRHEAD and W. G. V. ROSSER
Department of Natural Philosophy, University of Glasgow*

[Received December 15, 1952]

SUMMARY

Methods are described whereby stars produced in nuclear emulsions by protons, in the energy range 110 to 146 MeV may be separated into disintegrations produced in the light (carbon, nitrogen and oxygen), and heavy (silver and bromine) components of the emulsion. The cross sections obtained for nuclear disintegrations are compared with those predicted by the ‘ transparent nucleus ’ theory of Fernbach, Serber and Taylor (1949).

§ 1. INTRODUCTION

THE three components which determine the total cross section for the nuclear scattering of protons of high kinetic energies are :

(*a*) large angle coulomb scattering,

(*b*) diffraction or shadow scattering,

(*c*) inelastic nuclear scattering (Fernbach *et al.*, 1949 ; Gatha and Riddell 1952).

In a nuclear emulsion it is generally possible to separate inelastic events of the type (*c*) from events of the types (*a*) and (*b*). For events in category (*c*) a nuclear disintegration (‘ star ’) is produced, and/or the incident proton loses energy in the scattering ; for coulomb and diffraction scattering there is no large change of energy, and therefore no appreciable change in ionization of the track produced by the proton following the scattering process. Thus in a photographic plate it is possible to identify events of the type (*c*), and to submit them to study without the undesirable inclusion of events of the types (*a*) and (*b*). However, the photographic plate has the disadvantage that it has more than one constituent element. This disadvantage can be partially removed by comparison of the effects produced in normal and diluted emulsions ; the stars observed can then be separated into two main groups, namely those produced in the light elements carbon, nitrogen and oxygen, and those produced in the heavy elements silver and bromine.

In this laboratory an examination of the stars produced by protons with energies in the region of 130 MeV is being carried out. Separation of the stars into two nuclear groups, as a preliminary stage in their examination, will be described in this paper.

---

* Communicated by Professor P. I. Dee, F.R.S.

§ 2. EXPERIMENTAL PROCEDURE

(*a*) *Exposure of the Plates*

Ilford normal and × 4 diluted G5 plates were exposed to the external proton beam of the Harwell cyclotron. The exposure was carried out using the early uncollimated and unducted beam. The protons entering the plate assembly possessed an energy of 146 ± 3 MeV. After allowing for energy loss by ionization in the plates, the protons producing the stars may be considered to have kinetic energies between 110 and 146 MeV.

(*b*) *Examination of the Plates*

The plates were examined using × 50 and × 90 oil immersion objectives and × 6 eyepieces. The search for stars was carried out both by the 'along the track' and 'area' scanning methods (Bernardini *et al.* 1952).

A proton-induced star with *n* secondary charged prongs will be referred to as an np star. All scatterings of the type 1p in which the ionization of the secondary particle was not statistically greater than the ionization of the primary proton were rejected, as diffraction and large angle coulomb scatterings appear as events of this type. With this criterion, 251 and 122 stars were found by the 'along the track' method in the normal and × 4 diluted plates, for total proton path lengths of 8 460 and 7 290 cm respectively. Thus the mean free paths for star formation were $35{\cdot}1^{+2{\cdot}6}_{-2{\cdot}2}$ and $59{\cdot}5^{+6}_{-4{\cdot}5}$ cm respectively (the errors quoted throughout this paper will be the standard deviations). Before the cross sections for nuclear interaction in heavy and light nuclei can be calculated from the data given above, the mean free paths must be corrected for two factors.

(*a*) Sometimes fast protons undergo collisions with free protons, present in the emulsions as the nuclei of hydrogen atoms. These collisions yield events of the type 2p. The contribution to be expected from events of this type was estimated using the published values for the cross section for p–p collisions (Christian 1952, Pickavance and Cassels 1952). This contribution was subtracted from the number of 2p events observed.

(*b*) By rejecting all events in which a proton changes direction without observable change of ionization, some genuine inelastic collisions are rejected. Since the wavelength of the incident proton ($\sim 10^{-13}$ cm) is small compared with nuclear dimensions, the proton may be assumed to make its first collision with an individual nucleon inside the nucleus (Serber 1947). This collision can be of the form p–p (proton–proton) or p–n (proton–neutron), and following this encounter the energy of the two nucleons may vary from equality to the point where one has most of the available kinetic energy. If in a collision one of the nucleons receives most of the available kinetic energy, and this nucleon escapes from the nucleus without further collisions, the residual nucleus can receive only a small excitation energy and it is unlikely that slow charged particles will be emitted. In this case, if the fast secondary particle is a proton, a 1p type event can then occur, but is rejected due to our criterion for the selection of stars. If the fast secondary particle is a neutron, the incident proton can appear to stop in the emulsion with no resultant prongs ('0p star'). The recognition of 0p events is unambiguous. A correction for the genuine 1p stars rejected was therefore made by estimating the ratio of the number of stars with a single secondary proton of high energy to the number of 0p stars. This was done by using the published cross sections for free p–p and n–p scattering (Christian 1952, Pickavance and Cassels 1952), and assuming as a rough approximation that the target nucleons could be considered as stationary in a potential well. A value of 2·5* was obtained for the ratio. Therefore 2·5 times the number of 0p stars observed was added to the number of 1p stars accepted in the original measurements.

Following these corrections, the mean free paths for star production became $32{\cdot}6^{+2\cdot5}_{-2\cdot0}$ and 54^{+6}_{-5} cm for normal and ×4 diluted emulsions respectively.

§ 3. Separation of Stars

(*a*) *Method of Prong Distribution in Normal and Diluted Emulsions*

In the conditions of our experiment the mean free path, λ_n, for the production of a star with n prongs is related to the cross section for production by the equation

$$N_H\sigma_{H_n}+N_L\sigma_{L_n}=\frac{1}{\lambda_n}, \quad . \quad . \quad . \quad . \quad . \quad . \quad . \quad . \qquad (1)$$

where N_H=number of silver and bromine atoms per cm³ in the emulsion ($N_H=2{\cdot}06\times10^{22}$ and $0{\cdot}92\times10^{22}$ atoms per cm³ for normal and ×4 diluted emulsions respectively), N_L=number of carbon, nitrogen and oxygen atoms per cm³ ($N_L=2{\cdot}69\times10^{22}$ and $4{\cdot}33\times10^{22}$ atoms per cm³ for normal and ×4 diluted emulsions respectively), σ_{H_n}=mean cross section for the production of a star with n prongs in silver and bromine nuclei, σ_{L_n}=the corresponding cross section for carbon, nitrogen and oxygen nuclei.

Thus if λ_n is known, the cross section σ_{H_n} and σ_{L_n} may be derived by applying eqn. (1) to normal and ×4 emulsions. The total cross section for star production in light and heavy nuclei may be obtained in a similar fashion.

---

* There is little data on the maximum energy that can normally be transferred to a nucleon inside a nucleus without giving rise to the emission of a slow charged particle. An upper limit of 25 Mev was used in this calculation. This figure is suggested by the absorption of negative μ-mesons by protons in nuclei. The maximum energy transferred to the nucleus in this case is about 25 Mev (Tiomno and Wheeler 1949), and about 5% of the interactions are accompanied by the emission of slow charged particles (Fry 1952). The figure of 25 Mev also represented a rough lower limit on the energy loss that could be detected by grain counting on the incident and scattered tracks in 1p events. The factor 2·5 was found to be not very sensitive to the value assumed for the maximum energy transferred in the collision.

In order to improve the statistics for the prong distribution, data on stars found by area scanning was added to that obtained by along the track scanning. It was found that although the mean free path obtained from area scanning was considerably longer (×1·5) than that obtained from along the track scanning, the relative prong distributions were identical for stars other than of the 0p type. We attribute this result to the difficulty of properly overlapping scans, when using high power objectives with very small fields of view. The data obtained from area scanning was therefore normalized to the overall mean free path obtained by along the track scanning, for all stars other than of the type 0p. The frequency distribution of prong size for stars produced by 130 MeV protons in normal and ×4 emulsions is given in fig. 1. The number of stars with n prongs is given in terms of the parameter $1/\lambda_n$.

Fig. 1

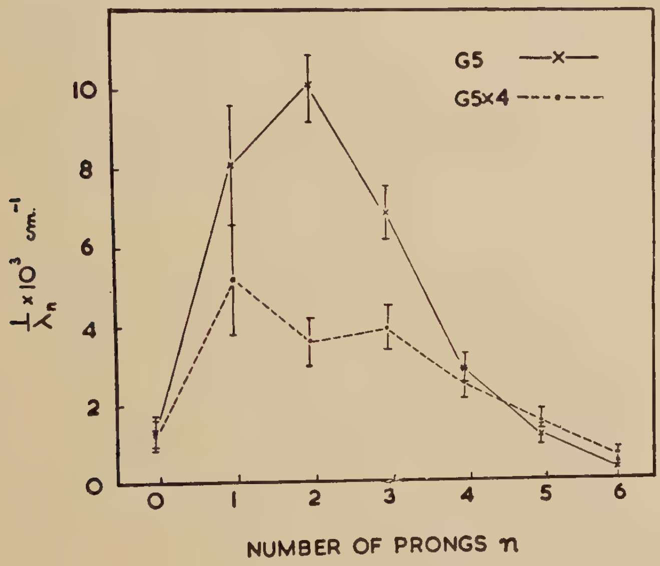

Table 1

Type of star	σ_{H_n} ($\times 10^{26}$ cm^2)	σ_{L_n} ($\times 10^{26}$ cm^2)
0p	4 ± 3	$2 \pm 1{\cdot}5$
1p	32 ± 12	5 ± 5
2p	53 ± 7	$-(3 \pm 4)$
3p	30 ± 5	3 ± 2
4p	9 ± 3	$4 \pm 1{\cdot}5$
5p	1 ± 2	$3{\cdot}5 \pm 1$
6p	$-(1 \pm 1)$	$1{\cdot}5 \pm 0{\cdot}5$

Using the values for $1/\lambda_n$ given in fig. 1, σ_{H_n} and σ_{L_n} were calculated using eqn. (1). The results are shown in table 1 ; it can be seen that σ_{L_n} only becomes larger than σ_{H_n} for 5 and 6 prong stars and that for all practical purposes the 1, 2 and 3p stars are all produced in heavy nuclei.

The overall cross sections obtained for star production were found to be $(128 \pm 16) \times 10^{-26}$ cm^2 in heavy nuclei, and $(16 \pm 7) \times 10^{-26}$ cm^2 in light nuclei.

(*b*) *Alpha-particle Method*

Considerable work has been performed on the numbers of α-particles which emerge from stars formed by the cosmic radiation. It has been found that the ratio of α-particles to all tracks of energy less than ~30 MeV is 0·27 for silver and bromine nuclei and 0·5 for gelatine nuclei (Rochester and Rosser 1951). We have examined the numbers of α-particle tracks appearing from stars initiated by 130 MeV protons in normal emulsions. In an analysis of this type an α-particle is given the overall definition of a particle whose track has a range greater than 5 microns, and whose charge is $\geqslant 2e$; we have followed this convention.

Fig. 2

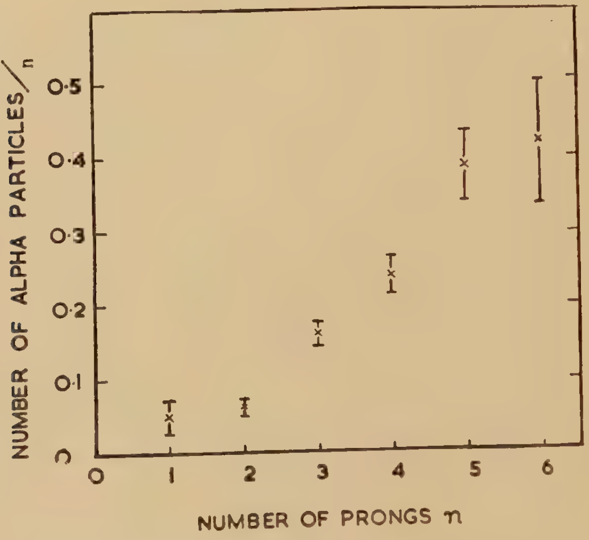

The ratio of the number of α-particle tracks to total number of prongs as a function of the latter figure is given in fig. 2. It can be seen that the ratio increases steadily with the number of prongs associated with a star and appears to flatten at the value of ~0·4 for 5 and 6 prong stars. The energy distributions of α-particles also show a difference for 1, 2 and 3p stars compared with 5 and 6p stars. This is illustrated in fig. 3.

The data presented in figs. 2 and 3 support the conclusion reached in the previous section regarding 5 and 6p stars—namely that they are mainly formed by the disintegration of the light gelatine nuclei. The energy distribution of α-particles from these stars shows a peak in the region of 4 Mev. This result is consistent with the low potential barrier confronting the α-particles in light nuclei. In addition the value of 0·4, for the ratio of α-particles to total prong number for 5 and 6p stars, is in good agreement with that found for stars formed by the cosmic radiation in pure gelatine (Harding 1951).

Fig. 3

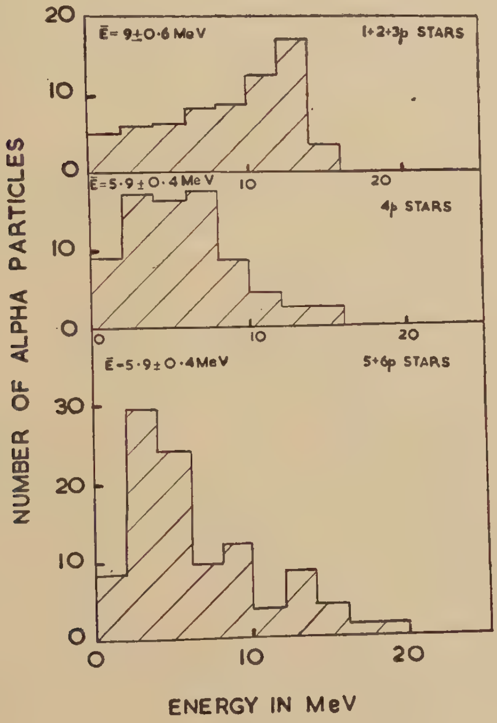

In the 1, 2 and 3p stars the ratio of α-particles to total prong number is considerably lower than that found in stars formed in silver and bromine nuclei by the cosmic radiation. This result is to be expected since the cosmic ray stars involve a considerably greater excitation of the nucleus than that produced by 130 Mev protons. Most of the particles of energy <30 Mev ejected in the cosmic-ray stars are evaporation particles and have a nearly isotropic prong distribution, whereas in our case the ratio of the number of slow protons travelling forward in the direction of the incident particle to the number in the backward direction was found to be 2·5. Seed (1952) has observed a similar effect for stars produced by protons with a kinetic energy of 100 Mev; the result may be interpreted in terms of protons directly knocked on in collisions produced by the primary particle. The energy distribution of α-particles from 1, 2 and 3p stars has a peak in the region of 12 MEV. This result is consistent with the high potential barrier presented to α-particles by silver and bromine nuclei. Thus the data obtained on the 1, 2 and 3p stars again supports the conclusion reached in the previous section.

A rough cross section for star production in light nuclei was estimated by assuming that all the 5 and 6p stars, and all the other stars with at least one α-particle of kinetic energy less than 9 MEV were produced in carbon, nitrogen or oxygen (Menon, Muirhead and Rochat 1950). This yielded a value of $\sim 15\times 10^{-26}$ cm^2 for the total cross section for star production in light nuclei. This figure is probably an underestimate, since reactions of the type $^{12}C(p, pn)^{11}C$ (Dickson and Randle 1950) would probably not be recognized as the disintegration of a light nucleus.

§ 4. CONCLUSIONS

Protons with a kinetic energy of 130 MEV produce larger stars in light than in heavier nuclei. Although the comparison of stars in normal and ×4 diluted emulsions allows a statistical separation of the stars to be made, it does not show the characteristics of the individual stars. The individual stars formed in the light nuclei may be recognized in many cases, however, by the high α-particle to total prong number ratio, and by the low energy of the α-particles emitted.

It is of interest to compare the measured cross sections for star production in light and heavy nuclei with the 'transparent nucleus' theory of Fernbach *et al.* (1949). These authors derive cross sections for the absorption and diffraction scattering of energetic nucleons by nuclei with the aid of an optical model, in which the effect of the passage of a nucleon wave through a potential well is examined. They derive a formula for the nuclear interaction of the following form:

$$\sigma=\pi R^2\left[1-\{1-(1+2KR)\,e^{-2KR}\}\frac{1}{2K^2R^2}\right], \quad . \quad . \quad . \quad (2)$$

where σ=cross section for nuclear interaction, R=nuclear radius, K=absorption coefficient (this term is the inverse of the mean free path, λ_0, of the incident particle in nuclear matter). A similar expression has been obtained by Bethe (1940).

Perry (1952) has shown that K and hence σ can be obtained from the single measurement of λ (the total mean free path for star production in any emulsion), if a value of R and the correctness of eqn. (2) are assumed. His method is equivalent to inserting the expression for σ in eqn. (2) into eqn. (1), giving

$$\sum_i N_i\pi R_i^2\left[1-\{1-(1+2KR_i)\,e^{-2KR_i}\}\frac{1}{2K^2R_i^2}\right]=\frac{1}{\lambda}, \quad . \quad . \quad (3)$$

(the subscripts i refer to the atomic constitution of the emulsion). Since both N_i and λ are known in this equation, K may be obtained if a suitable figure for the nuclear radius is assumed.

The term K is related to the cross sections for free proton–proton and proton–neutron scattering by the expression

$$K=\frac{1}{\lambda_0}=\frac{3A\alpha}{4\pi R^3}\,\frac{[Z\sigma_{pp}+(A-Z)\sigma_{pn}]}{A}, \quad . \quad . \quad . \quad . \quad . \qquad (4)$$

where A=atomic weight of the nucleus, Z=atomic number of the nucleus, σ_{pn}=total cross section for free proton–neutron scattering, σ_{pp}=total cross section for free proton–proton scattering, α=exclusion principle factor which reduces the free particle scattering inside the nucleus.

The quantities σ_{pn} and σ_{pp} have been measured (Christian 1952, Pickavance and Cassels 1952), and α may be calculated with the aid of a Fermi gas model for the nucleus (Goldberger 1948). Hence K may be obtained if a value for R is assumed. In table 2 the value of K expected from this formula is compared with that obtained from eqns. (2) and (3). Values for R equal to $1\cdot37\,A^{1/3}\times10^{-13}$ cm and $1\cdot47\,A^{1\cdot3}\times10^{-13}$ cm were assumed.

Table 2

Nuclear radius $\times10^{13}$ cm	Energy of protons in MeV	$K\times10^{-12}$ cm^{-1}	
		Transparent nucleus	Expected from eqn. (4)
$1\cdot37\,A^{1/3}$	130	$2\cdot9^{+0\cdot8}_{-0\cdot4}$	2·6
	220	$2\cdot9^{+0\cdot8}_{-0\cdot4}$	2·5
	375	$1\cdot7^{+1\cdot2}_{-0\cdot5}$	2·4
$1\cdot47\,A^{1/3}$	130	$2\cdot0^{+0\cdot4}_{-0\cdot3}$	2·1
	220	$1\cdot9^{+0\cdot3}_{-0\cdot3}$	2·0
	375	$1\cdot1^{+0\cdot7}_{-0\cdot3}$	1·9

Table 3

Cross sections $\times10^{26}$ cm^2	σ_H	σ_L
Measured	128 ± 16	16 ± 7
Transparent R $1\cdot37\,A^{1/3}\times10^{-13}$ cm	110^{+5}_{-4}	25^{+3}_{-2}
Nucleus theory R $1\cdot47\,A^{1/3}\times10^{-13}$ cm	111^{+6}_{-5}	23^{+2}_{-2}

In addition to our data, values of K are also compared with those obtained from the published values for λ at 220 MeV (Perry 1952), and at 375 MeV (Bernardini *et al.* 1952). In the latter case we have assumed that the values for the cross sections of the free proton–proton and proton–neutron scattering at 375 MeV may be estimated by extrapolation of the results obtained from measurements at somewhat lower energies.

In table 3 the experimental values given in § 3 for the cross sections for star production in light and heavy nuclei are compared with those obtained by substitution of K from table 2, column 3, into eqn. (2). The cross sections σ_H and σ_L obtained by both methods are in satisfactory agreement, thus indicating that eqn. (2) is reasonably accurate for both heavy and light constituents of the emulsion.

§ 5. ACKNOWLEDGMENTS

The authors wish to express their gratitude to Professor P. I. Dee, F.R.S. for his interest in the course of this work, and to Sir John Cockcroft, F.R.S. for his kindness in providing the facilities of the Harwell cyclotron. We are especially grateful to Dr. T. G. Pickavance and the members of the cyclotron group at Harwell for carrying out the exposures of the plates, and for their help in every possible way.

Lastly we wish to thank the Misses W. Green, E. Rose and M. Ross for their patience during the scanning of the plates.

REFERENCES

Bernardini, Booth and Lindenbaum, 1952, *Phys. Rev.*, **85**, 826.
Christian, 1952, *Rep. Progr. Phys.*, **15**, 68.
Dickson and Randle, 1950, *Nature, Lond.*, **166**, 235.
Fernbach, Serber and Taylor, 1949, *Phys. Rev.*, **75**, 1352.
Fry, 1952, *Phys. Rev.*, **85**, 676.
Gatha and Riddell, 1952, *Phys. Rev.*, **86**, 1035.
Goldberger, 1948, *Phys. Rev.*, **74**, 1269.
Harding, 1951, *Phil. Mag.*, **42**, 63.
Menon, Muirhead and Rochat, 1950, *Phil. Mag.*, **41**, 583.
Perry, 1952, *Phys. Rev.*, **85**, 497.
Pickavance and Cassels, 1952, *Nature, Lond.*, **169**, 520.
Rochester and Rosser, 1951, *Rep. Progr. Phys.*, **14**, 227.
Seed, 1952, *Phys. Rev.*, **87**, 182.
Serber, 1947, *Phys. Rev.*, **72**, 1114.
Tiomno and Wheeler, 1949, *Rev. Mod. Phys.*, **21**, 153.

XXXIV. *An Experimental Study of Radio Reflections from Meteor Trails*

By R. L. Closs, J. A. Clegg and T. R. Kaiser
Jodrell Bank Experimental Station, University of Manchester*

[Received November 13, 1952]

Abstract

The character of the radio echoes obtained from the ionized trails produced by meteors has been investigated. The dependence on the polarization of the incident wave has been studied and the existence of resonant scattering with transverse polarization verified. The magnitude of the resonance and its dependence on the electron line density, α, is found to be in good agreement with theory, as is also the variation of echo amplitude with α.

§1. Introduction

Various authors (Herlofson 1951, Feinstein 1951, Kaiser and Closs 1952) have made theoretical studies of the scattering of electromagnetic waves by the ionized column of air created by the passage of a meteor through the upper atmosphere. All predict that, under certain circumstances, resonant scattering may occur when the incident electric vector is normal to the axis of the meteor trail (transverse scattering). According to the theory of Kaiser and Closs, the echoes fall into two categories, depending on whether the electron line density produced by the meteor is greater or less than a few times 10^{12} cm^{-1}. The present investigation is concerned with an experimental study of the echo characteristics for comparison with this theory, the main predictions of which may be summarized as follows :—

(*a*) *Electron line density*, α, $<10^{12}$. If the incident electric vector is parallel to the trail axis (parallel scattering) it is sufficient to regard the electrons as an assembly of free scatterers, hence when the radius, r_0, of the column of ionization is small compared with $\lambda/2\pi$ (λ=free space wavelength) the scattering formula of Lovell and Clegg (1948) is valid. As r_0 increases (through diffusion), the echo amplitude will decay in a manner depending on the variation of electron volume density, n cm^{-3}, with radius r cm from the axis and time t sec. If, initially, $r_0 \ll \lambda/2\pi$ and if heating of the column may be neglected, solution of the diffusion equation gives

$$n=n_0 \exp\left[-(r/r_0)^2\right] , \qquad (1)$$

where $n_0=\alpha/\pi r_0^2$, $r_0^2=4Dt$, D cm^2 sec^{-1}=diffusion coefficient. The echo amplitude varies with time according to the law $\exp(-4k^2Dt)$, $k=2\pi/\lambda$. The duration to amplitude $\exp(-1)$ times the maximum is thus

$$\tau=(4k^2D)^{-1} . \qquad (2)$$

---

* Communicated by Professor A. C. B. Lovell.

The assumptions made concerning the diffusion process lead to results consistent with observation. The effect of neglecting factors such as heating of the column and of electron loss through recombination and attachment will be considered elsewhere.

With transverse scattering the reflection coefficient passes through a maximum at resonance, subsequently falling to the same value as for parallel scattering, followed by the exponential decay. The resonance occurs when the axial dielectric constant equals $-1{\cdot}4$, and its theoretical magnitude, η (measured as the maximum ratio between echoes obtained from a single meteor with transverse and parallel scattering) is $2{\cdot}0$ when $\alpha \ll 10^{12}$, decreasing to unity when α becomes a few times 10^{12} cm^{-1}. We have reproduced, in fig. 1, the predicted ratio between the amplitude reflection coefficients, $g_\perp/g_\parallel$ as a function of $4k^2Dt/\alpha$ for the case $\alpha \ll 10^{12}$.

Fig. 1

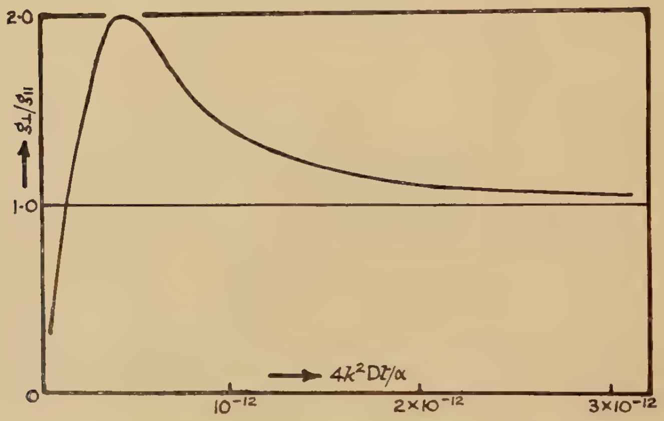

Theoretical polarization ratio, $g_\perp/g_\parallel$, as a function of $4k^2Dt/\alpha$, for $\alpha \ll 10^{12}$.

The additional assumption implicit in the above is that the meteor velocity is such that several Fresnel zones are traversed in a time small compared with τ; this is satisfied by the echoes obtained in the experiment.

(*b*) $\alpha \gg 10^{12}$. The incident wave no longer penetrates throughout the column, which reflects similarly to an expanding metallic cylinder. When $t > \tau$, $(r_0 > \lambda/2\pi)$, it is sufficient to assume total reflection at the surface of critical density, as in the case of ionospheric reflection, hence the echo persists until the axial electron density falls below the critical value. Except initially $(t < \tau)$, when $g_\perp < g_\parallel$, the theoretical reflection coefficients are equal and substantially constant in magnitude. In fact, echoes of duration greater than a few tenths of a second exhibit rapid amplitude fluctuations which Greenhow (1952) has ascribed to distortion of the trail by atmospheric turbulence and wind gradients.

For an echo of class (*a*) the duration is equal to τ, given by (2), i.e. independent of line density, while the amplitude is proportional to α.

For class (*b*) the amplitude varies only as $\alpha^{1/4}$ while the duration, τ' is greater than τ, being proportional to α. Both τ and τ' vary as $\lambda^2 D^{-1}$.

§ 2. The Apparatus

In order to test the above theoretical predictions it was decided to make independent measurements with transverse and parallel polarization of the echo amplitude obtained from a single meteor trail. The equipment was designed to operate during the activity of a major meteor stream with a fairly well defined radiant point, so that at any given time the meteors were travelling in parallel paths.

The complete aerial system consists of an array of six half wave dipoles mounted $\lambda/8$ in front of a conducting sheet which itself contains an array of six $\lambda/2$ slots. A second conducting sheet is mounted $\lambda/8$ behind the slot plane. The aerial is steerable in azimuth and elevation and during the experiment the fan-beam was continuously adjusted to maintain the polarization of the radiation from the slot and dipole arrays, parallel and transverse respectively to the meteor paths. The minimum elevation of the aerial beam, 30°, is such that effects of ground reflection may be neglected. Preliminary experiments had indicated that an aerial of this nature would ensure identical polar diagrams for the two polarizations; unfortunately the experimental results indicate that this ideal was not realized (see below).

Fig. 2

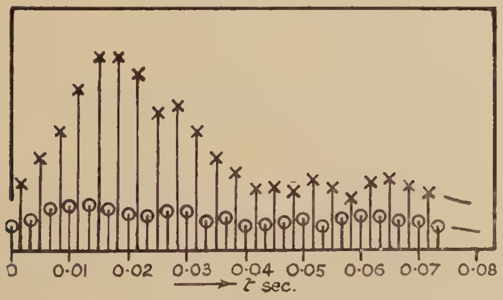

Short duration echo.
o Echo pulses received on slot array.
x ,, ,, ,, ,, dipole array.

The transmitter output of 40 kw, peak power, in 8 μsec pulses, is delivered equally to the two aerial arrays through twin T–R switches. By means of switched preamplifiers the slot and dipole array are connected to a 600 kc/s bandwidth receiver in alternate intervals between transmitter pulses, and thence to an automatic recorder of the type described by Ellyett and Davies (1948). The twin cathode ray tube recorder display has a fast time base for range measurements and a slow time base (duration 0·1 sec) which displays the individual echo pulses in sequence. A record of a short duration echo showing the two sets of echo pulses, is reproduced in fig. 2.

The mechanical design of the aerial system made it impossible to measure the polar diagrams by conventional methods. An overall check on the equipment was, however, attempted by attaching to a hydrogen filled balloon, a wire cage reflector so constructed as to be insensitive to polarization. Two successful flights were obtained but owing to the short time for which the reflector was in range of the equipment, sufficient measurements could not be obtained to predict the variation of the error over the complete polar diagram. Measurements made over a range of ±10° (in a vertical plane) from the supposed centre of the aerial beams showed an error which varied between 1·5 and 3·0 (in favour of the dipole array). It will be seen that this is consistent with the results discussed below.

§ 3. Experimental Results and Analysis

The complete equipment was first operated during the Geminid meteor shower of December, 1950, with the results described by Clegg and Closs (1951). Almost all echoes appeared with greater amplitude on the dipole aerial which was interpreted as indicating enhanced transverse scattering due to the plasma resonance effect. The transverse/parallel echo ratio ranged between 2 and 10.

Observations were continued in 1951 during the summer daytime meteor showers (Clegg *et al.* 1947, Aspinall *et al.* 1948, Aspinall and Hawkins 1951) and the analysis of these results is discussed in the following. The period covered is between June 4th and 12th when the predominant activity was from the Arietid radiant. In order to eliminate partially the sporadic meteors and meteors which may have been observed in the aerial side lobes, echoes with ranges outside the limits 100–250 km were rejected as were also those for which the larger signal was less than five times receiver noise level, leaving a total of 140. These were divided into two groups (i) and (ii), the former being echoes which did not exhibit a decay during the length of the slow time base (0·1 sec). A consideration of the expected range of values of the diffusion coefficient in the meteor ionization region, showed that this should result in the echoes of group (i) being exclusively of category (*b*) of § 1, while group (ii) would contain a large proportion of category (*a*).

Group (i)

These echoes exhibited in all cases a substantially constant ratio, ρ, throughout their lifetime, however ρ was often considerably greater than the theoretical value of unity, assuming the echoes to fall into category (*b*) of § 1. A histogram showing the distribution of polarization ratio among the 46 echoes is given in fig. 3. It is our belief that the deviations from unity of ρ are due to experimental errors, mainly arising from defects in the slot aerial array, which result in a reduced sensitivity and a distorted polar diagram. This is substantiated in the following discussion, hence fig. 3 may be interpreted as a distribution of experimental errors, in which case the 46 echoes correspond to electron line densities large compared with 10^{12} cm^{-1}.

Group (ii)

The majority of these had an echo ratio which varied during the echo lifetime. Each echo was plotted and the ratio, ρ, was evaluated as a function of time, t. Figure 4 gives ρ vs t for the echo of fig. 2. Of the 94 echoes, 45 were of this general type for which ρ first increased to a maximum value, ρ_{m}, and then decreased to a fairly constant value, ρ_{∞}. Except for the deviations of ρ_{∞} from unity these are of the form predicted for echoes exhibiting the plasma resonance with transverse scattering. Of the

Fig. 3

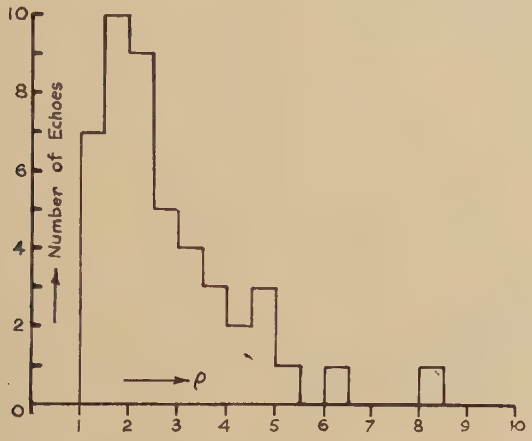

Distribution of measured polarization ratio, ρ, for the 46 echoes of group (i) (long duration echoes).

Fig. 4

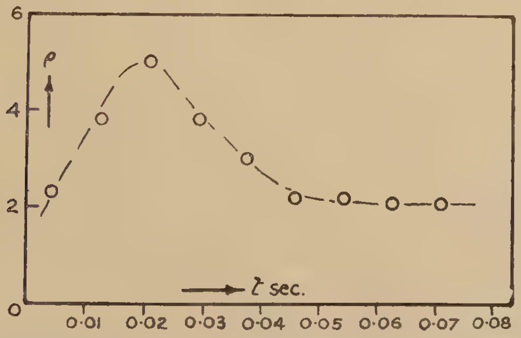

Experimental polarization ratio, ρ, vs t for the echo of fig. 2. Each point represents an average over several echo pulses.

remainder, 31 were similar to the echo shown in fig. 5. In these cases, ρ was either substantially constant or else increased monotonically to a steady value, ρ_∞, while the echoes had an initial rapid rise, a short period of fairly constant amplitude (in most cases) followed by an approximately exponential decay. Except again for the deviations of ρ_∞ from unity, these echoes have the general form expected from line densities greater than a few times 10^{12} cm^{-1} namely category (*b*) of § 1.

Thirteen echoes of doubtful character were eliminated from this part of the analysis, and for 5 which did not exhibit a signal on the slot aerial, only a lower limit could be set for ρ_∞.

Fig. 5

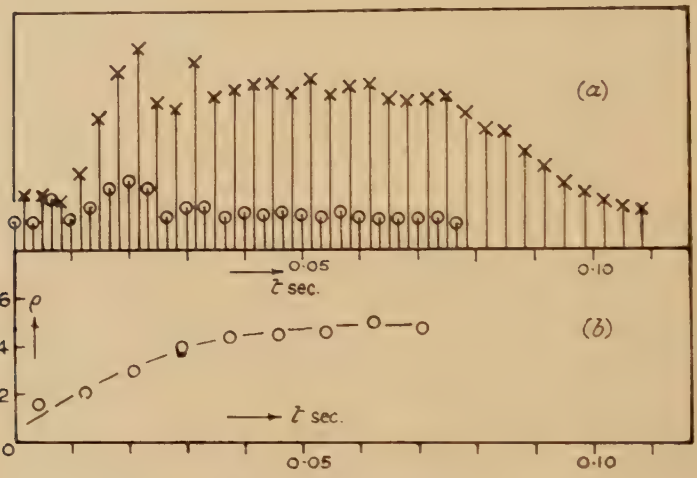

(*a*) Non-resonant echo.
(*b*) ρ vs t for the echo of (*a*).

Figure 6, which gives the distribution of ρ_∞ amongst these echoes is remarkably similar to fig. 3. To facilitate comparison, fig. 3 has been normalized by the factor 81 : 46 (the ratio of the number of echoes in the two groups) and reproduced as the broken line of fig. 6. The agreement strongly supports the assumption which we make in the following analysis that these distributions represent experimental errors. The ratios of fig. 6 are slightly greater, on the whole, than those of fig. 3 which may, in part, be due to decay of the slot echo into receiver noise before the asymptotic limit, ρ_∞, is reached.

On these assumptions, the ratio ρ_m/ρ_∞ represents the true resonant polarization ratio, η. The values of η obtained for the 76 echoes are given in fig. 7. The 45 echoes which appear to exhibit the resonance effect show a maximum in the distribution corresponding to $\eta=1{\cdot}7$, in good agreement with the theoretical value of 2·0.

§4. Electron Line Densities

The existence or otherwise of the resonance enables the echoes of group (ii) to be divided into the two electron line density categories (*a*) and (*b*) of § 1. In addition, since the resonance should occur when the axial

Fig. 6

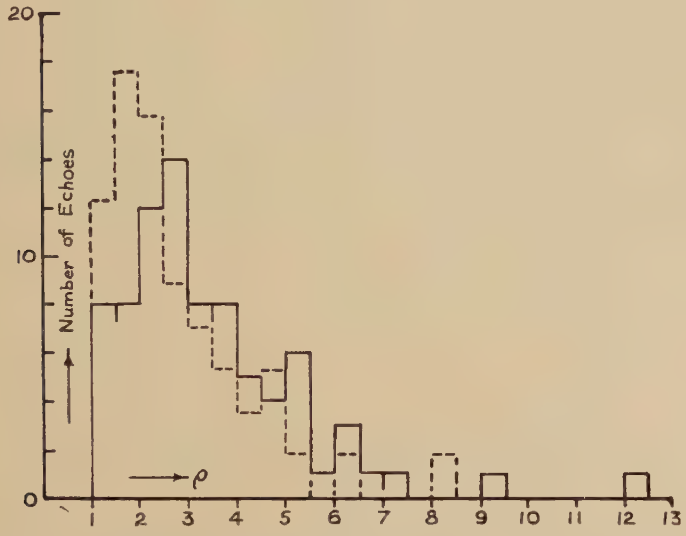

——— Distribution of values of ρ_∞ for the echoes of group (ii).
– – – – – As for fig. 2, with ordinates increased in the ratio 81 : 46.

Fig. 7

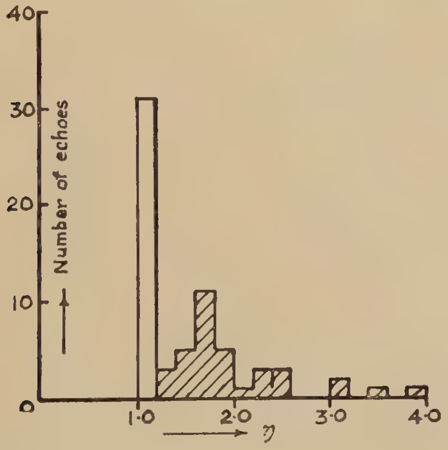

Distribution of values of the true resonant polarization ratio, η, for the echoes of group (ii). The shaded portion represents the echoes exhibiting the resonance effect.

dielectric constant is $-1{\cdot}4$, the line density of an individual trail may be estimated, if the instant, t_r, when $\rho=\rho_m$, and the time constant, τ, of the exponential decay are known. The appropriate relation is

$$\alpha=2{\cdot}14\times10^{12}\, t_r/\tau\,. \qquad (3)$$

For the non-resonant echoes (category (*b*)) a similar estimate may be obtained from a knowledge of τ and of τ', the total echo duration. Figure 8 shows the dependence of α on τ'/τ derived from the theory of Kaiser and Closs. Using (3) and fig. 8, line densities were estimated in 66 cases.

The echo amplitude is also a function of α, as well as of range ($\propto R^{-3/2}$) and of the position of the meteor trail in the aerial polar diagram. The amplitude of the slot and dipole echoes were recorded in arbitrary units, reduced to a common range of 100 km and for the former group, corrected by the factor ρ_∞. In order to eliminate partially the polar diagram effect, the results were divided into groups according to the estimated line density, namely, 1 $-<2$, 2 $-<4$, 4 $-<8$, 8 $-<16$, 16 $-<32$, 32 $-<64\times10^{11}$ cm^{-1} containing 4, 9, 17, 12, 9, 15 echoes respectively, and the line densities and corrected amplitudes were averaged for each group. The result is plotted in fig. 9; the amplitude scale of the theoretical curves given for comparison has been adjusted so that they fit the experimental points for the smaller line densities. The agreement is satisfactory with the possible exception of the group $16\text{–}32\times10^{11}$ cm^{-1}.* The saturation of echo amplitude for line densities above 10^{12} cm^{-1} is particularly apparent.

Fig. 8

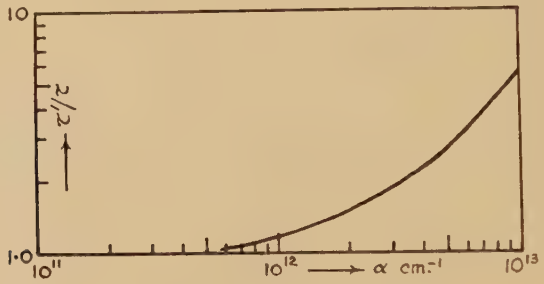

α vs τ'/τ according to Kaiser and Closs.
τ =decay constant defined by (2).
τ'=total duration to exp (-1) times maximum amplitude.

The variation of η with α, obtained from the averaged results, is given in fig. 10, together with the theoretical curve.

---

* Due to various factors (e.g. finite meteor velocity and finite transmitter pulse interval) it is possible that some category (*a*) echoes arising from low electron densities, would not exhibit the polarization effect. The above analysis, however, would place these in the line density group $16\text{–}32\times10^{11}$cm^{-1} with the effect of depressing the average amplitude for this group.

The amplitude scale of fig. 9 is such that the value at line density $1{\cdot}65\times10^{11}$ corresponded to a signal received on the dipole aerial with a maximum amplitude about 5 times the receiver noise level. The mean

Fig. 9

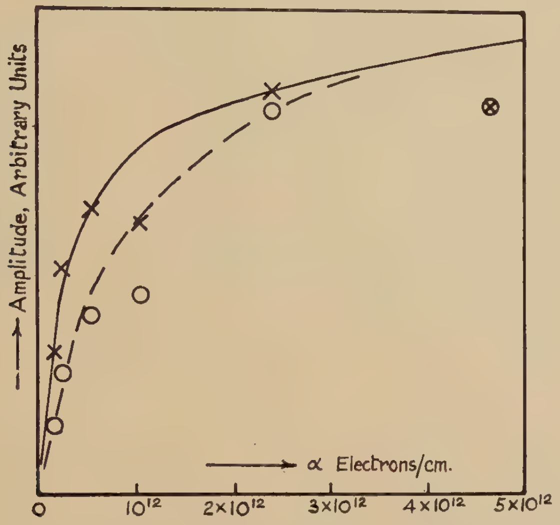

Echo amplitude (reduced to range 100 km and corrected for experimental errors) vs electron line density.

x Transverse scattering. o Parallel scattering.
———— } Theoretical curves adjusted to fit the experimental
– – – – – } points for small line densities.

Fig. 10

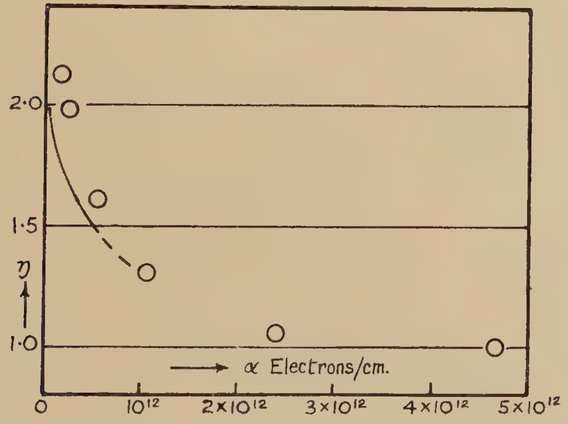

True resonant polarization ratio, η, vs electron line density.
o Experimental.
—— Theoretical.

range for this group of echoes was 130 km giving an estimate of the equipment sensitivity. An independent estimate may be obtained from the equipment parameters previously given. Assuming a receiver noise factor of 10 db, a mean integrated sky background temperature of 2000° K, an aerial gain of 20 (referred to an isotropic radiator) and taking account of the polarization ratio, a 5× noise echo on the dipole aerial would require a line density of $1{\cdot}5\times10^{11}$ at the above range.

§ 5. Diffusion Coefficients

For 76 echoes of group (ii) it was possible to estimate the decay constant, τ, and hence, using (2) the diffusion coefficient D. The results are given in fig. 11, the most probable value being $2\text{–}2{\cdot}5\times10^4$. This value should be related to the conditions of the atmosphere at the corresponding height, which, for the Arietid shower, has been determined independently by Evans and Kaiser (unpublished) at 88 km.

Fig. 11

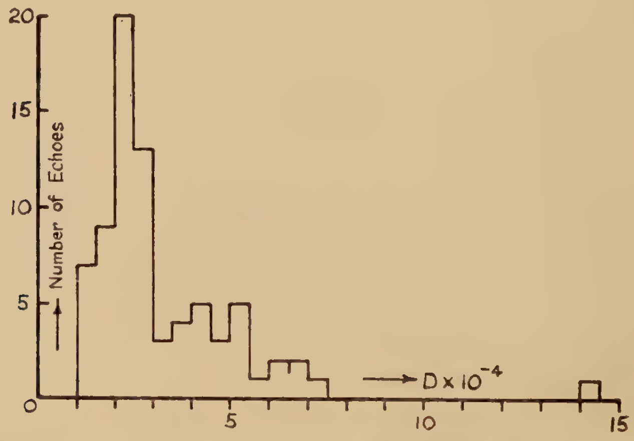

Distribution of diffusion coefficient for the echoes of group (ii).

A simple theory of ambipolar diffusion suggests that, as a result of the space charge electric field within the ionized column, the effective diffusion coefficient is related to the classical kinetic theory value of the ionic diffusion coefficient, D_i, by

$$D=D_i\,(1+T_e/T_i)\,, \qquad \ldots\ldots\ldots \quad (4)$$

where T_e and T_i are the electron and ion temperatures respectively. Putting $T_e=T_i=T$ and assuming the ionic mass, m g, to equal the mass of the neutral air molecules (this should be approximately true, even for ionized meteor atoms) we obtain

$$D=\frac{4}{3}\,\lambda_i\left(\frac{8kT}{\pi m}\right)=3{\cdot}6\times10^3\,\lambda_i\,T^{1/2}\ \mathrm{cm^2\ sec^{-1}} \qquad \ldots\ldots \quad (5)$$

where λ_i cm = ionic mean free path, k = Boltzmann's constant, $m=29$ a.m.u.

Using the above data for D, with $T \sim 200°$ K, we obtain $\lambda_i \sim 0{\cdot}5$ cm. If the cross section for ion-neutral molecule collisions is assumed to be the same as for collisions between neutral molecules ($\sim 10^{-15}$ cm^2), the atmospheric particle density, N, can be calculated from the kinetic theory formula for λ_i. Table 1 compares the result with the values at 88 km height, interpolated from the data of other authors. It is seen to be closest to that of Whipple (1943); however an increase of about three times in the assumed collision cross section would bring it into agreement with the value obtained by Havens *et al.* from V-2 rocket flights.

Table 1

Source	A	B	C	D
Particle Density, N cm^{-3}	4×10^{14}	3×10^{14}	$2{\cdot}2 \times 10^{14}$	$1{\cdot}2 \times 10^{14}$

A From decay of Arietid meteor trails.
B Whipple (1943).
C Gerson (1951).
D Havens *et al.* (1952).

§6. SUMMARY

Although the majority of Arietid meteors observed gave larger signals with transverse than with parallel scattering, this has been shown to have been partly due to errors inherent in the equipment.

It proved possible, in the majority of cases, to allow for these errors and hence to derive the true polarization ratio. For a substantial fraction of the echoes, this ratio varied approximately as predicted for trails with line densities less than a few times 10^{12} cm^{-1}, exhibiting the plasma resonance effect. The most probable value of the resonant polarization ratio was 1·7 in fair agreement with the theoretical value of 2·0. Almost all of the remaining echoes were of the form expected from higher line densities.

Individual line densities were estimated independently of the equipment parameters. Both echo amplitude and resonant polarization ratio were found to vary with line density in the manner predicted by theory.

The sensitivity of the apparatus, determined from the estimated line densities and echo amplitudes, is in good agreement with the value calculated from the equipment parameters.

From the decay of the echoes, the coefficient of diffusion of the Arietid meteor trails was determined. The most probable value lies between 2·0 and 2·5 cm^2 sec^{-1}.

ACKNOWLEDGMENTS

We wish to thank the Department of Scientific and Industrial Research for making the above work possible, both by financial support for the experiment and through provision for the maintenance of one of us (R.L.C.); another (T.R.K.) is indebted to Messrs. I.C.I. Ltd., for a Research Fellowship.

REFERENCES

ASPINALL, A., CLEGG, J. A., and LOVELL, A. C. B., 1948, *Mon. Not. Roy. Ast. Soc.*, **109,** 352.

ASPINALL, A., and HAWKINS, G. S., 1951, *Mon. Not. Roy. Ast. Soc.*, **111,** 18.

CLEGG, J. A., HUGHES, V. A., and LOVELL, A. C. B., 1947, *Mon. Not. Roy. Ast. Soc.*, **107,** 369.

ELLYETT, C. D., and DAVIES, J. G., 1948, *Phil. Mag.*, **40,** 614.

FEINSTEIN, J., 1951, *Jour. Geophys. Res.*, **56,** 37.

GERSON, N. C., 1951, *Phys. Soc., Rep. Prog. Phys.*, **14,** 316.

GREENHOW, J. S., 1952, *Jour. Atmos. Terr. Phys.*, **2,** 282.

HAVENS, R. J., KOLL, R. T., and LA GOW, H. E., 1952, *Jour. Geophys. Res.*, **57,** 59.

HERLOFSON, N., 1951, *Arkiv För Fysik*, **3,** 247.

KAISER, T. R., and CLOSS, R. L., 1952, *Phil. Mag.*, **43,** 1.

LOVELL, A. C. B., and CLEGG, J. A., 1948, *Proc. Phys. Soc.*, **60,** 491.

WHIPPLE, F. L., 1943, *Rev. Mod. Phys.*, **15,** 246.

XXXV. *Alpha Particles from* ^{10}B+D

By P. B. Treacy
Research School of Physical Sciences,
Australian National University, Canberra*

[Received October 28, 1952]

Abstract

Thin targets containing separated ^{10}B have been bombarded by deuterons of energies 0·59, 0·78 and 1·07 Mev, and the emitted alpha particles observed using a differential ionization chamber. Transitions proceeding via the ground state and first excited state of ^{8}Be have been identified. On the basis of the dispersion theory of Wigner and Eisenbud, the shape of the alpha particle spectrum is used to indicate properties of the first excited state of ^{8}Be.

A study has been made of the groups of alpha particles emitted under deuteron bombardment of the separated isotope ^{10}B. Using deuteron energies between 0·59 and 1·07 Mev, alpha particles corresponding to transitions to the ground state and first excited state of ^{8}Be have been observed. The energy release in the ground-state transition has been measured. From the shape of the distribution curve corresponding to the excited state of ^{8}Be, properties of this level have been assigned on the basis of a form of dispersion formula due to Wigner and Eisenbud.

Thin targets of B_2O_3 (approximately 0·3 mm air equivalent) were evaporated on brass backings by slowly heating boric acid in a vacuum. This boric acid was prepared originally from metallic ^{10}B. The beam from the 1·25 Mev Philips High Tension Set was allowed to strike the target through a 5/16 in. stop, and alpha particles were detected at 90° using a differential ionization chamber (French and Treacy 1950), with an air absorption cell and mica foils as stopping media. The chamber subtended an angle of 16° at the target. Chamber and foils were calibrated with α-particles from ThC and C′, the mean ranges being taken as 4·72 and 8·57 cm respectively. The chamber resolution, after allowing for straggling, was found to be $0{\cdot}25 \pm 0{\cdot}02$ cm of range. Allowance was made for variation of stopping power of the mica foils with alpha energy (Livingston and Bethe 1937). The bombarding voltage scale was calibrated by using gamma rays from well-known resonances in the proton bombardment of ^{19}F (Chao *et al.* 1950).

Results are shown in fig. 1, for a deuteron energy of 0·78 Mev. Peaks labelled B and C are due to alphas accompanying transitions to the first

---

* Communicated by Professor E. W. Titterton.

excited state and ground state of ^{8}Be respectively, and peak A to alphas from a contamination of carbon formed in the target in the evaporating process. Under bombardment the targets were maintained at a temperature of 120° c, and there was no evidence for an increase of carbon contamination throughout each run. Peak C was located accurately at different bombarding energies and, allowing for target thickness, occurs at a mean range of 15·05 cm for 0·78 Mev deuterons. With the range–energy relation of Livingston and Bethe (1937) this gives an energy of 12·33 Mev, and a Q-value of 17·91±0·06 Mev, for the

Fig. 1

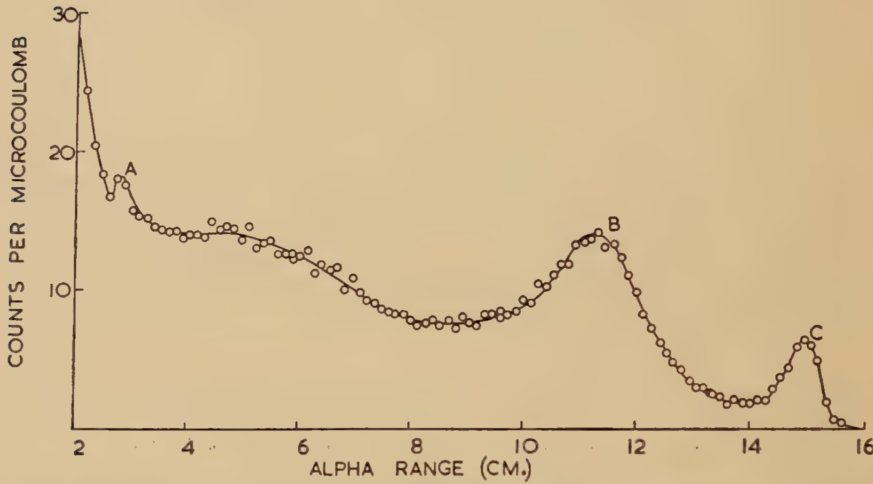

Alpha particles emitted in the bombardment of ^{10}B by deuterons of energy 0·78 Mev.

Fig. 2

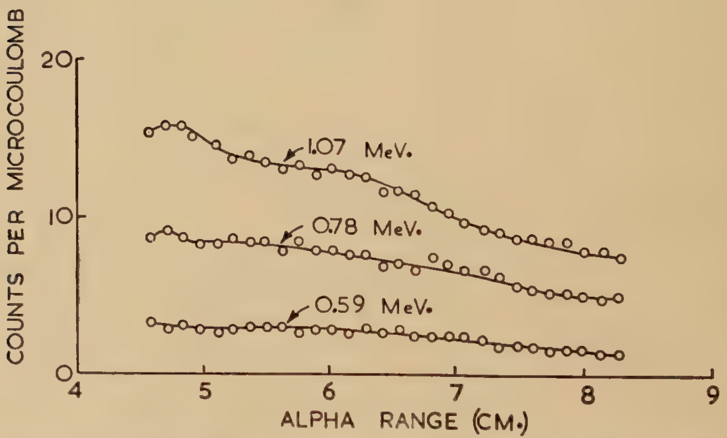

Alpha particles of ranges near 6 cm emitted in the ^{10}B+D process at deuteron energies of 0·59, 0·78 and 1·07 Mev.

ground-state transition. The energy of ^8Be corresponding to the top of peak B is 2·88±0·08 MeV, above the ground state. No well-defined peak, such as has been observed previously in this process, appears in the vicinity of 6 cm range. This was confirmed in separate runs, shown in fig. 2, in which alphas were observed at deuteron energies of 0·59, 0·78 and 1·07 MeV. (The peak appearing below 5 cm range in fig. 2 can be attributed to a trace of ^{11}B present in the target.) Separate bombardments at 0·78 MeV, on cold ^{10}B and natural boron targets showed no evidence for further peaks. This agrees with results of Cockcroft and Lewis (1936) but not with those of Smith and Murrell (1939) and Whitehead (1951). Counting rates used in the present experiments were not sufficiently great for the detection, by 'pile-up', of protons at 5½ cm range from the ^{16}O (d, p) process (French and Treacy 1950), which might account for this apparent discrepancy.

If no transitions are involved other than those to the two lowest levels of ^8Be, it should be possible to describe completely the shape of the observed alpha particle spectrum between ranges of 2½ and 14 cm, assuming only a form of curve for the shape of the broad peak (B of fig. 1) and the angular distributions of the disintegration products in each stage of the process. Effects of straggling and chamber resolution may be neglected in so broad a peak. We have assumed that the peak follows the form

$$n(E) \sim \frac{\Gamma a \cdot \Gamma b}{(E_0+\Delta-E)^2+\Gamma_b{}^2/4},$$

where

$$\Gamma b = \frac{2\,k\,\gamma^2}{F^2+G^2},$$

$$\Delta = -\frac{\gamma^2}{a}\left(\frac{ka}{(F^2+G^2)^{1/2}} \cdot \frac{d\,(F^2+G^2)^{1/2}}{d\,(ka)}+l\right),$$

suggested by the work of Wigner and Eisenbud (1947) and Adair (1952). The width Γa was assumed constant, as it varies slowly with the Q-value for formation of ^8Be, which is itself not a sensitive function of E, the energy of ^8Be with respect to emission of two alpha particles. In these formulae E_0 and γ^2 are constants, k the wave-number of the reduced mass particle and l the spin of the excited state of ^8Be, assumed 0 or 2. Coulomb wave functions F and G, evaluated at an effective ^8Be radius a, for orbital angular momentum l, were obtained from tables (Bloch *et al.* 1951). The peak was fitted at its low E side by a method of successive approximations, using values $4{\cdot}48\times10^{-13}$ cm for the radius a (Christy and Latter 1948) and 0·078 MeV for the energy of the ground state of ^8Be (Carlson 1951). The following values of the parameters E_0 and γ^2 were obtained :

For $l=0$: $E_0=2{\cdot}90$ MeV, $\gamma^2=2{\cdot}29\times10^{-13}$ MeV cm,

For $l=2$: $E_0=5{\cdot}29$ MeV, $\gamma^2=13{\cdot}4\times10^{-13}$ MeV cm.

The shape of the continuum of alphas resulting from the disintegration of the excited ^8Be was calculated in each case, assuming that all alphas involved are emitted isotropically with respect to their parent nuclei. The resulting total distributions are shown in fig. 3, together with the experimental energy spectrum.

The experimental results agree better with the curve for $l=2$. The discrepancy between either calculated curve and the experimental one may be due to a contribution from a direct disintegration into three alpha particles, or to the presence of a very broad peak in the continuum, not sufficiently intense to be observed in an experimental range spectrum.

Fig. 3

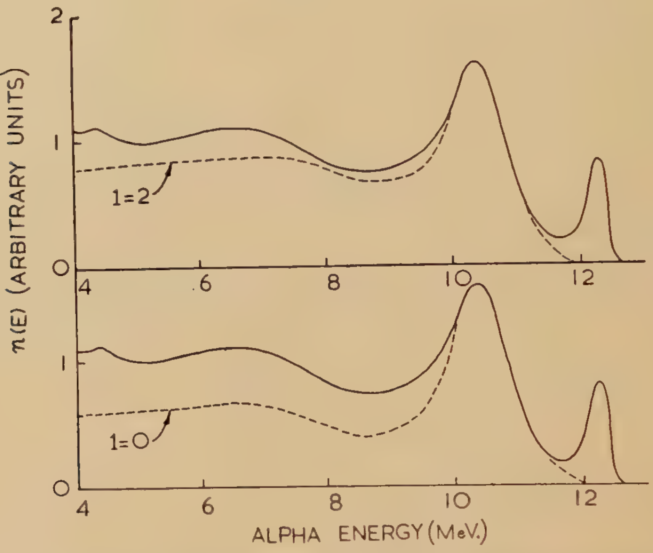

Experimental energy spectrum (full curves) and theoretical distributions (dotted curves) for ^{8}Be spins l of 0 and 2.

I wish to thank Dr. F. C. Barker for helpful discussions on this work. Acknowledgments are due to Mr. N. F. Bowkett for operating the High Tension Set. The boric acid used in these experiments was prepared from metallic ^{10}B through the courtesy of Dr. F. Dwyer, of the University of Sydney.

References

Adair, R. K., 1952, *Phys. Rev.*, **86,** 155.
Bloch, I., Hull, M. M., Jr., Broyles, A. A., Bouricius, W. G., Freeman, B. E., and Breit, G., 1951, *Rev. Mod. Phys.*, **23,** 147.
Carlson, R. R., 1951, *Phys. Rev.*, **84,** 749.
Chao, C. Y., Tollestrup, A. V., Fowler, W. A., and Lauritsen, C. C., 1950, *Phys. Rev.*, **79,** 108.
Christy, R. F., and Latter, R., 1948, *Rev. Mod. Phys.*, **20,** 185.
Cockcroft, J. D., and Lewis, W. B., 1936, *Proc. Roy. Soc.* A, **154,** 246.
French, A. P., and Treacy, P. B., 1950, *Proc. Phys. Soc.* A, **63,** 665.
Livingston, M. S., and Bethe, H. A., 1937, *Rev. Mod. Phys.*, **9,** 245.
Smith, C. L., and Murrell, E. B., 1939, *Proc. Camb. Phil. Soc.*, **35,** 298.
Whitehead, W. D., 1951, *Phys. Rev.*, **82,** 553.
Wigner, E. P., and Eisenbud, L., 1947, *Phys. Rev.*, **72,** 29.

XXXVI. *Self Energy of Slow Electrons in Polar Materials**

By M. GURARI†
Department of Theoretical Physics, University of Liverpool‡

[Received November 4, 1952]

SUMMARY

A new variational method is developed to treat the properties of slow electrons in ionic crystals, and similar problems. It is shown that the true energy of the ground state is always lower than the energy obtained from second order perturbation theory, however strong the interaction. The corresponding wave functions differ, however, from those of perturbation theory unless the interaction is sufficiently weak. For NaCl the energy of the ground state is found lower than by any previous method, and hence closer to the true energy. The effective mass is of the order of twice the electronic mass ; no trapping takes place, therefore.

§1. INTRODUCTION AND DISCUSSION

IT is well known that slow electrons in strictly periodic crystal lattices behave in many respects like free electrons. A slow electron, however, polarizes an ionic lattice so that the field in which the electron moves is no longer periodic. Fröhlich, Pelzer and Zienau (1950, quoted as I) have pointed out that this energy corresponds to the self energy of the electron in a field theory if the polarization of the crystal is considered as a field. They found that although the energy of the ground state is depressed by this interaction, the electron together with the polarization attached to it can still move nearly freely through the lattice. This result differs from an earlier suggestion by Landau (1933) who neglected the dynamic properties of the lattice. He thus treated the electron as moving in a static field due to the polarization produced by the electron. This would lead to the trapping of an electron near a given point in space. Although such a trapped electron could still move through the lattice, its effective mass might be very large, in contrast to the result of I.

The calculations in I hold only for relatively weak interaction. The purpose of the present paper is to develop a new variational method which applies also to stronger interaction. The result shows that for a very general type of interaction the energy of the ground state is the same as found from second order perturbation theory. Since a variational method has been used now, however, it follows that this energy is always higher than the true energy, however strong the interaction. The wave functions used in the variational method tend towards those of perturbation theory only in the case of weak interaction. They may differ from them very considerably for strong interaction.

---

* Based on E. R. A. Report L/T 284.

† Mark Gurari died on May 8, 1952. The present paper was prepared from notes left by him.—H. Fröhlich.

‡ Communicated by Professor H. Fröhlich.

In the case of ionic crystals assumed to have a single vibrational frequency $\omega/2\pi$ for long longitudinal waves, a static dielectric constant ϵ and an optical refractive index $\epsilon_\infty^{\frac{1}{2}}$ the energy $E(0)$ of the ground state is then (cf. 2.29) found to be $-W$ where (cf. I, 1.5)

$$W=\frac{1}{2}\left(\frac{1}{\epsilon_\infty}-\frac{1}{\epsilon}\right)e^2u. \quad . \quad . \quad . \quad . \quad . \quad . \quad . \quad (1.1)$$

Here u is an inverse length satisfying

$$\hbar\omega=\hbar^2u^2/2m. \quad . \quad . \quad . \quad . \quad . \quad . \quad . \quad . \quad . \quad (1.2)$$

It should be noted (cf. I, 4.1) that ω is connected with the frequency $\omega_t/2\pi$ of residual waves by

$$\omega=\omega_t(\epsilon/\epsilon_\infty)^{\frac{1}{2}}. \quad . \quad . \quad . \quad . \quad . \quad . \quad . \quad . \quad (1.3)$$

It will also be shown below that the ratio of effective mass m^* to the electron mass is†

$$\frac{m^*}{m}=1+\frac{W}{6\hbar\omega}. \quad . \quad . \quad . \quad . \quad . \quad . \quad . \quad . \quad (1.4)$$

In the case of NaCl (for numerical values of parameters cf. I) (1.1) leads to $-W=-0{\cdot}17$ ev. This value is lower than both Markham and Seitz's (1948) value of $-0{\cdot}13$ ev obtained by Landau's method, and Pekar's (1949) value of $-0{\cdot}10$ ev (obtained with an approximation which is good for large $W/\hbar\omega$) and it thus represents a better approximation. Since $\hbar\omega\simeq0{\cdot}03$ ev it follows from (1.4) that the effective mass is only about twice the electronic mass. It is thus confirmed that as was suggested in I no trapping takes place.

§ 2. DERIVATION OF THE RESULTS

Consider the Hamiltonian used in I, eqn. (2.6),

$$H=H_{\text{osc}}+H_{\text{int}}+p_{\text{op}}{}^2/2m \quad . \quad . \quad . \quad . \quad . \quad . \quad . \quad (2.1)$$

where $\mathbf{p}_{\text{op}}$ is the momentum operator of the electron,

$$H_{\text{osc}}=\sum_{\mathbf{w}} H_{\mathbf{w}} \quad . \quad . \quad . \quad . \quad . \quad . \quad . \quad . \quad . \quad (2.2)$$

refers to the oscillators representing the lattice vibrations and H_{int} is their interaction with the electron. The lattice vibrations can be expressed in terms of plane waves with wave number $\mathbf{w}$, and $H_{\mathbf{w}}$ refers to a single one of them. Clearly if $|\mathbf{K}\rangle$ is the electronic wave function,

$$\frac{p_{\text{op}}{}^2}{2m}|\mathbf{K}\rangle=\frac{\hbar^2K^2}{2m}|\mathbf{K}\rangle \quad . \quad . \quad . \quad . \quad . \quad . \quad . \quad (2.3)$$

---

† From a preprint received recently I found that Tsung-Dao Lee and David Pines have independently derived the same results. They have not yet published details.—H Fröhlich.

where $\hbar\mathbf{K}$ is the electronic momentum. Also if $|n_{\mathbf{w}}\rangle$ is an oscillator wave function

$$H_{\mathbf{w}}|n_{\mathbf{w}'}\rangle=\delta_{\mathbf{w}\mathbf{w}'}n_{\mathbf{w}}\hbar\omega|n_{\mathbf{w}}\rangle \quad . \quad . \quad . \quad . \quad . \quad . \quad (2.4)$$

where the quantum number $n_{\mathbf{w}}$ is a positive integer or zero. Here we have omitted the zero point energy of the oscillator which can be done by an appropriate choice of the zero of energy. Clearly

$$(H-H_{\text{int}})\{|\mathbf{K}\rangle\prod_{\mathbf{w}}|n_{\mathbf{w}}\rangle\}=\left(\frac{\hbar^2K^2}{2m}+\sum_{\mathbf{w}}n_{\mathbf{w}}\hbar\omega\right)\{|\mathbf{K}\rangle\prod_{\mathbf{w}}|n_{\mathbf{w}}\rangle\} \quad . \quad . \quad (2.5)$$

which means that the product of the electronic and all oscillator wave functions are eigenfunctions of the operator $H-H_{\text{int}}$. They form a complete set, obtained by using all combinations of all possible values for the quantum numbers $n_{\mathbf{w}}$ and for $\mathbf{K}$.

It has been shown in I that the interaction term H_{int} leads to transitions between these eigenfunctions provided the total wave number

$$\mathbf{k}=\mathbf{K}+\sum_{\mathbf{w}}n_{\mathbf{w}}\mathbf{w} \quad . \quad . \quad . \quad . \quad . \quad . \quad . \quad . \quad (2.6)$$

is not altered. It is useful, therefore, to denote these eigenfunctions by $|\mathbf{k};\ldots n_{\mathbf{w}}\ldots\rangle$. Clearly in ordinary space ($\mathbf{r}$) representation the normalized electronic wave function is

$$|\mathbf{K}\rangle=V^{-\frac{1}{2}}\exp(-i\mathbf{K}\,.\,\mathbf{r}) \quad . \quad . \quad . \quad . \quad . \quad . \quad . \quad (2.7)$$

where V is the volume. Thus using (2.6),

$$|\mathbf{k};\ldots n_{\mathbf{w}}\ldots\rangle=|\mathbf{K}\rangle\prod_{\mathbf{w}}|n_{\mathbf{w}}\rangle=V^{-\frac{1}{2}}\exp(i\mathbf{k}\,.\,\mathbf{r})\prod_{\mathbf{w}}\exp(-in_{\mathbf{w}}\mathbf{w}\,.\,\mathbf{r})|n_{\mathbf{w}}\rangle \quad . \quad . \quad . \quad (2.8)$$

are the eigenfunctions of $H-H_{\text{int}}$. Hence with (2.5),

$$\langle\ldots n_{\mathbf{w}}'\ldots;\mathbf{k}'|(H-H_{\text{int}})|\mathbf{k};\ldots n_{\mathbf{w}}\ldots\rangle=\delta_{\mathbf{k}\mathbf{k}'}\ldots\delta_{n_{\mathbf{w}}n_{\mathbf{w}}'}\ldots\frac{\hbar^2}{2m}$$
$$\times\{(\mathbf{k}-\sum_{\mathbf{w}}n_{\mathbf{w}}\mathbf{w})^2+\sum_{\mathbf{w}}n_{\mathbf{w}}u^2\} \quad . \quad . \quad . \quad (2.9)$$

where use has been made of eqn. (1.2). Thus in the matrix representation based on the eigenfunctions (2.8) the operator $H-H_{\text{int}}$ has diagonal elements only. For the interaction operator H_{int} on the other hand all diagonal elements vanish. The non-diagonal elements are different from zero only for transitions which leave $\mathbf{k}$ as well as all $n_{\mathbf{w}}$ but one unaltered, the excepted one differing by unity. Thus from I, eqns. (2.15) and (2.16)

$$\langle\ldots,n_{\mathbf{w}''},\ldots,n_{\mathbf{w}},\ldots n_{\mathbf{w}'},\ldots;\mathbf{k}|H_{\text{int}}|\mathbf{k};\ldots,n_{\mathbf{w}'},\ldots,n_{\mathbf{w}}+1,$$
$$\ldots,n_{\mathbf{w}''},\ldots.\rangle=\langle n_{\mathbf{w}}|H_{\text{int}}|n_{\mathbf{w}}+1\rangle=\frac{C}{w}\left(\frac{n_{\mathbf{w}}+1}{V}\right)^{\frac{1}{2}}. \quad (2.10)$$

where using (1.2)

$$C=(4\pi W\hbar^2u/2m)^{\frac{1}{2}}. \quad . \quad . \quad . \quad . \quad . \quad . \quad . \quad (2.11)$$

To find an approximate solution of our problem with the help of the variational method it is required that

$$\delta\langle\psi(\mathbf{k})|H|\psi(\mathbf{k})\rangle=0 \quad . \quad . \quad . \quad . \quad . \quad . \quad . \quad (2.12)$$

where δ represents a variation of the normalized trial wave function $|\psi(\mathbf{k})\rangle$. The latter will be assumed of the form

$$|\psi(\mathbf{k})\rangle = V^{-\frac{1}{2}} \exp(i\mathbf{k}\,.\,\mathbf{r}) \prod_{\mathbf{w}} |\psi(\mathbf{k},\ \mathbf{w})\rangle \quad . \quad . \quad . \quad (2.13)$$

where

$$|\psi(\mathbf{k},\ \mathbf{w})\rangle = \frac{|0_{\mathbf{w}}\rangle + V^{-\frac{1}{2}} c(k,\ w,\ x) \exp(-i\mathbf{w}\,.\,\mathbf{r})\,|\,1_{\mathbf{w}}\rangle}{(1+V^{-1}c^2(k,\ w,\ x))^{\frac{1}{2}}} \quad . \quad . \quad . \quad (2.14)$$

Here the coefficients $c(k,\ w,\ x)$ are assumed to depend on the magnitudes k and w and on the angle between $\mathbf{k}$ and $\mathbf{w}$ whose cosine is denoted by x; they will be determined from (2.12). As required the wave functions (2.13) using (2.14) can be written as a linear superposition of eigenfunctions (2.8). They all have the same value of $\mathbf{k}$ and contain all combinations of the values $n_{\mathbf{w}}=0$, and $n_{\mathbf{w}}=1$ of all $\mathbf{w}$'s. We thus admit states which may contain a very great number of vibrational quanta provided they all belong to different wave vectors $\mathbf{w}$. In contrast more restrictive wave functions were used in I where, as in perturbation theory, no states were used with more than a single quantum.

Using orthogonality and normalization of the wave functions, eqns. (2.1), (2.13), (2.14), together with (2.3), (2.4), (1.2), (2.6), (2.7) and (2.10) yield

$$\begin{aligned}\langle\psi(\mathbf{k})\,|\,H\,|\,\psi(\mathbf{k})\rangle = \frac{\hbar^2}{2m}\Bigg\{k^2 &+ \sum_{\mathbf{w}} \frac{V^{-1}c^2(k,\ w,\ x)(u^2+w^2-2kwx)}{1+V^{-1}c^2(k,\ w,\ x)} \\ &+ \sum_{\mathbf{w}_1,\mathbf{w}_2}{}' \frac{V^{-2}c^2(k,\ w_1,\ x_1)c^2(k,\ w_2,\ x_2)(\mathbf{w}_1\,.\,\mathbf{w}_2)}{(1+V^{-1}c^2(k,\ w_1,\ x_1))(1+V^{-1}c^2(k,\ w_2,\ x_2))}\Bigg\} \\ &+ 2C\sum_{\mathbf{w}} \frac{V^{-1}c(k,\ w,\ x)}{w(1+V^{-1}c^2(k,\ w,\ x))}. \quad . \quad . \quad . \quad . \quad . \quad . \quad (2.15)\end{aligned}$$

Here the dash at the summation sign means that $\mathbf{w}_1 \neq \mathbf{w}_2$. The last term arises from H_{int}; the rest are due to the electronic terms apart from u^2 which is due to H_{osc}. Clearly as $V \rightarrow \infty$, $V^{-1}c^2$ can be neglected against unity (anticipating c to be independent of V). Furthermore, if polar coordinates in $\mathbf{w}$-space are introduced with $\mathbf{k}$ as axis and ϕ as azimuth then only $\mathbf{w}_1\,.\,\mathbf{w}_2$ depends on ϕ,

$$\mathbf{w}_1\,.\,\mathbf{w}_2 = w_1 w_2(\cos\theta_1 \cos\theta_2 + \sin\theta_1 \sin\theta_2 \cos(\phi_1-\phi_2)). \quad (2.16)$$

Clearly ϕ integration removes the $\cos(\phi_1-\phi_2)$ term so that in (2.15), $\mathbf{w}_1\,.\,\mathbf{w}_2$ can be replaced by

$$w_1 w_2 \cos\theta_1 \cos\theta_2 = w_1 x_1 w_2 x_2. \quad . \quad . \quad . \quad . \quad . \quad . \quad (2.17)$$

For $V \rightarrow \infty$, eqn. (2.15) can thus be written as

$$\begin{aligned}\langle\psi(\mathbf{k})\,|\,H\,|\,\psi(\mathbf{k})\rangle = {}& \frac{\hbar^2(k^2+\gamma^2)}{2m} \\ &+ V^{-1}\sum_{\mathbf{w}}\left\{\frac{\hbar^2}{2m}(u^2+w^2-2kwx)c^2(k,\ w,\ x) + \frac{2Cc(k,\ w,\ x)}{w}\right\} \quad . \quad (2.18)\end{aligned}$$

where

$$\gamma = V^{-1}\sum_{\mathbf{w}} wxc^2(k,\ w,\ x). \quad . \quad . \quad . \quad . \quad . \quad . \quad . \quad (2.19)$$

According to (2.12) the variation of (2.18) with respect to all coefficients $c(k, w, x)$ must vanish. Hence

$$(u^2+w^2-2kwx+2\gamma wx)c(k, w, x)=-\frac{2m}{\hbar^2}\frac{C}{w}, \quad . \quad . \quad . \quad (2.20)$$

which requires that

$$u^2+w^2-2(k-\gamma)wx\neq 0. \quad . \quad . \quad . \quad . \quad . \quad . \quad . \quad (2.21)$$

Denoting by $E(k)$ the expectation value of H when these values of $c(k, w, x)$ have been inserted one finds from eqns. (2.18), (2.19) and (2.20)

$$E(k)=\frac{\hbar^2(k^2+\gamma^2)}{2m}+\frac{2m}{\hbar^2}V^{-1}C^2\sum_{\mathbf{w}}\frac{1}{w^2}\left\{\frac{u^2+w^2-2kwx}{(u^2+w^2-2(k-\gamma)wx)^2}\right.$$
$$\left.-\frac{2}{u^2+w^2-2(k-\gamma)wx}\right\}=\frac{\hbar^2(k^2-\gamma^2)}{2m}$$
$$-\frac{2m}{\hbar^2}V^{-1}C^2\sum_{\mathbf{w}}\frac{1}{w^2(u^2+w^2-2(k-\gamma)wx)}. \quad . \quad . \quad . \quad (2.22)$$

Introducing now for γ the dimensionless variable

$$v=(k-\gamma)/u, \quad . \quad . \quad . \quad . \quad . \quad . \quad . \quad . \quad (2.23)$$

we find from (2.22) and (2.21) the following parametric representation of $E(k)$,

$$E(k)=\frac{\hbar^2}{2m}[k^2-(k-uv)^2]-\frac{2m}{\hbar^2}V^{-1}C^2\sum_{\mathbf{w}}\frac{1}{w^2(u^2+w^2-2uvwx)}, \quad . \quad . \quad (2.24)$$

$$k-uv=\left(\frac{2m}{\hbar}\right)^2V^{-1}C^2\sum_{\mathbf{w}}\frac{wx}{w^2(u^2+w^2-2uvwx)^2}. \quad . \quad . \quad (2.25)$$

To evaluate the sums they will be replaced by integrals,

$$V^{-1}\sum_{\mathbf{w}}\ldots\to\frac{2\pi}{(2\pi)^3}\int\ldots w^2\,dw\,dx. \quad . \quad . \quad . \quad . \quad . \quad . \quad (2.26)$$

The w-integration can be extended to infinity as has been discussed in I. All integrations are elementary. With the use of (2.11) and (1.2) eqns. (2.24) and (2.25) then become

$$E(k)=\hbar\omega\left[\frac{k^2}{u^2}-\left(\frac{k}{u}-v\right)^2\right]-W\frac{\sin^{-1}v}{v}, \quad . \quad . \quad . \quad (2.27)$$

and

$$\frac{k}{u}-v=\frac{W}{\hbar\omega}\frac{1}{2v^2}\left(\frac{v}{(1-v^2)^{\frac{1}{2}}}-\sin^{-1}v\right). \quad . \quad . \quad . \quad (2.28)$$

Clearly if $v=0$ then from (2.28) also $k=0$. Hence

$$E(0)=-W. \quad . \quad . \quad . \quad . \quad . \quad . \quad . \quad . \quad (2.29)$$

If $v\to 1$ then from (2.28) $k\to\infty$ and with (2.27) $E(k)\simeq 2\hbar\omega k/u\to\infty$. The case $v>1$ has to be excluded to satisfy condition (2.21). It cannot be expected that the choice of the wave function (2.13) and (2.14) permits a successful treatment of energies $E(k)$ which are above the ground state by more than $\hbar\omega$. For states below this energy $v \ll 1$. In this case (2.27) and (2.28) can be developed into a power series in v, i.e.

$$E(k)=-W+\hbar\omega\left(2\frac{k}{u}v-v^2\left(1+\frac{W}{6\hbar\omega}\right)+\dots\right) \quad . \quad . \quad (2.30)$$

and

$$\frac{k}{u}=v\left(1+\frac{W}{6\hbar\omega}\right)+\dots . \quad . \quad . \quad . \quad . \quad . \quad . \quad (2.31)$$

Eliminating v leads to

$$E(k)=-W+\frac{\hbar^2k^2}{2m^*}+\dots \quad . \quad . \quad . \quad . \quad . \quad . \quad (2.32)$$

with a value of m^* given by (1.4). Its validity requires

$$E(k)-E(0)\ll\hbar\omega. \quad . \quad . \quad . \quad . \quad . \quad . \quad . \quad . \quad (2.33)$$

§ 3. GENERALIZATION FOR $k=0$

Equation (2.29) shows that for $k=0$ the energy $E(0)$ is the energy obtained from second order perturbation theory (although the wave functions in the two cases are equal only if $W/\hbar\omega \ll 1$). This result holds not only for the model used in § 2 but also in a much more general case obtained by the replacements

$$C/w \rightarrow g(w), \qquad u \rightarrow u(w), \quad . \quad . \quad . \quad . \quad . \quad . \quad (3.1)$$

where $g(w)$ and $u(w)$ are arbitrary functions of w, provided no divergent integrals occur. This can best be seen by making the replacements (3.1) in eqns. (2.24) and (2.25). Then $v=0$ requires $k=0$ because the integrand in (2.25) becomes antisymmetric in x. Equation (2.24) is then equal to the second order perturbation formula. This result can also be derived by a more elegant method which will be presented here because it will probably be of use in the discussion of excited states.

Consider the matrix representation of the Hamiltonian H given in § 2, and write H as the sum of two terms

$$H=H'+H'', \quad . \quad . \quad . \quad . \quad . \quad . \quad . \quad . \quad . \quad . \quad (3.2)$$

such that H'' is a diagonal matrix with elements

$$\langle \dots n_{\mathbf{w}} \dots | H'' | \dots n_{\mathbf{w}} \dots \rangle=\frac{\hbar^2}{2m}\{(\Sigma_{\mathbf{w}} n_{\mathbf{w}}\mathbf{w})^2-\Sigma_{\mathbf{w}} n_{\mathbf{w}} w^2\} \quad . \quad (3.3)$$

Then since the diagonal elements of H_{int} vanish the diagonal elements of H are obtained from (2.9) by putting $k=k'=0$ and $n_{\mathbf{w}}=n_{\mathbf{w}}'$. Use of (3.1), (3.2) and (3.3) then gives

$$\langle \dots n_{\mathbf{w}} \dots | H' | \dots n_{\mathbf{w}} \dots \rangle=\frac{\hbar^2}{2m}\Sigma_{\mathbf{w}} n_{\mathbf{w}}(w^2+u^2(w)), \quad . \quad . \quad (3.4)$$

as diagonal elements of H'. The non-diagonal elements are the same as those of H_{int}, given by (2.10). Clearly then, the operator H' can be written as

$$H' = \sum_{\mathbf{w}} H'(\mathbf{w}), \qquad (3.5)$$

where

$$\langle n_{\mathbf{w}} \,|\, H'(\mathbf{w}) \,|\, n_{\mathbf{w}} \rangle = n_{\mathbf{w}} \frac{\hbar^2}{2m} (w^2 + u^2(w)), \qquad (3.6)$$

are the diagonal elements of $H'(\mathbf{w})$. All non-diagonal elements vanish except those next to the diagonal; they are given by

$$\langle n_{\mathbf{w}} \,|\, H'(\mathbf{w}) \,|\, (n_{\mathbf{w}}+1) \rangle = g(w) \left(\frac{n_{\mathbf{w}}+1}{V} \right)^{\frac{1}{2}}. \qquad (3.7)$$

Thus $H'(\mathbf{w})$ is identical with the Hamiltonian of an harmonic oscillator (apart from its zero point energy) with frequency $\hbar(w^2+u^2(w))/2m$ whose origin, through a linear term, has been displaced by

$$\Delta = \{16m^3 g^2(w)/V\hbar^4(w^2+u^2(w))^3\}^{\frac{1}{2}}, \qquad (3.8)$$

assuming its mass to be unity. If $|\,\psi_0'(\mathbf{w})\rangle$ is its eigenfunction in the ground level, clearly

$$H'(\mathbf{w}) \,|\, \psi_0'(\mathbf{w}) \rangle = - \frac{g^2(w) 2m}{V\hbar^2(w^2+u^2(w))} \,|\, \psi_0'(\mathbf{w}) \rangle. \qquad (3.9)$$

Using (3.5), therefore,

$$H' \,|\, \psi_0' \rangle = E_0 \,|\, \psi_0' \rangle, \qquad (3.10)$$

where

$$|\, \psi_0' \rangle = \prod_{\mathbf{w}} |\, \psi_0'(\mathbf{w}) \rangle, \qquad (3.11)$$

and

$$E_0 = -\frac{1}{V} \sum_{\mathbf{w}} \frac{g^2(w) 2m}{\hbar^2(w^2+u^2(w))}. \qquad (3.12)$$

Thus the lowest eigenvalue of H' is exactly equal to the expression for the lowest state of H calculated with the help of perturbation theory.

To compare the eigenfunctions it will be noticed that the function $|\,\psi_0'(\mathbf{w})\rangle$ of the displaced oscillator can be developed in a series of eigenfunctions $|\, n_{\mathbf{w}} \rangle$ of the undisplaced oscillator. It is found that

$$|\, \psi_0'(\mathbf{w}) \rangle = \exp(-s_w^2) \sum_{n_{\mathbf{w}}} \frac{(-2^{\frac{1}{2}} s_w)^{n_{\mathbf{w}}}}{(n_{\mathbf{w}}\,!)^{\frac{1}{2}}} \,|\, n_{\mathbf{w}} \rangle, \qquad (3.13)$$

where

$$s_w = \frac{g(w) 2m}{(2V)^{\frac{1}{2}} \hbar^2 (w^2+u^2(w))}. \qquad (3.14)$$

It follows that terms with $n_{\mathbf{w}} \geqslant 2$ can be neglected if $V \to \infty$. The eigenfunction $|\,\psi_0'\rangle$ is then seen to be identical with $|\,\psi(\mathbf{k})\rangle$, eqns. (2.13) and (2.14) if $\mathbf{k}=0$ and if the coefficients c are introduced from (2.20) considering the replacements (3.1). Also, since for $\mathbf{k}=0$ the c's are independent of the direction of $\mathbf{w}$, the diagonal elements (3.3) of H'' vanish for $n_{\mathbf{w}}=0$ and $n_{\mathbf{w}}=1$. Clearly then

$$\langle \psi_0' \,|\, H'' \,|\, \psi_0' \rangle = 0, \qquad (3.15)$$

and hence

$$\langle \psi_0' \,|\, H \,|\, \psi_0' \rangle = E_0. \qquad (3.16)$$

It now follows from the variational principle (2.12) that E_0 is larger than the lowest eigenvalue of H.

It is hoped that the present method will permit treatment of excited states by using solutions of H' different from the ground state. Also use of H'' as a perturbation should lead to an estimate of the accuracy of the above solutions.

REFERENCES

Fröhlich, Pelzer and Zienau, 1950, *Phil. Mag.*, **41,** 221.
Landau, 1933, *Z. Phys. Sowjet.*, **3,** 664.
Markham and Seitz, 1948, *Phys. Rev.*, **74,** 1014.
Pekar, 1949, *J. Exp. Theor. Phys., U.S.S.R.*, **19,** 796.

XXXVII. *A Dislocation Mechanism for the Growth of Hopper Crystal Faces and the Growth of Salol Crystals from Solution and from the Melt*

By S. Amelinckx
Laboratorium voor Kristalkunde, Geologisch Instituut, Rijksuniversiteit
Gent Rozier, 6, Ghent (Belgium)*

[Received December 16, 1952]

The influence of dislocations on the growth of crystals has been fully discussed by Burton, Cabrera and Frank (1951). It has been shown that in the case of normal growth (i.e. when the considered crystal face is completely surrounded by the phase out of which it grows) the exposed edge of the screw dislocation will wind itself up into a *spirally terraced hill* (vicinal faces), centred on the emerging dislocation.

Salol (phenyl ester of salicylic acid) crystals, when grown from a solution, exhibit sometimes growth spirals of the Frank type (Amelinckx 1952). In many cases, however, especially when grown slowly from heavy organic solvents, they show *spirally terraced pits* (hopper faces) not foreseen as a growth feature by Frank's theory. On the basis of Frank's theory spirally terraced pits could indeed only be generated by dissolution or evaporation, and not as a consequence of growth.

It will be shown here how a dislocation mechanism can be devised to account for the occurrence of ' spiral growth pits '.

As is well known, hopper crystals are formed e.g. when crystals grow whilst floating on the surface of a solution or of a melt. In this case diffusion will make growth possible, but only on a relatively narrow strip along the crystal's edge. Let us suppose that at a certain moment, when the supersaturation is low enough, a screw dislocation is created in such a floating crystal. Similarly, as for the Frank mechanism, growth will start at the exposed edge AB (fig. 1 (*a*)), but only a narrow strip parallel to the crystal's edge will be developed, e.g. BC. When this strip approaches the crystal boundary at C another strip CD (fig. 1 (*b*)) can develop which, when having reached D, will be able to go on growing towards E (fig. 1 (*c*)). At the end a growth layer will have surrounded completely the crystal face. After having reached B again, the crystal (at least its outer part) will have grown by a layer equal in thickness to the screw component of the Burgers vector of the dislocation (fig. 1 (*d*)). As in the meantime the crystal has grown laterally, this new layer will have its inner edge a little more outward than the previous one, and the result will be a spirally terraced pit (fig. 1 (*e*)).

An example of a spiral pit on a salol crystal is shown in fig. 2 (Plate 12). Stepheights cannot be measured with extreme accuracy because multiple beam interferometry cannot be used in this case. Step-heights measured by means of two-beam fringes ranged from some 400 up to 18 000 Å.

---

* Communicated by Professor Dr. W. Dekeyser.

To decide whether a feature was a pit or a hill we made use of the asymmetry of the diffraction pattern at an edge when going off focus.

Similar growth features have also been observed on citric acid crystallized from alcohol.

The proposed mechanism and its experimental confirmation emphasize once more the important role played by dislocations in various types of growth.

Fig. 1

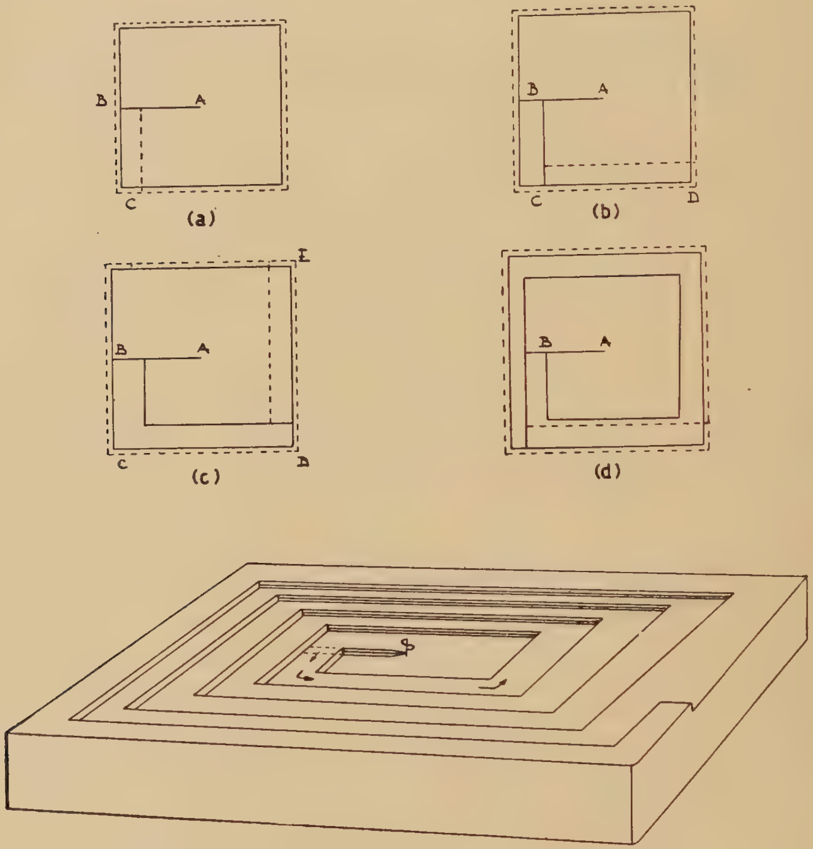

(a) (b) (c) (d) (e)

Another instance where dislocations were thought to play no essential role is growth from the melt. It has been shown by Burton, Cabrera and Frank (*loc. cit.*) that above a certain critical temperature T_c the surface roughness s could probably account for the growth of crystals, so that neither two-dimensional nucleation nor dislocations would be necessary. Chalmers and Martius (1952) have proposed another mechanism for growth from the melt which is not based on dislocations.

On crystals prepared by slow cooling of molten salol we observed that on almost every crystal growth spirals either of the Frank type or of the type discussed above were visible (figs. 3, 4, Plate 12).

Two alternative conclusions are now possible. The first is that the surface roughness will play no role when growth-promoting dislocations are present. The second that T_c is superior to the melting point in the actual case, a possibility which was already considered on theoretical grounds by Burton, Cabrera and Frank (*loc. cit.*).

A striking feature for spirals from the melt is that the Burgers vectors are most of the time very large (up to a few thousand ångströms). Nevertheless no craters (Frank 1951) were observed, the dislocations being dissociated into ribbons of dislocations. For growth from solution there is evidence of craters in some rare cases, although the Burgers vectors were most of the time much smaller.

It is hoped to publish elsewhere a detailed account of these observations and a more elaborate theory of the proposed mechanism.

ACKNOWLEDGMENTS

I wish to thank Professor Dr. W. Dekeyser for interesting discussions and for his continuous encouragement. This work is part of a research scheme supported by C.N.B.C.P.M.

Note added in proof.—Thymol has now been found to be a second example of a compound exhibiting the here described growth features (Votava, Amelinckx and Dekeyser, to be published in *Naturw.*).

REFERENCES

AMELINCKX, S., 1952, *Naturwissenschaften*, **23,** 547.
BURTON, W. K., CABRERA, N., and FRANK, F. C., 1951, *Phil. Trans. Roy. Soc.*, **243,** 299.
CHALMERS, B., and MARTIUS, U. M., 1952, *Phil. Mag.*, **43,** 686.
FRANK, F. C., 1951, *Acta Cryst.*, **4,** 497.

XXXVIII. *The Formation of the Helium Film*

By D. F. BREWER and K. MENDELSSOHN, F.R.S.
Clarendon Laboratory, Oxford*

[Received December 27, 1952]

ABSTRACT

The formation of the unsaturated helium II film has been studied by measurements of superfluidity and adsorption isotherms on glass between 1·35°K and 2·27°K. Whereas with decreasing percentage saturation the onset of superflow is depressed to lower temperatures, the coverage shows a discontinuity at the normal lambda-point of the bulk liquid. Formation of liquid clusters has been advanced as a possible explanation and the existence of an anomalous surface tension effect has been suggested.

A YEAR ago we reported on experiments in which the transfer rates of unsaturated helium II films on a german silver surface were determined thermally (Bowers, Brewer and Mendelssohn 1951). These experiments have since been extended to film transfer over glass surfaces, and have been supplemented by measurements of the adsorption isotherms of helium from 0 to 95 % saturation between 1·35° K and 2·27° K. Comparison of the flow phenomena on german silver and on glass, as well as the transfer of the saturated film over different surfaces (Mendelssohn and White 1950), indicates that the microscopic state of the surface very strongly influences the film, particularly at high percentage saturations. Since glass appears to be the only surface on which simple and reproducible phenomena of film flow have been observed, the adsorption was studied on a glass surface. Excepting the earlier and rather qualitative adsorption observations of Kistemaker (1947), glass has not been used in recent measurements of the adsorption isotherms.

The results obtained on a glass surface of about 0·5 m^2 area are shown in fig. 1, where the adsorbed volume for different percentage saturations is plotted against the temperature. Our results differ from those of Long and Meyer (1949), and of Frederikse and Gorter (1950), obtained on Fe_2O_3 and on steel, in that for constant percentage saturation the coverage rises with temperature until the lambda point (2·19° K) is reached, when there is a sharp drop in the volume adsorbed.

The flow measurements of the unsaturated film on glass have confirmed our observation on german silver that for each percentage saturation, there exists a definite temperature, *below* 2·19° K, above which *no* film transfer takes place. This is in disagreement with the earlier report of Long and Meyer (1952 a) that even films of only $1\frac{1}{2}$ statistical layers show superflow up to the lambda point of the bulk liquid.*

---

* Communicated by the Authors.

Combining the results of the flow experiments and of the adsorption experiments, a (dotted) line has been drawn in fig. 1 dividing the diagram into a region where superflow takes place and one where no anomalous film transport occurs. It seems remarkable that (except for very low percentage saturations) the adsorption curves all break only at the lambda point of the bulk liquid, while the onset of superfluidity occurs at lower temperatures. The adsorption isotherm for 1·552° K, shown in fig. 2, has been measured with particular care in the region where the onset of superfluidity occurs, but no anomaly which is larger than the experimental scatter of the points was observed.

Fig. 1

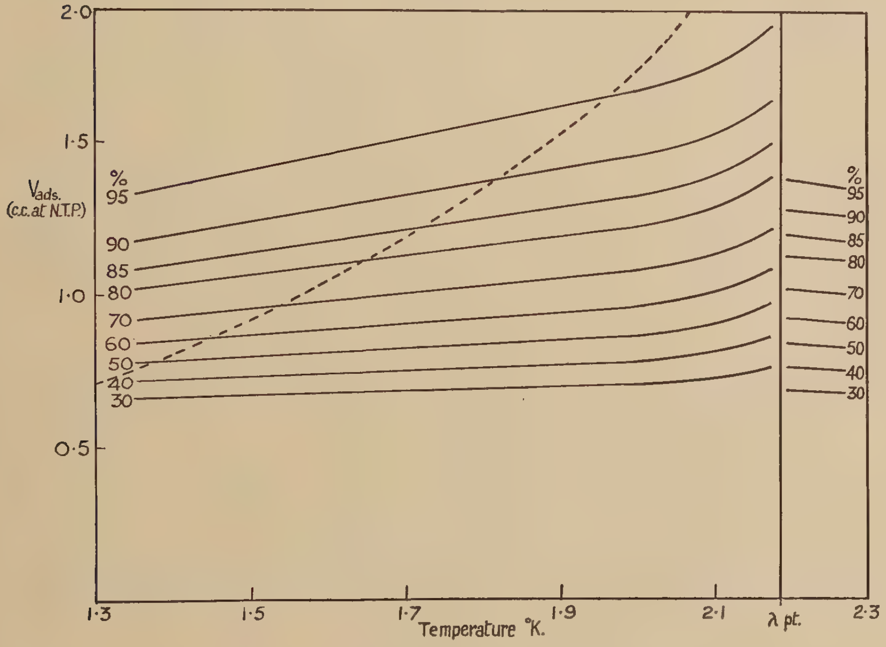

Volume of the gas adsorbed on 0·5 m² of glass for varying percentage saturation in dependence on temperature. The dotted line indicates the onset of superfluidity.

A number of explanations suggest themselves for the curious fact that the films show a definite break in coverage at 2·19° K but become superfluid only at lower temperatures, depending on the percentage saturation. First of all, one may think that the lambda phenomenon and superfluidity are not closely connected, but this would be out of keeping with almost all other observations on helium II. Secondly, it cannot be ruled out that the moving film differs in its properties from the stationary one, although, at least for the saturated film, the observations of Henshaw and Jackson (1953) do not indicate this. Finally, one might regard the break at 2·19° K as due to the presence of bulk liquid. This cannot be due to ordinary capillary condensation, which should be the same just below the lambda point as just above. However, it is possible that the formation of an unsaturated film covering a solid surface may be different in helium below the lambda point from that with any other gas. There are indications that the de Broglie wavelength

---

* However, these authors have quite recently, using our method, confirmed that the temperature of onset of superfluidity is depressed as the thickness of the film is decreased (Long and Meyer 1952 b).

Fig. 2

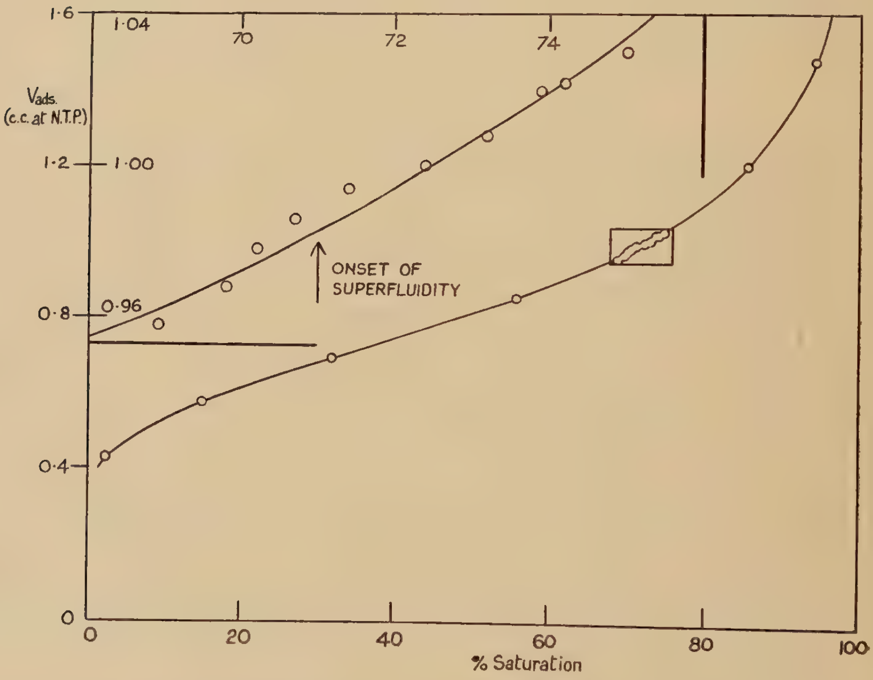

The adsorption isotherm for 1·552° K.
Inset: The region between 68 and 76% saturation where superfluidity begins.

d in helium II is much greater than in helium I. As the pressure of helium over a solid surface is increased, it may therefore be energetically preferable to form clusters of liquid of the order of magnitude of *d*, rather than to pile on further layers of adsorbed gas. On the basis of such a model it would be wrong, as has hitherto been done, to interpret throughout the measured coverages as a 'number of layers' of the unsaturated helium film. In fact the formation of the helium II film would proceed by the adsorption on the plane surface of a number of layers which is not greater just below the lambda point than just above, on which clusters of bulk liquid appear, which ultimately aggregate on saturation to the well-known film, with about 10^{-6} cm thickness. Using the relation proposed by one of us (Mendelssohn 1947),

$$T_\lambda = \text{const.} \left(\frac{1}{l^2} - \frac{1}{d^2} \right),$$

where l is the mean free path in helium I, we see that d must be at least of the order of magnitude of $\sim 10^{-6}$ cm in order to maintain the break of the curves in fig. 1 within 0·01° K of the normal lambda temperature. The same formula can also be used to estimate the thickness of the adsorbed unsaturated film whose lambda point is depressed to temperatures indicated by the dotted line. For a percentage saturation of about 55%, which has a lambda point of $\sim$1·4° K, a thickness of $\sim 10^{-7}$ cm is obtained.

Another consequence of the suggested model of film formation should be an anomalous condensation in capillaries of the order of d below 2·19° K, far in excess of that calculated from the measured (Allen and Misener 1938) surface tension. We might further expect that ^{3}He, besides not showing superfluidity, should also not form thick films.

REFERENCES.

ALLEN, J. F., and MISENER, A. D., 1938, *Proc. Camb. Phil. Soc.*, **34**, 299.
BOWERS, R., BREWER, D. F., and MENDELSSOHN, K., 1951, *Phil. Mag.*, **42**, 1445.
FREDERIKSE, H. P. R., and GORTER, C. J., 1950, *Physica*, **16**, 402.
HENSHAW, D. G., and JACKSON, L. C., 1953, *Phil. Mag.*, **44**, 14.
KISTEMAKER, J., 1947, *Physica*, **13**, 81.
LONG, E. A., and MEYER, L., 1949, *Phys. Rev.*, **76**, 440; 1952 a, *Phys. Rev.*, **85**, 1032; 1952 b, *Ibid.*, **87**, 153.
MENDELSSOHN, K., 1947, *Phys. Soc. Camb. Conf. Report*, 35.
MENDELSSOHN, K., and WHITE, G. K., 1950, *Proc. Phys. Soc.* A, **63**, 1328.

XXXIX. CORRESPONDENCE

Electromagnetic Radiation from Radium E

By D. G. E. Martin and G. Parry
George Holt Physics Laboratory, Liverpool*

[Received February 2, 1953]

Abstract

A scintillation spectrometer has been used to study the electromagnetic radiation from a RaE source, to determine if a monochromatic line exists in the region of 85 kev. It appears that the intensity of such radiation is not greater than 1 quantum per 6000 beta disintegrations. The number of gamma quanta in the bremsstrahlung above 90 kev is estimated to be $2 \cdot 5 \times 10^{-3}$ per disintegration.

According to Zavelski, Umarov and Matushevski (1949), the beta-spectrum of RaE is complex, 92% of the beta transitions going to an excited state of ^{210}Po with an energy of 85 kev above the ground state. They found a line in the beta-spectrum at 66 kev with an intensity of 0·1% per disintegration, and they attributed this to the internal conversion of the de-excitation energy. The external gamma radiation was, however, weak.

One would expect that this gamma radiation would be found in experiments on the inner bremsstrahlung of RaE. The spectrum of Madansky and Rasetti (1951) does show an anomaly at about 90 kev, but their curve for ^{32}P shows a similar anomaly in the same region. It therefore seemed worthwhile to investigate the RaE spectrum again.

We have used an apparatus similar to that of Madansky and Rasetti. A source of about 200 μc of RaE, prepared from material supplied by the Radiochemical Centre, was deposited on a thin Zapon film (100 μg/cm^2) and the gamma radiation from it measured by a cylindrical crystal of NaI(Tl) (3 cm diameter × 1·8 cm) used in conjunction with an E.M.I. type 5311 photomultiplier. The pulses from the photomultiplier were fed to a scaling circuit through a linear amplifier and a single channel analyser, and energy calibration of the pulse heights was obtained from the gamma-ray lines of RaD and ^{60}Co. The primary beta radiation of RaE was absorbed in perspex, and the gamma-rays were allowed through a hole of 1·25 cm diameter in a lead screen 4 cm thick.

---

* Communicated by Professor H. W. B. Skinner, F.R.S.

Figure 1 shows the observed distribution from RaD and fig. 2 that due to the electromagnetic radiation from the RaE source corrected for absorption. From this data, there may be a slight sign of a monochromatic radiation in the region of 85 kev but its intensity would not be more than 1 quantum per 6000 disintegrations. This result appears to be in agreement with that of Novey (1952).

Fig. 1

Observed distribution due to radiation from RaD.

Fig. 2

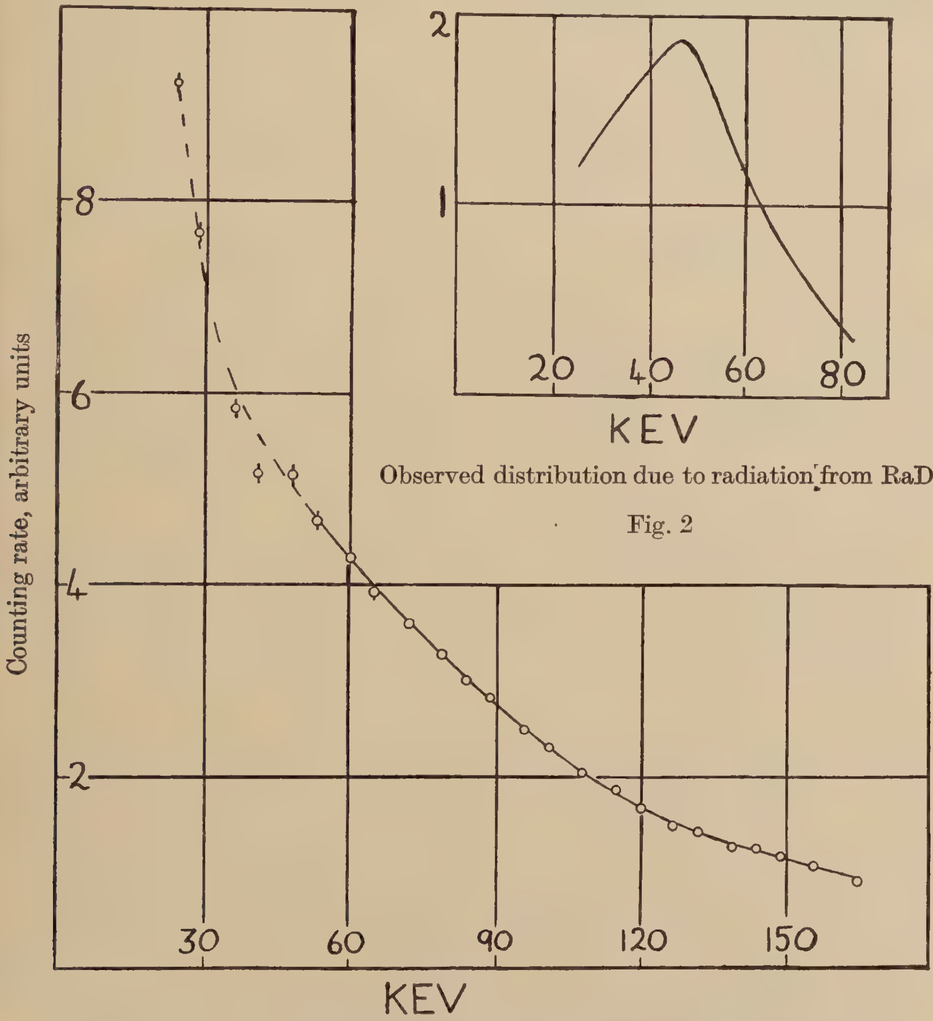

Observed distribution, corrected for absorption, due to radiation from RaE.

There may be a non-uniformity in the curve at about 45 kev, but this could be entirely due to statistical error. To investigate it further would require an apparatus having better resolution, and a lower absorption correction in this region. Certainly, less than 1 in 500 of the counts at 46 kev can be attributed to RaD contamination.

It seems probable that practically the whole of the observed distribution is due to inner bremsstrahlung, and an estimate of the number of quanta above 90 kev is $2{\cdot}5\times10^{-3}$ per beta disintegration.

REFERENCES

MADANSKY, L., and RASETTI, F., 1951, *Phys. Rev.*, **83,** 187.
NOVEY, T. B., 1952, *Phys. Rev.*, **86,** 619.
ZAVELSKI, A. S., UMAROV, G., and MATUSHEVSKI, S. KH., 1949, *J. Exp. Theor. Phys., U.S.S.R.*, **19,** 1136.

The Virial Theorem in Free Electron and Generalized Thomas–Fermi Models

By N. H. MARCH
Department of Physics, The University, Sheffield*

[Received February 3, 1953]

IN a recent paper (March 1952, referred to as I) the writer has discussed the virial theorem in the Thomas–Fermi (T.F.) and Thomas–Fermi–Dirac (T.F.D.) theories. These models refer to absolute zero, and have recently been generalized to apply when $T\neq0$. The purpose of this note is to record briefly some results arising from an investigation of the form of the virial theorem in these generalized models.

Marshak and Bethe (1940) have extended the T.F. theory to the case of low temperatures, whilst a full account of the temperature has been taken by Sakai (1942) and Feynman, Metropolis and Teller (1949, referred to as F.M.T.).

In the case of a single centre F.M.T. have obtained the result

$$2\mathscr{T}+U=3pv, \qquad . \quad . \quad . \quad . \quad . \quad . \quad . \quad . \quad . \quad . \quad (1)$$

where $\mathscr{T}$ is the kinetic energy, U the potential energy, v the volume and p the pressure. In the many-nuclei case, not hitherto discussed when $T\neq0$, the methods of I give the result

$$2\mathscr{T}+U=\frac{4\pi}{3h^3m}(2m\mathbf{k}T)^{5/2}\int I_{3/2}\left(\frac{eV}{\mathbf{k}T}-\eta\right)\mathbf{r}\,.\,d\mathbf{s}+\lim_{a=0}\sum_k e_k\mathbf{r}_k\,.\,\boldsymbol{\epsilon}_a(\mathbf{r}_k), \qquad (2)$$

the notation being that used by F.M.T. and in I.

One remark aside from the virial theorem is worth making here. It is that the entropy S in the T.F. model can be written down immediately from the free electron result (see for example, Wohlfarth 1950) as

$$S=-\frac{\mathbf{k}}{\pi^2}\int d\tau\int_0^\infty\{f\ln f+(1-f)\ln(1-f)\}k^2\,dk, \qquad . \quad . \quad . \quad (3)$$

where

$$f=\left[\exp\left(\frac{h^2k^2/(8\pi^2m)-eV}{\mathbf{k}T}+\eta\right)+1\right]^{-1}.$$

---

* Communicated by Professor C. A. Coulson.

This procedure is much more direct than that of Brachman (1951) who obtained S by integrating the Gibbs–Helmholtz equation. Brachman's eqn. (7 b) follows easily from our expression.*

The generalization of the T.F.D. model presents more difficulties. Yokota (1949) has given a discussion in which he takes the distribution function $f(k, T)$ to be the Fermi–Dirac function. However, this is not correct (as Yokota in fact noted), and improved approximations to f have been obtained recently by Wohlfarth (1950) and Lidiard (1951). It is somewhat surprising to find that with both these approximations for f the virial theorem in the free electron model is exactly satisfied and may be written

$$2\mathscr{T}+A=3pv, \qquad (4)$$

where A is the exchange energy and p the pressure obtained from the free energy F by means of the relation

$$p=-\left(\frac{\partial F}{\partial v}\right)_T. \qquad (5)$$

If, on the other hand, following Yokota, one takes f to be the Fermi–Dirac function, then the theorem is no longer satisfied.

We can improve the T.F.D. model of Yokota if we use Lidiard's approximation for f. The equations obtained by minimizing the free energy are somewhat complicated and we do not propose to give them here.† But again in the case of a single centre one obtains after some manipulation

$$2\mathscr{T}+U+A=3pv. \qquad (6)$$

That the virial theorem should be satisfied when approximate distribution functions are used seems to be closely related to the fact that the free energy has been minimized with respect to the parameters in the forms chosen for f, but up to the moment we have achieved no general result.

REFERENCES

BRACHMAN, M. K., 1951, *Phys. Rev.*, **84,** 1263.
FEYNMAN, R. P., METROPOLIS, N., and TELLER, E., 1949, *Phys. Rev.*, **75,** 1561.
KOPPE, H., 1947, *Z. Naturforsch.*, **2A,** 429.
LIDIARD, A. B., 1951, *Phil. Mag.*, **42,** 1325.
MARCH, N. H., 1952, *Phil. Mag.*, **43,** 1042.
MARSHAK, R. E., and BETHE, H. A., 1940, *Astrophysical Journal*, **91,** 239.
SAKAI, T., 1942, *Proc. Phys. Math. Soc., Japan*, **24,** 254.
WOHLFARTH, E. P., 1950, *Phil. Mag.*, **41,** 534.
YOKOTA, I., 1949, *J. Phys. Soc. Japan*, **4,** 82.

---

* Brachman uses $-\eta$ in place of our η.

† Professor K. Umeda (private communication to Professor C. A. Coulson) has indicated that he is making a detailed investigation of the results of the T.F.D. model for $T\neq 0$ along similar lines.

Delayed Disintegration of a Heavy Nuclear Fragment: I *

By M. Danysz and J. Pniewski
Institute of Experimental Physics, University of Warsaw †

[Received December 1, 1952]

A remarkable coincidence of two events recorded in a photographic emulsion has recently been observed in this laboratory. It occurred in a G5 emulsion, 600 μ thick, which had been exposed to cosmic radiation at an altitude of 85 000 feet,‡ and consists of two stars marked A and B in the photo-micrograph reproduced in Plate 13. The centre of the star B coincides with the end of the track of a heavy fragment ejected from the star A. If this coincidence is not accidental, it must be considered as an example of the delayed disintegration of a heavy fragment. The probability of a fortuitous coincidence is very small, and it therefore seemed appropriate to analyse the events more closely. It is clear, of course, that any novel conclusions drawn from a single observation should be treated with proper reserve.

The disintegration referred to as star A represents the result of a high-energy interaction, presumably between a singly-charged particle and a silver or bromine nucleus. In the nomenclature of Brown *et al.* (1949), the star A may be described as of type 21+18p. The track p—see Plate 13—is the only track in the upper hemisphere with minimum grain density, of which the direction coincides approximately with the 'axis' of the cone of the emitted shower particles. It therefore probably represents the incident particle which produced the disintegration A. Scattering measurements do not allow an accurate evaluation of its energy, but they are not inconsistent with the above assumption. Using statistical data of Camerini *et al.* (1951), and of Daniel *et al.* (1952), we estimate the energy of the primary particle to be about 30 Bev. Energy measurements on some of the longer tracks produced by the shower particles are also in agreement with this estimate.

From the analysis of the 'black' and 'grey' tracks of star A, we could identify nine α-particles, one heavy fragment and eleven singly-charged particles. As no slow mesons were detected, the latter were probably due to protons, deuterons or tritons. The comparison of the shape of the track 'f' with those of other multiply-charged particles stopping in the emulsion allows a rough estimate of the charge of fragment f; the most probable value is about 5.

The initial kinetic energy of the fragment 'f', estimated from its range (90 μ) and charge (Perkins 1950), is of the order of 60 Mev. The fragment appears to stop in the emulsion exactly in the centre of star B.

---

* A preliminary report of this observation was given by Professor A. Soltan at the meeting of the Polish Academy of Science held on 20th October 1952.

† Communicated by Professor C. F. Powell, F.R.S.

‡ We are indebted to Professor C. F. Powell for the opportunity of exposing the plates in a balloon flight and processing them at Bristol.

Its final energy, as deduced from the characteristics of the end of its track is very small and certainly much less than that necessary to produce the star B. The time of flight of the fragment was of the order of 3×10^{-12} sec.

The results of the analysis of the star B, which is a four-prong star of low energy are given in the following table :

Track	Range	Grain density	Identity	Energy
1	9 μ	Black	p, d, t, or α	0·7 MeV assumed proton
2	123 μ	Black	p, d, t, or α	16 MeV assumed α-particle
3	—	$3{\cdot}7 \pm 0{\cdot}2$	p, d, t, or π	82 MeV assumed proton
4	2 μ	Black	Recoil	—

Taking into account the binding energy of the emitted particles, we find for the total energy released in event B, a value equal to or greater than 120 MeV. We may, however, expect that some neutrons should also be emitted. If so, the total internal energy of the fragment should be increased to $\sim$140 MeV. If track 3 was produced by a π-meson, the total energy, including the rest-mass of the particle, is of the order of 180 MeV, not taking into account possible neutron emission.

The probability of a chance coincidence between the end of the track f and the centre of star B, in the conditions of the experiment, was calculated from, (*a*) the average star density in the exposed plate and the local increase in the radiation density, due to the proximity of star A ; and, (*b*) the known optical resolution of the microscope. This probability is less than 1 in 10^7.

CONCLUSION

Assuming that the event is not due to a chance coincidence, we are left with various alternative possibilities. It might be attributed either to an interaction between a heavy fragment and a nucleus of the emulsion, or to the spontaneous decay of the heavy fragment (Schopper 1947, Lovera 1947, Hodgson and Perkins 1949). The first interpretation fails because of the small, if not zero, final kinetic energy of the fragment. For the second interpretation to be valid, the fragment must have been emitted with a high internal energy, at least 120 MeV and probably more. Further, it must have remained stable, against both γ-transitions and the emission of particles, during a time greater than 3×10^{-12} sec. These considerations make it difficult to interpret the event in terms of a highly excited state of the nucleus.

It might be supposed alternatively, that the explosion was due to a π-meson capture at B, the meson being picked up in a Coulomb orbit round the heavy fragment as the latter left the disintegration at A.

B would then be regarded as a kind of ' delayed ' σ star. The weight to be given to this assumption depends on estimates of the probability of the heavy fragment picking up the meson in the disintegration A—if such a process is indeed possible— and of the time likely to elapse between the instant of capture of the meson into the orbit and its interaction with the nucleus. This time interval is generally considered to be of the order of 10^{-12} sec or less.

An alternative explanation of the event may be sought in terms of the heavy neutral V_1^0-particle, or of similar *charged* particles, which may be considered as a nucleons in excited states, with mean lifetime greater than 10^{-10} sec. It is possible that such particles exist not only as free particles, but also in bound states within nuclei. If the fragment were formed with such an excited particle among its nucleons, this could perhaps account for the delayed disintegration as well as for the observed release of energy. The kinetic energy Q, released in the decay $V_1^0 \rightarrow p^+ + \pi^-$ would be augmented by the rest-energy of the created π-meson, if the latter were absorbed in the same nucleus.

REFERENCES

Brown, R. H., Camerini, U., Fowler, P. H., Heitler, H., King, D. T., and Powell, C. F., 1949, *Phil. Mag.*, **40**, 862.
Camerini, U., Davies, J. H., Fowler, P. H., Franzinetti, C., Muirhead, H., Lock, W. O., Perkins, D. H., and Yekutieli, G., 1951, *Phil. Mag.*, **42**, 1241.
Daniel, R. R., Davies, J. H., Mulvey, J. H., and Perkins, D. H., 1952, *Phil. Mag.*, **43**, 753.
Hodgson, P., and Perkins, D. H., 1949, *Nature, Lond.*, **163**, 439.
Lovera, G., 1947, *Ric. Sci. Ricostruz.*, **17**, 2045.
Perkins, D. H., 1950, *Proc. Roy. Soc.* A, **203**, 399.
Schopper, E., 1947, *Naturwiss.*, **34**, 118.

Delayed Disintegration of a Heavy Nuclear Fragment: II

By D. A. Tidman, G. Davis, A. J. Herz and R. M. Tennent
Imperial College, London, S.W.7*

[Received December 15, 1952]

Soon after Dr. Menon of Bristol University had informed us about the event found by Danysz and Pniewski (see the preceding note), a similar observation was made in this laboratory. Photo-micrographs of the event are shown in Plate 14.

The event occurred in a G5 emulsion, 400 μ thick, exposed in a balloon flight at geomagnetic latitude 40° N. The balloon floated for eight hours at about 96 000 feet. The parent disintegration (star A) is of type 16+0p, excluding the heavy fragment f. The track of the ejected fragment has a length of 219 μ, and its end coincides with the centre of a three-track star. The following table shows the results of measurements on the tracks. The references given refer to the method of analysis.

---

* Communicated by Dr. E. P. George.

(i) Fragment f.

Range	219 μ
Charge determined by comparison with tracks of identified particles—see Plate 15	2 or 3 e
Number of delta-rays of more than 15 kev	None observed

(ii) Star A.

Energy (excluding fragment f) (Brown *et al.* 1949)	1620 Mev
Kinetic energy of fragment f, if a helium nucleus	20 Mev
Total visible energy released in star A	1640 Mev
Energy of primary (Camerini *et al.* 1951)	6000 Mev

(iii) Star B.

Energies of particles

Particle	Range	Grain density	Kinetic energy in Mev if proton	 if α-particle
B1	24 μ	black	1·6	6·4
B2	117 μ	black	4·0	16·0
B3	leaves emulsion	109 gr/100 μ ($5\cdot1\ g_{\mathrm{min}}$)	48 ± 3	
Total visible energy			54 ± 3	70 ± 3

Scattering measurements on track B3 gave $\bar{\alpha}_{100}=(0\cdot4\pm0\cdot15)^\circ$, and this suggests that the track is that of a proton rather than that of a π-meson. If the particle were a π-meson its energy would be 6 Mev.

It is of interest to make a rough estimate of the probability that the star B occurred by chance at the end of the range of the ejected particle from star A, the two disintegrations being unrelated. It seemed best to estimate a safe upper limit for such a chance juxtaposition. This involves estimating the probability that the centre of a star of 3, 4 or 5 tracks shall occur inside the cubic micron of emulsion at the end of the range of a heavy particle ejected from a star of six or more tracks. We assume that every star of six or more tracks contains one heavy fragment ending in the emulsion (Perkins 1950).

Lord (1951) gives the rate of production of stars of 3, 4 and 5 tracks at great altitudes as 1000 $\mathrm{cm}^{-3}\mathrm{d}^{-1}$. The average duration of balloon flights is not more than about eight hours. It follows that the probability of observing a small star in a specified cubic micron of emulsion is $3\cdot3\times10^{-10}$.

The rate of production of stars with six or more tracks is given by Lord (1951) as about 1600 $\mathrm{cm}^{-3}\mathrm{d}^{-1}$. Assuming that 1000 cm^3 of emulsion have so far been examined carefully in laboratories all over the world, we find that $5{\cdot}3\times10^{+5}$ large stars, each containing a heavy fragment, should have been observed. The probability of observing one chance coincidence would thus be 10^{-4}. The probability of finding two such chance events in the 1000 cm³ of emulsion would be 10^{-8}.

It appears certain that the charge of the ejected heavy particle from star A is not greater than 3 e (see Plate 15). It is rather unlikely that the event can be attributed to the capture of a negative π-meson by the heavy fragment (Danysz and Pniewski, preceding letter), for the visible energy in star B is somewhat high for such an event (Menon, Muirhead and Rochat 1950). The observations are, however, not inconsistent with the view that one of the nucleons of the fragment was a $V_1{}^0$-particle. The observed release of energy among the charged particles can be reconciled with this assumption and the measured mass of the $V_1{}^0$-particle.

REFERENCES

CAMERINI, U., DAVIES, J. H., FOWLER, P. H., FRANZINETTI, C., MUIRHEAD, H., LOCK, W. O., PERKINS, D. H., and YEKUTIELI, G., 1951, *Phil. Mag.*, **42**, 1241.

LORD, J. J., *Phys. Rev.*, **81**, 901.

MENON, M. G. K., MUIRHEAD, H., and ROCHAT, O., 1950, *Phil. Mag.*, **41**, 583.

PERKINS, D. H., 1950, *Proc. Roy. Soc.* A, **203**, 399.

A Neutral V-Particle from a Low-Energy Nuclear Interaction

By J. P. ASTBURY, J. S. BUCHANAN, G. D. JAMES, D. D. MILLAR,
J. A. NEWTH, D. I. PAGE, A. B. SAHIAR and A. RYTZ
The Physical Laboratories, The University, Manchester 13

[Received February 3, 1953]

THE study of low-energy interactions in which V-particles are produced has a double importance. In the first place, it can be expected to provide fundamental information about the production process—whether, for example, the $V_1{}^0$-particle should be regarded as an excited nucleon or as a produced particle. Secondly, in the design of a large particle accelerator, the likely yield of V-particles and heavy mesons must be a major consideration. This yield can only be estimated at present from observations made on cosmic-ray nuclear interactions.

In a recent paper (Astbury *et al.* 1952) we have drawn attention to the fact that charged V-particles can be produced in nuclear interactions where the total energy involved is $\sim 5\times10^9$ ev. In this letter we describe an event which shows that at least one type of neutral V-particle can be produced in interactions of similar energy.

During the course of the cloud chamber experiment previously reported some 25 000 photographs have been taken. Among these there are fifty showing characteristic nuclear ‘ stars ’ in the gas of the cloud chamber.

Thirty of these stars correspond to low-energy disintegrations in which no fast charged particles are produced. In the remaining twenty events there is evidence for the production of π-mesons or of fast protons.

The photograph of one of these last events (see Plate 16) shows the decay of a neutral *V*-particle at a distance of 3·5 cm from the nuclear interaction. Figure 1 shows a scale drawing of the event in which all the relevant tracks are numbered; the measurements made on them are given in the table. From the geometry and dynamics of the decay it is clear that the *V*-particle came from the star in the gas.

Fig. 1

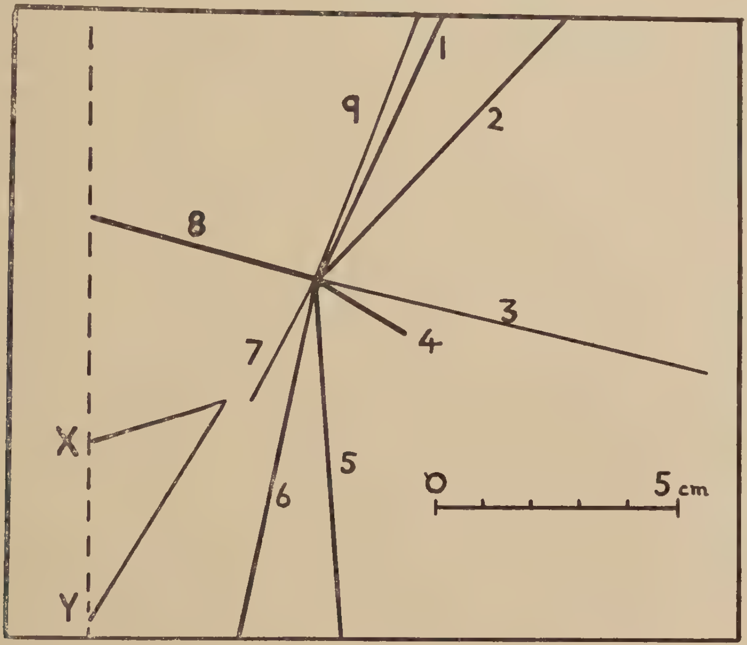

Diagram of the interaction showing the primary particle (1) and the eight charged products (2–9). *X* and *Y* are the decay products of the *V*-particle produced in the interaction.

If the star is related to the main shower occurring in the lead above the cloud chamber either particle 1 or a nearby neutral particle must be the primary causing the interaction. We consider it most improbable that particle 1 should be a secondary particle from the star since only one fast charged particle is emitted in the forward direction and all three identified light mesons move backwards in the laboratory system. Were particle 1 a secondary, this asymmetry would be even more pronounced. For this reason, our interpretation of the event assumes particle 1 to be the primary.

Excluding particle 7, the energy given to the charged secondary particles from the star is $\sim 10^9$ ev ; this figure includes the rest-energy of three π-mesons. From measurements made on stars in photographic emulsion (Camerini, Lock and Perkins 1952) it is known that the average energy of shower particles in low multiplicity stars is less than 10^9 ev. It is reasonable to take this as an estimate of the energy of particle 7 although the photographic plate work shows that there are large fluctuations about the average value.

Table of Measurements

Track number	Sign and momentum* (10^8 ev/c)	Ionization density (I/I_0)	Nature of particle	Kinetic energy (Mev)
1	? >5	<2	?	?
2	$-0{\cdot}6$	3 to 6	π-meson	13
3	$+2{\cdot}0$	<2	π-meson	100
4	? ?	>5	proton	$\leqslant 65$
5	$+3{\cdot}6$	3 to 6	proton	60
6	$+3{\cdot}0$	5 to 10	proton	50
7	? >1	<2	?	?
8	$+2{\cdot}0$	>10	proton	22
9	$+3{\cdot}2$	<2	π-meson	210
X	$-1{\cdot}0$	1·5 to 3	light meson	See text
Y	>3	<2	?	See text

* No errors are given for the measurements of momenta since their effect is negligible in computing the energy of the interaction.

The total energy of the neutral mesons and neutrons emitted from the star is unlikely to be very much larger than that of the protons and charged mesons. What evidence there is suggests that the number of π^0-mesons from showers of low multiplicity is about the same as the number of charged mesons (Camerini *et al.* 1951). The numbers of neutrons and protons must, of course, be very nearly the same.

Owing to the shortness of the tracks X and Y, the V-decay cannot be fully analysed. The plane of the fork can only be determined to within 5° and, to this accuracy, the star is coplanar with the decay tracks. The angle between the tracks is $55° \pm 5°$ and the measurements are all equally consistent with the decay of a $V_1{}^0$- or a $V_2{}^0$-particle (Armenteros *et al.* 1950). Assuming a $V_1{}^0$-decay, the kinetic energy, total energy and time of flight of the particle were about 390 Mev, 1 500 Mev and 10^{-10} sec ; the corresponding figures for a $V_2{}^0$-particle are 330 Mev, 800 Mev and 7×10^{-11} sec.

From the preceding argument we consider that the best estimate of the energy of the interaction is $\sim 6 \times 10^9$ ev and that the value is unlikely to be much greater than 10^{10} ev.

It is interesting to consider how this event would have appeared had it occurred in a lead plate in a cloud chamber or in photographic emulsion. Only the secondary particles 3, 7 and 9 have ranges in lead greater than one centimetre and, of these, 3 has a nearly horizontal trajectory and would probably not emerge from a horizontal lead plate 1 cm thick. Thus the only secondary particles seen would be 7 and 9 and, of course, the *V*-particle.

If it had occurred in photographic emulsion the event would have been classified as a star with three shower particles (either 3, 7, and 9 or 1, 3, and 9 depending upon which of the particles 1 and 7 were taken as primary) and the energy roughly estimated at 6 to 10×10^9 ev. The *V*-decay would not have been observed.

The photograph discussed here was obtained at the Hochalpine Forschungsstation, Jungfraujoch, Switzerland. We are indebted to the administration of the station and to Mr. H. Wiederkehr for enabling us to work there.

We are grateful to Mr. R. W. Wilkins and Mr. A. H. Chapman for assistance in running the apparatus and to Miss P. Miles for making many of the measurements.

REFERENCES

ARMENTEROS, R., BARKER, K. H., BUTLER, C. C., and CACHON, A., 1951, *Phil. Mag.*, **42,** 1113.

ASTBURY, J. P., CHIPPINDALE, P., MILLAR, D. D., NEWTH, J. A., PAGE, D. I., RYTZ, A., and SAHIAR, A. B., 1952, *Phil. Mag.*, **43,** 1283.

CAMERINI, U., DAVIES, J. H., FOWLER, P. H., FRANZINETTI, C., LOCK, W. O., PERKINS, D. H., and YEKUTIELI, G., 1951, *Phil. Mag.*, **42,** 1241.

CAMERINI, U., LOCK, W. O., and PERKINS, D. H., 1952, Article in *Progress in Cosmic Ray Physics* (North Holland Publishing Co.).

XL. *Notices of New Books and Periodicals received*

Light. By R. W. Ditchburn. (Blackie & Son Ltd.) [Pp. 680.] Price 45*s.*

Professor Ditchburn's book is very well produced and is a pleasure to read ; it is a valuable addition to the range of post-war English textbooks. The aim stated is " to describe the wave theory in such a way that the quantum theory may appear as a natural development rather than as an alternative theory ", and the treatment throughout adheres closely to this ideal. The book covers the requirements of a full Honours Degree Course and has been arranged to be read through twice. The material for omission on a first reading is clearly marked, but it may perhaps be doubted whether a student starting with only an ' Intermediate ' knowledge of Mathematics could understand all the earlier analysis.

The material discussed has been very thoughtfully selected, the sequence in which topics are arranged presents a satisfactorily coherent picture, and, in general, the book can be strongly recommended as a thoroughly suitable basis for an Honours Course.

S. H. P.

Theoretical Nuclear Physics. By J. M. Blatt and V. F. Weisskopf. (Wiley & Sons.) [Pp. 864.] Price $12.50.

The enormous development of nuclear physics during the last fifteen years has made obsolete most of the books and reviews written during the 1930's. Several new phenomena have come to light, and many others are found to require fresh theoretical treatment. This book deals mainly with the physics of nuclear processes involving energies less than about 50 mev, a notable exception being the analysis of n–p and p–p scattering up to energies of 350 mev. It is essentially, and in the best sense, an elementary book, dealing more with the broad physical principles of nuclear physics than with detailed mathematical solutions ; nevertheless, several sections are devoted to more mathematical aspects of the theory. There is full discussion of the experimental data, and some of the interpretation has not been published elsewhere.

It is easy to find fault with a work of such magnitude written while the subject matter is still growing and changing. For example, no account is given of the fruitful Butler theory of (d, p)-reactions, while all mention of the important interference terms in β-decay is relegated to a footnote. There is a general tendency towards repetition, especially through the use of over-simplified models to pave the way for a more exact and complicated treatment later on. Thus, the theory of β-decay is first formulated non-relativistically : this might be helpful if it enabled me to avoid a matrix formulation of the problem, but naturally it does not. Again, a one-particle model is used for a first discussion of the dispersion theory of nuclear reactions in spite of the fact that much the same results can be obtained with greater validity and hardly more complication from a Kapur–Peierls treatment.

It is a pity that very little recent work published outside the Physical Review has been included : the authors' apology in the preface does not excuse this omission in a work which promises to be a standard text. And it is strange that in an expensive book of over 800 pages, ten per cent of the space is devoted to lists of symbols. Nevertheless, the book gives an excellent comprehensive picture of low energy nuclear physics, and no nuclear physicist today can afford to do without it.

B. H. F.

[*The Editors do not hold themselves responsible for the views expressed by their correspondents.*]

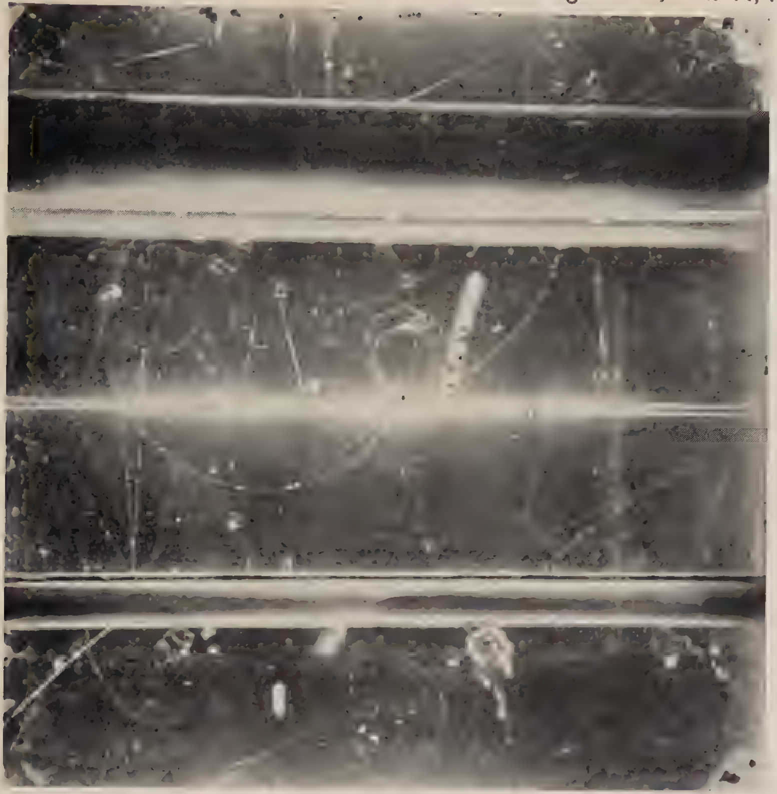

(*a*) Event DP22. A negative heavy particle comes from a low-energy interaction in the lower lead plate. (See table 1.)

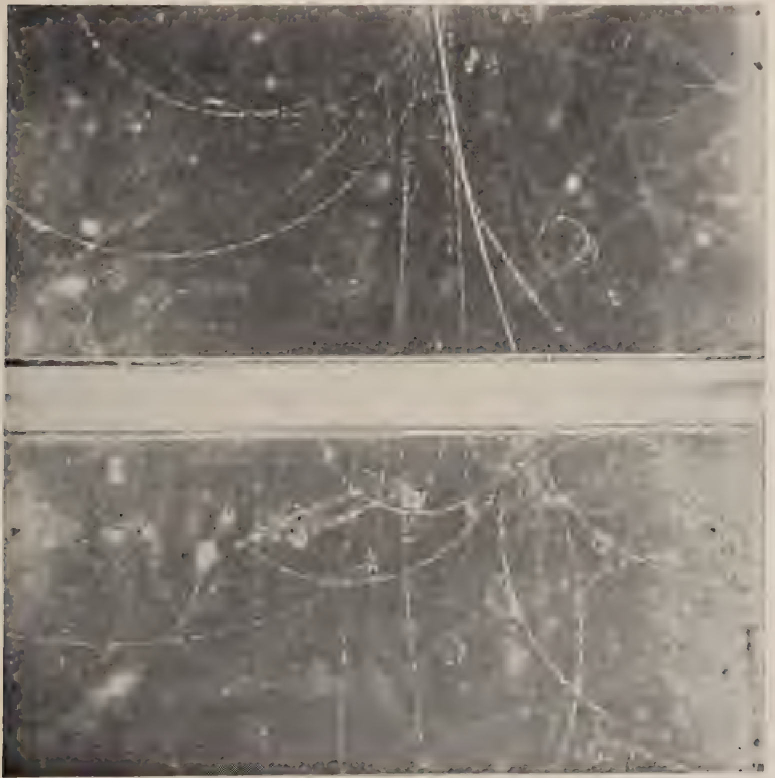

(*b*) Event JM41. A negative heavy particle from a nuclear interaction above the cloud chamber stops in the lead plate. (See table 1.)

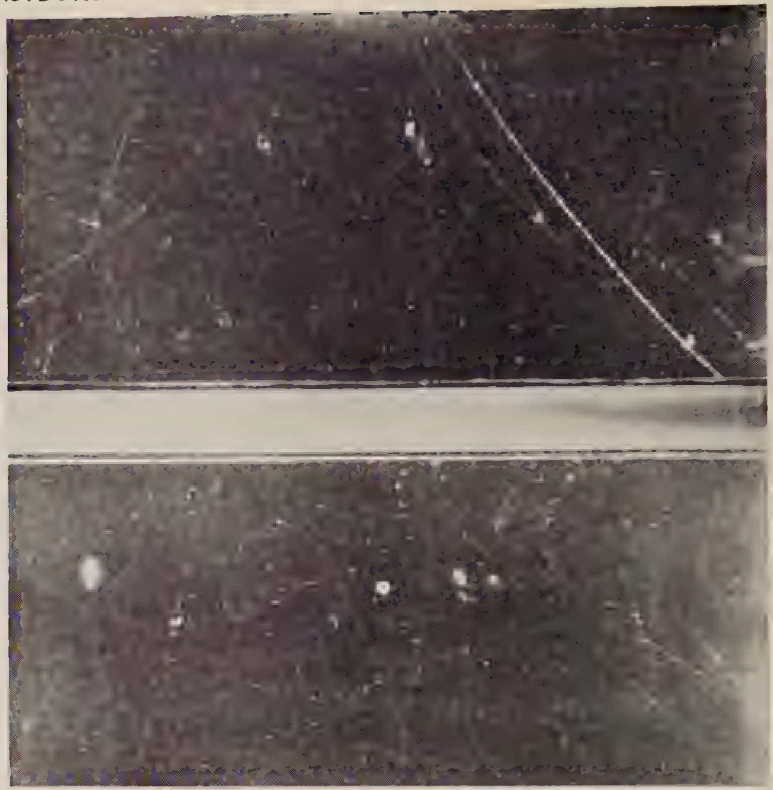

(*a*) Event KD79. A negative heavy particle with a time of flight in the cloud chamber of 3×10^{-9} sec. (See table 1.)

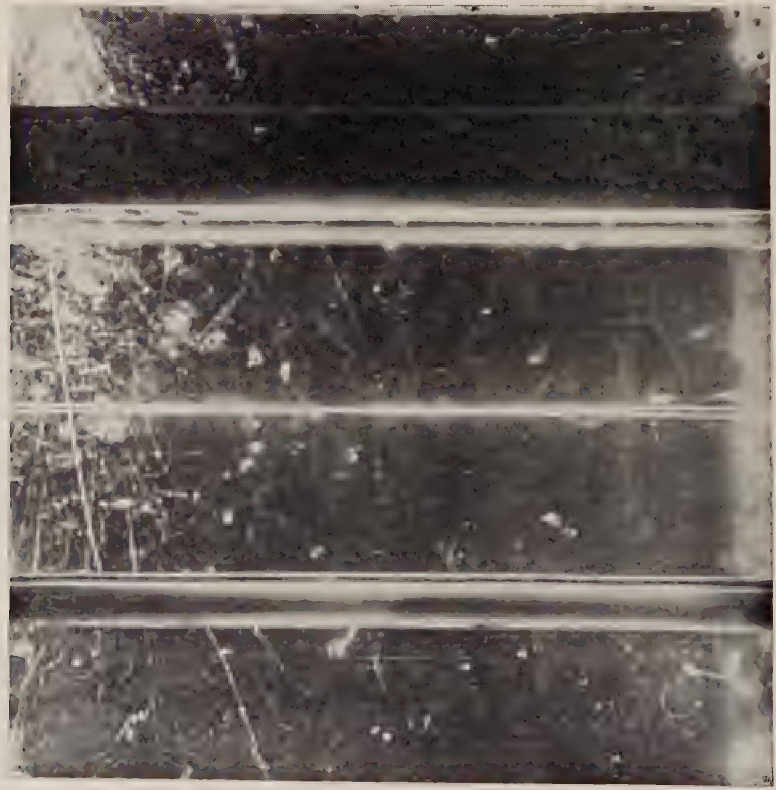

(*b*) Event CC17. A slow particle whose direction of travel cannot be determined definitely. If it is moving downwards its charge is negative.

Fig. 2

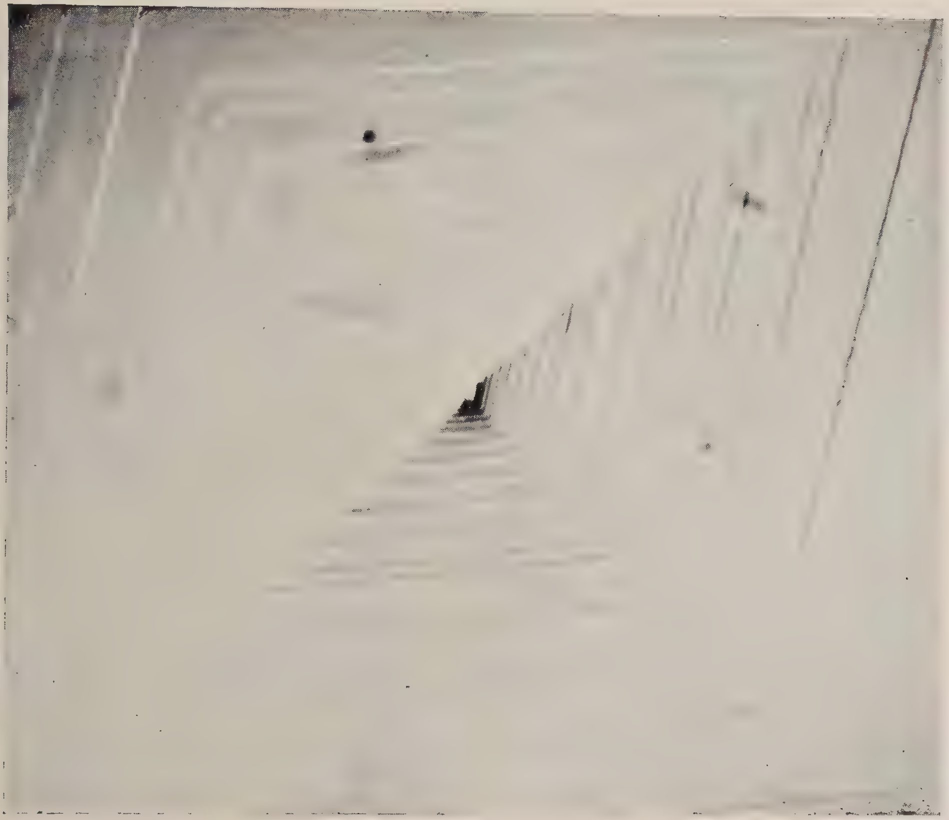

×45

Fig. 3

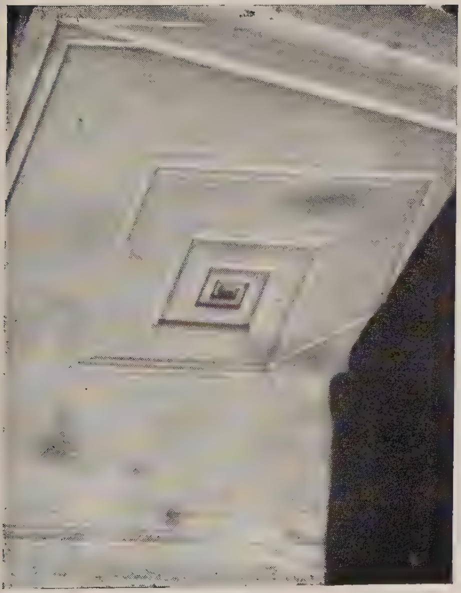

×60

Fig. 4

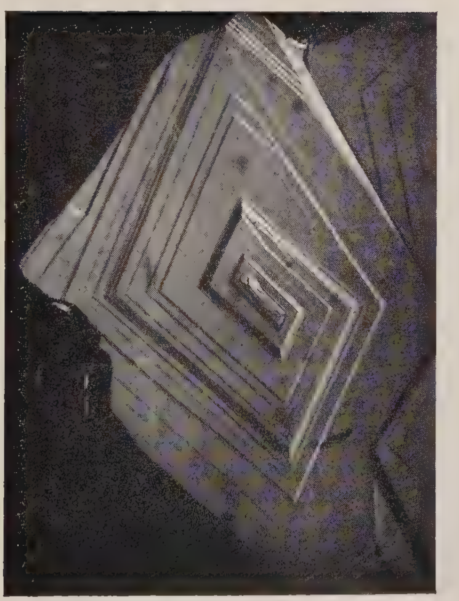

×60

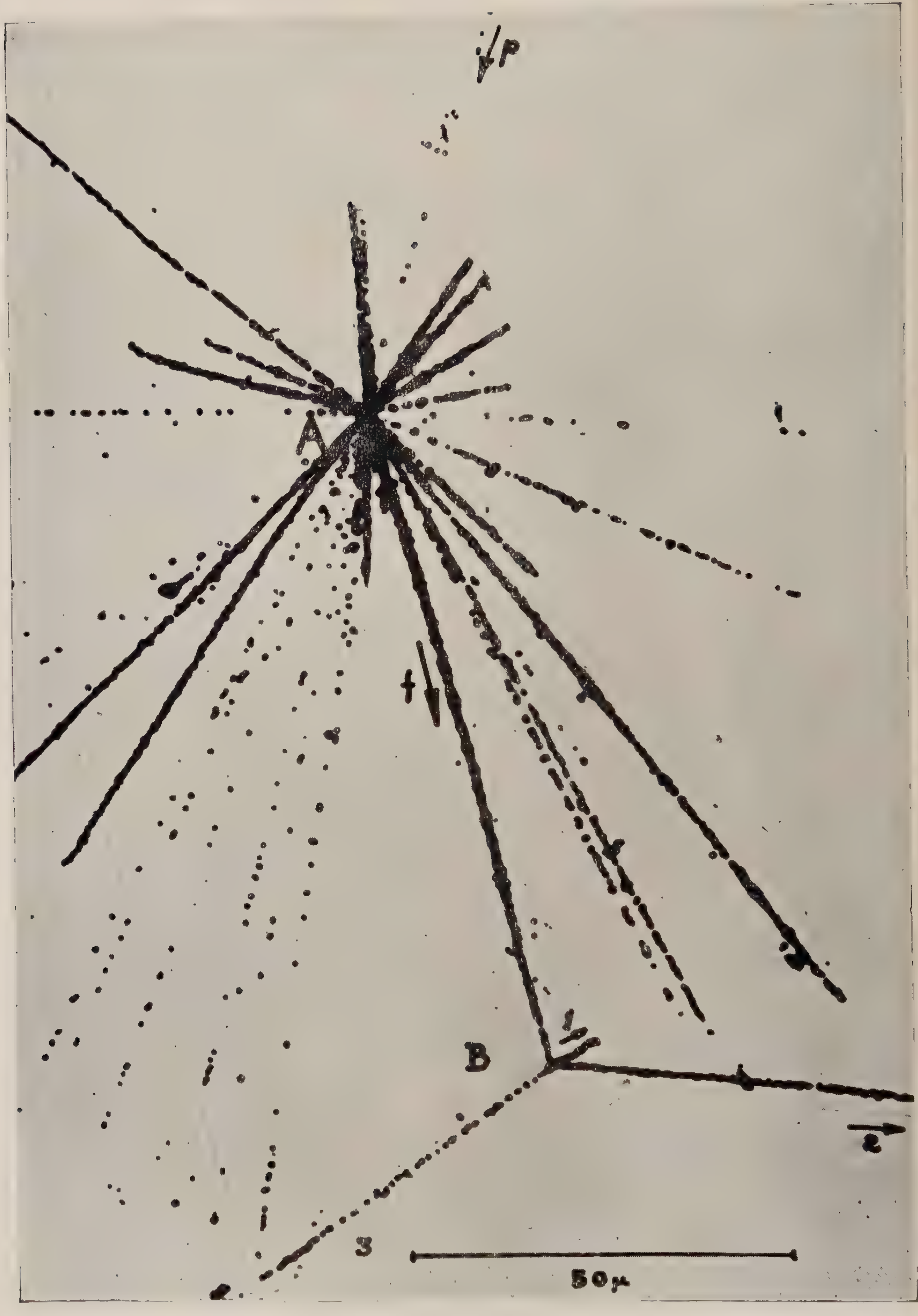
p
A
f
B
1
2
3
50μ

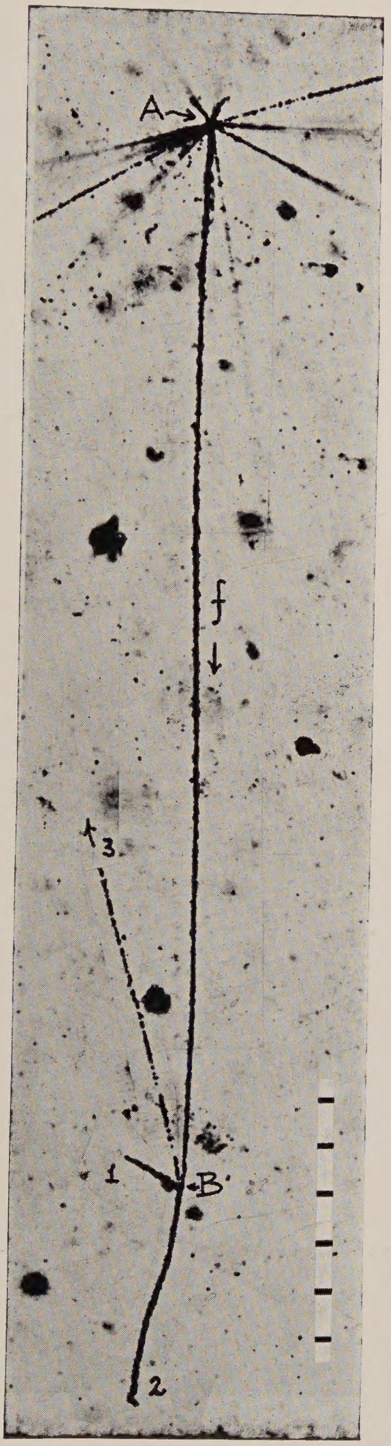
A
f
3
1
B
2

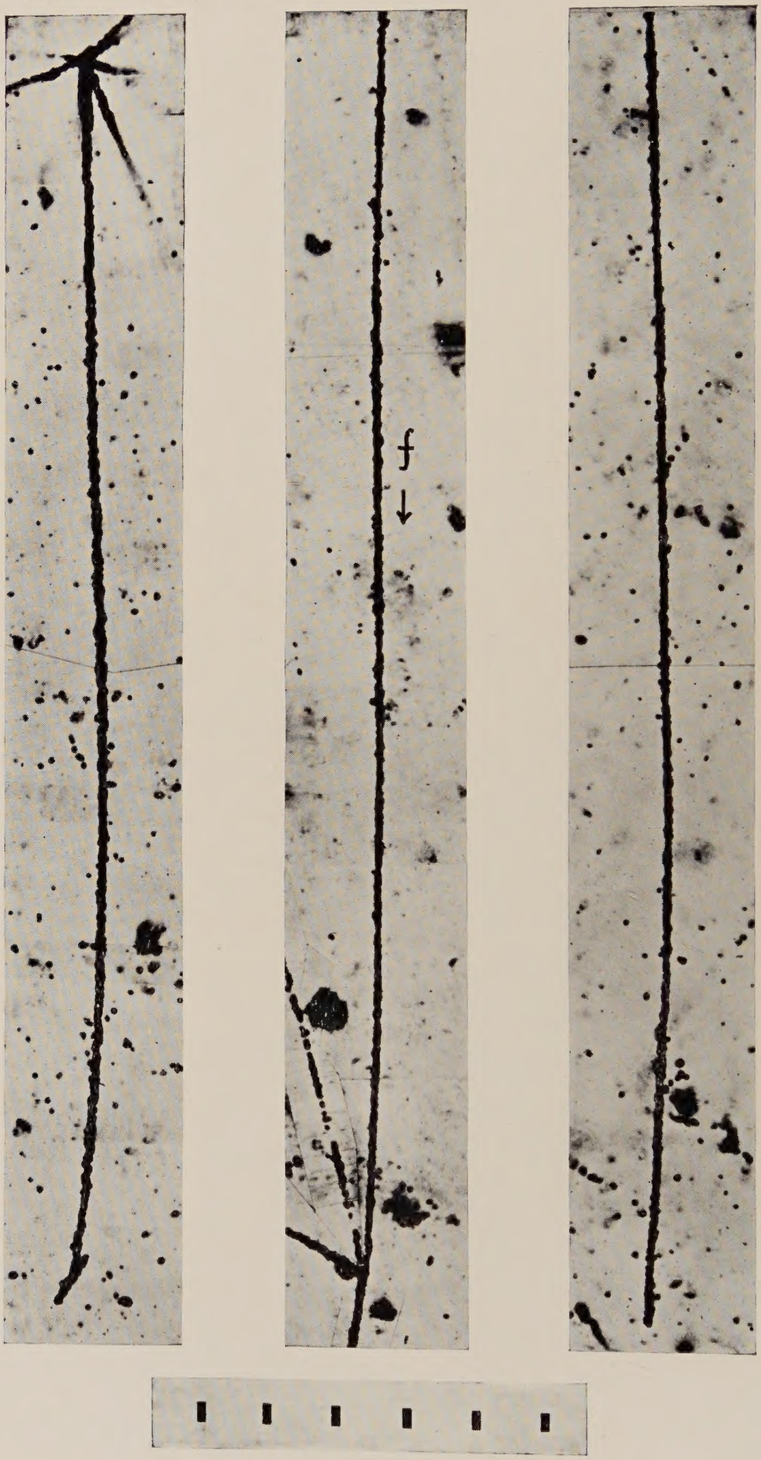

(*a*) (*b*) (*c*)

Track (*a*) Lithium nucleus (z=3).
(*b*) Heavy fragment f.
(*c*) α-particle.

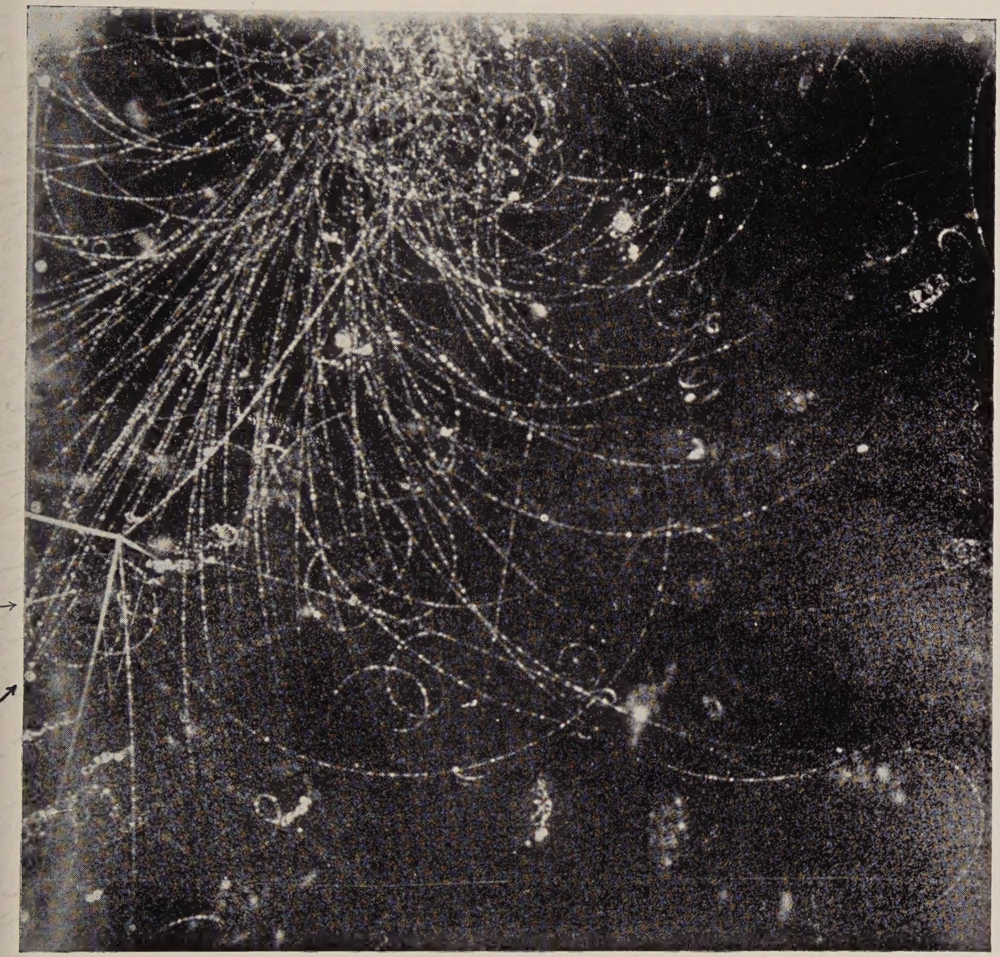

Nuclear interaction in the gas of a cloud chamber showing the production of a neutral V-particle.